https://doi.org/10.1016/j.rser.2019.109289

This is the Pre-Published Version.

Mechanical failure and mitigation strategies for the membrane in a proton exchange membrane fuel cell

Diankai Qiu[1,2,*], Linfa Peng[1], Xinmin Lai[1], Meng Ni[3], Werner Lehnert[2,4]

1=State Key Laboratory of Mechanical System and Vibration, Shanghai Jiao Tong University, Shanghai 200240, China

2=Forschungszentrum Jülich GmbH, Institute of Energy and Climate Research, IEK-3: Electrochemical Process Engineering, 52425, Jülich, Germany

3=Department of Building and Real Estate, The Hong Kong Polytechnic University, Hung Hom, Kowloon, Hong Kong, China

4= RWTH Aachen University, Modeling Electrochemical Process Engineering, 52062 Aachen, Germany

*=diankaiqiu@sjtu.edu.cn

Phone: 86-15216712064

Submitted to the Renewable and Sustainable Energy Reviews

© 2019. This manuscript version is made available under the CC-BY-NC-ND 4.0 license http://creativecommons.org/licenses/by-nc-nd/4.0/

Abstract

Proton exchange membrane (PEM) fuel cells are promising zero-emission power source for automobiles, portable devices, backup power system and stationary applications. However, their relatively short lifespan remains a major obstacle to the commercial deployment of this type of fuel cell. The membrane's mechanical degradation is the main cause of early-stage failure in fuel cell lifetimes. In order to provide engineers and researchers with a basis for extending fuel cell durability, this paper presents an overview of important issues relating to mechanical failure and mitigation strategies for PEM fuel cell membranes, drawing on a survey of the existing literature. This review begins with a sketch of failure mechanisms in an effort to establish an unambiguous definition of membrane degradation in each stage of its lifespan. The material properties of typical membranes are outlined below to illustrate the fundamentals of their mechanical behavior and cell degradation. Following the lifespan of a membrane, the causes and mechanisms of mechanical degradation in the fabrication process, cell assembly process, short-term phase and long-term phase of cell operation are discussed in detail. Practical strategies for reducing the degradation rate are introduced to each process. Finally, in-situ and ex-situ methods for the evaluation and characterization of mechanical durability are summarized to pursue the measurement methods and protocols of membranes. The aim is to assess which mechanisms affect the mechanical failure of membranes and how degradation should be mitigated across the entire lifetime of fuel cells. A summary of further work in this area is also provided to give a direction to future research.

Keyword: Fuel cell; membrane durability; mechanical degradation; cyclic relativity humidity; mitigation methods

Hightlight:

Mechanical degradation of membranes across fuel cell's lifetime are discussed
Mitigated strategies for failure are proposed for each stage of membrane's lifespan
A standard set of evaluation method and protocol for membrane durability is discussed
A summary of key points and research interests is given based on our understanding

Word count: (32075)

1. Introduction

By virtue of their clean, quiet and highly efficient operation, proton exchange membrane (PEM) fuel cells are an attractive alternative to traditional power sources and have many potential applications, including automobiles, portable devices, backup power systems and stationary applications[1]. However, their relatively short lifespan is still a major obstacle to the commercial deployment of fuel cells [2, 3]. The US Department of Energy (DOE) [4] has set durability targets of 5000 h for automotive applications and over 40000 h for power stations by 2020, which have not been satisfied by contemporary practical tests around the world. Unquestionably, the last decades have seen significant progress. Nevertheless, extensive research and development efforts are necessary for improving durability, including the lifetime of component durability, the stability of stack design and strategies for system operation.

One of the key technical challenges with PEM fuel cells is proton exchange membrane durability. A typical stack is primarily composed of a bipolar plate (BPP) and a membrane electrode assembly (MEA), constituting part of a five-layer structure with a PEM at the center. A PEM, with thicknesses ranging from 10 μm to 200 μm, plays multiple roles in the fuel cell operation, such as: (1) separating the fuel and oxidant gases; (2) transporting protons to the cathode side from the anode; and (3) preventing direct electron conduction between the two sides . The degradation characteristics of the membrane are a critical underpinning of fuel cell performance and lifetime. Table 1 summarizes the PEM fuel cell endurance tests of available in the literature. Unfortunately, the lifetime of fuel cells in the laboratory is currently less than 3000 h if membranes fail during operation, as is shown in Table 1. It is notable that fuel cell stacks for real transportation application need to work in more severe working conditions, which accelerate membrane failure.

Table 1 PEM fuel cell stack with membrane failure in lifetime test

Stack description	Testing hours (h)	Test loading (mA/cm^2)	Operating conditions				Failure type and evaluation [a]	Ref. /Publication year
			RH (%)	Stack temperature (℃)	Gas pressure	Stoichiometry		
Single cell, 25 cm^2, ①[b] GORE-SELECT® A with ePTFE; ② GORE-SELECT® B with ePTFE; ③ FSM without PTFE; ④ Nafion® 101 without PTFE; ⑤ Nafion® 1035 without PTFE; Gore electrodes with a loading of	① 700 ② 1600 ③ 70 ④ 350 ⑤ 450	800	D.P.a/c= 83/83℃	70	H_2:5 psi Air:15 psi	H_2:1.2; Air:2.0	Gas crossover, 10 mA/cm^2	[5], 2001

0.4 mg/cm^2 Pt on both the anode and cathode sides								
Ballard 8-cell stack, Nafion® membranes, 0.4 mg/cm^2 Pt on both the anode and cathode sides	11000	538 (<1000 h), 861(>1000 h)	-	-	-	-	Voltage decay<2 μV/h	[6], 2002
Single cell Nafion® membranes	2500	800	-	-	-	-	Gas crossover	[7], 2004
Ballard eight-cell stack, 0.7 mg/cm^2 Pt on cathode side and 0.3 mg/cm^2 Pt on anode side	2500	1080	H2:100%; Air:70%	75	fuel pressure slightly higher than air pressure	-	Large Gas crossover	[8], 2004
Single cell, 45 cm^2, Nafion 112 membrane, 0.5 mg/cm^2 carbon-supported Pt on both the cathode and anode sides	2088	300	H2:100%; Air:100%	75	At atmosphere	H2: 1.43; Air: 2.5	1）Gas crossover, 27.71 mA/cm^2 (Rate dramatically increases at 1900h), 2）Slow decrease of the electrochemically active surface area (EAS) of Pt	[9], 2005
20-cell stack, 110 cm^2	5000	250	H2:57%; Air:74%	75	At atmosphere	-	-	[10], 2005
Single cell, 45 cm^2, Nafion 112 membrane, 0.5 mg/cm^2 Pt loading on both the cathode and anode sides	① 500 ② 1000	① Cyclic current (maximum 1060 mA/cm^2) ② Constant current 1060	H2:100%; Air:100%	80	Backpressure 20 psi	H_2: 200 sccm; Air: 500 sccm	1) Gas crossover, ① 60 mA/cm^2, ② 10 mA/cm^2, 2) EAS decrease	[11], 2006

		mA/cm^2						
Ballard 10-cell stack	7863	Dynamic load cycle	H2:70%; Air:56%	60-65	H2:2.6 bar Air:2.4 bar	H2: 1.5; Air: 1.8	-	[12], 2008
Six cell stack, $50cm^2$, GoreTM PRIMEA® series 57, 0.4 mg/cm^2 Pt loading on both the cathode and anode sides	1200	10	H2:100%; Air:100%	70	-	H_2: 0.5 SLPM; Air:2.0 SLPM	1) Gas crossover, , 2.15 mA/cm^2@800h, 20.71 mA/cm^2@1200h; 2) EAS decrease from 0.037 C cm^{-2} to 0.021 C cm^{-2} at 800h, and 0.002 C cm^{-2} at 1200h	[13], 2010
4-cell stack, 50 cm^2, ① Nafion® N117; ② Nafion® N115; ③ Nafion® NR212; ④ Nafion® NR211, 0.3 mg/cm^2 carbon-supported Pt loading on both the cathode and anode sides	1000	10	H2:100%; Air:100%	70	-	H_2: 1 SLPM; Air:2.0 SLPM	Gas crossover in NR211, ④ 40 mA/cm^2	[14], 2010
Two 55-cell stack, 90 cm^2, Nafion® NR211, Pt/C catalys type	1500	Constant current in different level	-	-	-	-	28 cells with high gas crossover	[15], 2012
30-cell stack, 142 cm^2, PFSA-membrane from Johnson Matthey Fuel Cells	1200	500	H2: 50% (0-50A) and 15%: (>50A); Air: 60%	80	150 Kpa	H_2:1.5; Air: 2.5	1) Gas crossover, Maximum : 6.3 mA/cm^2, 2) Particle size of cathode catalyst increase from 3.5 nm to 4.0 nm	[16], 2016
24-cell stack,	3500	447	H2:80%;	75	H_2:2.4	H_2:1.26-	-	[17],

80 μm thick membrane, 0.4 mg/cm^2 carbon-supported Pt loading on both the cathode and ande sides			O_2:60%		bar Air:2.5 bar	1.0 Air: 1.26-1.0		2016

[a] The failure type of gas crossover is evaluated by the electrochemical H_2 crossover rate

[b] ①②③④⑤ mean different experiments in the study

The degradation of membranes takes two main forms: mechanical and chemical degradations, which induce the respective mechanical and chemical failure of membranes in a synergistic process [18]. Chemical failure, which takes the form of damage to the ionomer and diminished membrane integrity and functionality, has been extensively studied by a significant body of work. It is usually caused by free radical attack, that is generated in the course of hydrogen peroxide decomposition on the cathode side, cationic contaminants or the reaction of hydrogen and oxygen at the platinum catalyst [19-21]. The thinning and divot generated in the PEMs are the main modes of chemical failure and result from attack by radicals on the carboxylic acid end group sites of the primary chain and sulfonic acid groups from the side chain [22-24]. The mechanical failure results from the local stress concentration and mechanical stress variation on the constrained membrane under the alternating swelling and shrinking in response to the changes in water content and temperature. As a result, material fatigue, creep and the generation of wrinkles, delamination, pinholes, tears or cracks are initiated and propagated on the surface or across the bulk of the membrane, which would be exacerbated by inherent defects in the membrane occurring during the fabrication process or the improper assembly of fuel cell stacks [25]. Liu and Case's [11] results show that hydrogen crossover is the primary source of degradation after 500 h of operation. Although PEM mechanical failure is considered to have the highest occurrence potential and is regarded as the main cause of fuel cell failure in the early period of the cell's lifetime [26, 27], comprehensive understanding of this type of failure is lacking.

The mechanical failure of the membrane, such as that resulting from a pinhole or crack, provides a passage by which the hydrogen and oxygen mix and which can trigger a combustion reaction and high heat spot, thus leading to instantaneous performance decay and the failure of the fuel cell. In particular, recent stacks have been designed to use especially thin membranes so as to minimize ohmic loss and enhance proton conductivity [28]. Therefore, the membrane's mechanical integrity and durability has emerged as a critical challenge. Although the mechanical degradation of membrane is unavoidable, the material durability could be improved and degradation rate could be reduced by differentiating between failure modes and the resulting effects, deeply understanding the failure mechanisms, and optimizing the mitigation strategies [29].

In recent years, automobile manufacturers and fuel cell developers have realized the importance of understanding membrane mechanical failure and improving mechanical durability.

Figure. 1 displays the literature from ScienceDirect that has focused on the mechanical durability of PEM fuel cells. Before 2005, comparatively few publications had been reported, since most attention was paid to performance improvement. With fuel cell development in recent years, the mechanical durability of membranes has become a challenge to ensuring their low cost and long life in practical applications. Increasing attentions have been paid to this issue in the fuel cell. Although considerable progress has been made in the last few years to improve the membrane durability, it remains a major obstacle that hinders fuel cell lifetime. Considering the complex assembly and operating processes of fuel cells, the causes and mechanism of the gradual mechanical degradation in each stage of membrane lifespan remain unclear. New in-situ techniques of detecting the failure process and mitigating mechanical degradation are urgently required to guide the improvement of membranes. Moreover, novel ex-situ methods should be established to evaluate membrane property and durability. However, to date, no review has been dedicated to this topic. The purpose of this paper is to review current studies and encourage the development of more techiques to understand the mechanical failure of membranes.

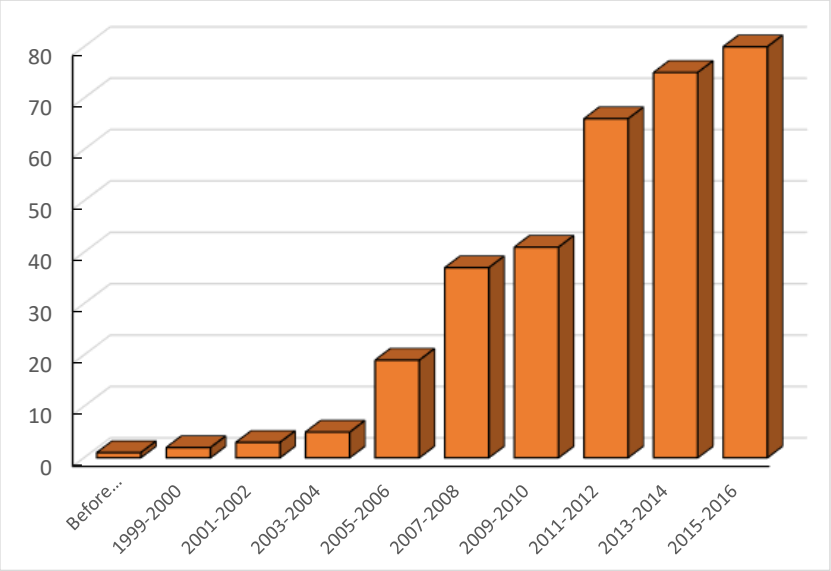

Figure. 1 Trend in publications for PEM mechanical degradation studies in recent years

In this paper, studies conducted on the mechanical failure of membranes are summarized to offer a clear overview of the concepts of membrane mechanical failure and performance decay. This review begins with a sketch of failure mechanisms and modes according to the process of a membrane's life path, followed by typical membrane material properties to illustrate the basis of understanding mechanical behavior in the cell. A detailed description of the main contributions to mechanical degradation in the fabrication process, stack assembly, short-term operation and long-term operation stage and their mitigation strategies is presented. Finally, in-situ and ex-situ methods of evaluation and the characterization of membrane mechanical failure are summarized to outline membrane measurement methods and protocols. The aim of this is to assess which mechanisms

affect mechanical failure and how degradation should be mitigated to provide a guideline for improving membrane durability.

2. Mechanism of mechanical failure

The durability of any device is broadly defined by the feasibility of it reaching functional purpose in its service lifetime. In order to obtain a complete fuel cell, the life path of a PEM is displayed in Figure. 2, which can be divided into four processes: the fabrication process of the membrane, the assembly process of the fuel cell, its short-term and long-term operation stages. The manufacturing quality of the membrane determines its material properties and capability to resist degradation. Then the PEM, as a central component of the MEA, is assembled in the cell alongside the BPP, gasket and endplate. At the beginning of the fuel cell operation, the membrane's stress state changes significantly with relatively humidity (RH) and temperature, requiring high mechanical flexibility in the constrained cell environment. Some extreme conditions could result in a dramatic failure of the membrane. During the long-term operation, the membrane undergoes repetitive swelling and shrinkage (water absorption and thermal effect), gas pressure and chemical attacks during the duty cycles. It is obvious that the fuel cell's efficacy would decline if mechanical failure occurs in the membrane at any stage of its life path.

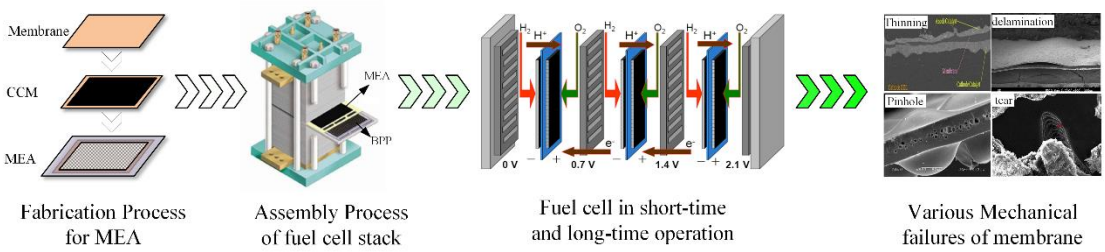

Figure. 2 Schematic representation of the membrane life path in the fuel cell (Permission from [24, 30-33], copyright Elsevier)

1) The first process primarily relates to the quality of the manufactured product. The thin PEM has important functions that require high end qualities with respect to the mechanical and geometric properties. However, defects are unavoidable in the course of mass production, such as with the micro pinhole, higher roughness and thickness variation. These undesirable variables tend to create non-uniform mechanical and chemical properties in the membrane, and give rise to adverse effects on membrane durability and fuel cell performance as a result of low mechanical strength, hot-spots and radical attack [34].

2) A fuel cell stack is usually assembled with multiple single cells in series to meet the voltage and power requirements. The PEM is installed with the MEA between two BPPs in a sandwich structure. Under the constraint of the sealing edge (MEA frame) and flow field, in which the ribs and channels are arranged at regular intervals, the mechanical failure of the membrane is affected by the non-uniform mechanical stress or localized concentrated stress. The current manual assembly

process and manufacturing error of the components could aggravate the fluctuating mechanical stresses in the membrane, which may trigger the membrane's tearing.

3) Once the assembled fuel cell begins running, humidified reactant gases are supplied to it at a certain temperature. The constrained membrane is exposed to the pressure fluctuation of reactant gases and cycling hygrothermal conditions especially when during startup or shutdown, resulting in sharp tensile and compressive stresses in the membrane due to the expansion and shrinkage [35]. Plastic deformation is also a potential threat, in which residual stress is caused if the compressive/tensile stress exceeds the yield strength. In addition, the freeze-thaw of a fuel cell and weak area at the joint region between the membrane and MEA frame may cause a rapid membrane failure during the short-term operation phase. These environmental factors present major mechanical challenges to membranes.

4) For the fuel cell's long-term operation, the membrane experiences cyclic loading conditions. Accordingly, the swelling and shrinkage induce fluctuating mechanical stress in the membrane, causing wrinkles, creep and fatigue in the material. With the long-time accumulation, the mechanical failure of membrane is eventually caused by the initiation and propagation of micro-pinhole or crack, especially within the defective area [18]. It should be noted that in real working environments, the mechanical failure process would be intensified by delamination from the catalyst layer (CL) and chemical degradation.

As can be seen, the mechanical failure of a membrane is influenced by many external and internal factors, such as its fabrication, the fuel cell's assembly, the quality of the assembled components, acceleration of chemical degradation and operational conditions. Figure. 3 summarizes the main factors influencing membrane mechanical failure in terms of four procedures. This work outlines and discusses how and why membrane mechanical failure occurs during its life path. In order to provide the fundamentals of mechanical behavior and degradation in the cell environment, the material properties of typical membranes are first illustrated.

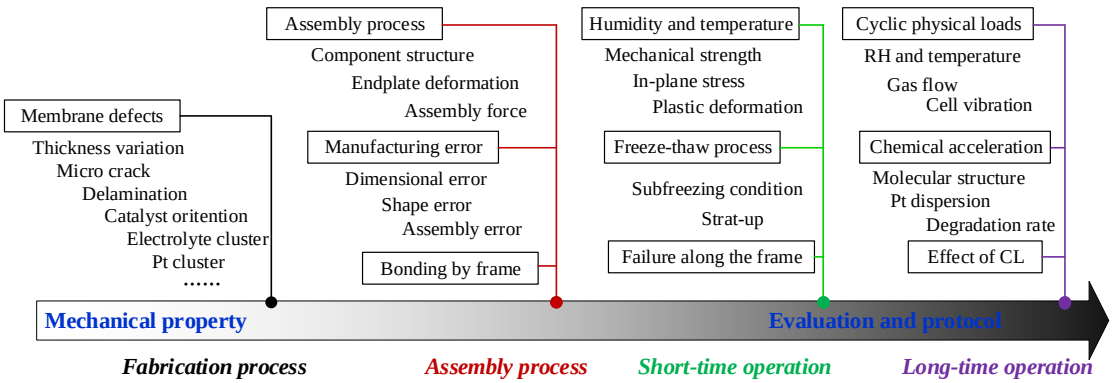

Figure. 3 The main factors that influence mechanical failure during the lifespan.

3. Membrane mechanical properties

The mechanical properties of membranes are crucial to their mechanical durability when

subjected to cell environments [5]. They not only influence the deformation behavior of the membrane, but also dominate mechanical resistance to sustained or cyclic stresses. For a particular material, its mechanical property can be evaluated by stress-strain behavior, which is tested by recording the amount of deformation (strain) at various loadings (stress). The elastic modulus, yield stress, ultimate tensile strength (UTS) and final strain are usually used to evaluate the results of stress-strain curves. For membranes, these parameters are determined by micro molecular chains mobility and interchain interaction in the material. The elastic modulus can be used as indications of the membrane stiffness, an ability to withstand deformation when loading is applied. Yield stress is defined as the strength at which plastic deformation of a material starts to occur. The final strain and UTS are defined as the total strain and maximum tensile stress before fracture, respectively. In addition, the stress-strain behavior of the membrane is dependent on temperature, humidity and time due to the change in intermolecular force and amorphous domain of the material in cell conditions. In recent years, a wide range of studies have emerged to address the membrane's mechanical properties in the context of the fuel cell. These studies fall into three primary categories: (1) the improvement of membrane materials; (2) the testing of membrane properties, and (3) the constitutive model developed for describing material properties.

3.1 Materials

In 1955, Thomas Grubb, a General Electric (GE) Company worker, proposed using a polymer membrane as an electrolyte with the goal of modifying and simplifying the original fuel cell design [36]. Based on this concept, the first type of PEM fuel cell was designed with an ion-exchange polystyrene sulphated membrane, and had a very limited lifetime. From the 1960s, the broadly utilized PEM materials incorporated perfluorosulfonic acid (PFSA) such as DuPont Nafion® on the basis of its good proton conductivity and mechanical and chemical stability. PFSA membranes comprise a perfluorinated backbone (tetrafluoroethylene, TFE) to provide the chemical and thermal stability and hydrophilic sulfonated side chains (HSO_3^-) for proton conduction as shown in Figure 4. In order to change the poor mechanical property of neat PFSA membranes, especially with thin thickness, reinforcement technologies are developed to incorporate PTFE-based woven fabrics and microfibrils as a composite membrane [37]. Currently, PFSA-based membranes are developed by several companies such as Nafion® (Dupont™), Gore-Select® (Gore™), Aquivion with shorter side chains (Solvay Solexis) and Aciplex® with longer side chains (Asahi™) [38, 39]. For a long time, Nafion® has been regarded as the state-of-the-art membrane in the PEM fuel cell.

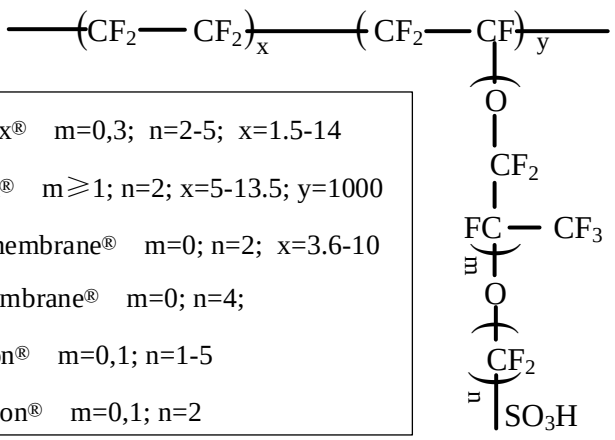

Figure 4. Chemical structures of perfluorinated PEMs.

However, the PFSA-based membranes exhibit high material costs, undesired reactant permeability and are dependent on water content, which in turn increase the fuel cell's costs and reduce the efficiency and durability of fuel cell at high operation temperature [40-42]. Recently, some novel non-fluorinated and partially fluorinated hydrocarbon membranes have also been presented as potential candidates for fuel cell electrolytes [43, 44], such as sulfonated perfluorocyclobutane (PFCB) [40, 45], sulfonated styrene/ethylene-butylene/styrene (S-SEBS) copolymers [46], poly(ether ether ketone)s (PEEKs) [2, 47], polyimides (PI) [48-50], and aromatic ABA triblock copolymers[51]. More recent development of materials are reviewed by Zhang and Shen [52]. PFCB membranes have promising proton conductivity but poor mechanical stability. In Jiang et al.'s work [40], an obvious crossover gas leak was observed in the improved PFCB membrane with 30 wt.% poly(vinylidene fluoride) (PVDF) after only 7000 RH cycles. For PEEK membranes, a fairly brittle behavior with a strain of only 6% was obtained when breaking in the tensile test. Better mechanical durability with above 80 % final strain can be achieved when PEEK membranes were sulfonated (above 70%) [53]. The higher breaking strain is caused by the increase of the chain bulkiness and decrease of chain entanglement after –SO3H groups were introduced. However, durability remains a major obstacle that hinders PEEK membrane application due to the hydroxy radical initiated degradation. For PI membranes, the respective stress and final strain when breaking are obviously higher and smaller than conventional Nafion®. However, PI degration is sentive to hydrolysis, and lifetimes of a few hours to 1000 h are observed for PI membranes in cell conditions under various operating temperatures and material ion exchange capacity [54]. In general, the stability and durability of these polymer membranes are insufficient in the cell conditions, and significant improvements are still necessary to achieve commercial application. PFSA membranes continue to maintain their positon as the proton conducting polymer of choice. Hence, considering the application range, the contributions to the mechanical issues of PFSA-based membranes are primarily reviewed in this work, unless otherwise stated.

3.2 Mechanical properties

As synthetic polymers with ionic properties, the mechanical properties of membranes are robust in terms of humidity, temperature and time. In a humidified environment, the nano-sized clusters separated from sulfonated (SO3-) end groups absorb a large amount of water, leading to the swelling of the ionomer. Accordingly, higher proton conductivity will be achieved by increasing humidity [55, 56]. The polymer material is also sensitive to thermal effects. As is shown in Figure 5 of regarding the uniaxial test with Nafion® 112 (conditions with temperatures of 25 ℃, 45 ℃, 65 ℃ and 85 ℃ and relatively humidities of 30%, 50%, 70% and 90%) [57], the stress-strain curves of the membrane monotonically drop with the increasing humidity and temperature, which resulted in a reduced Young's modulus and yield stress because of a declining intermolecular force and amorphous domain. As can be seen, the effect of temperature on the decrease of elastic modulus and yield stress is more significant than humidity. Lower UTS and higher final break strain at the fracture are caused in the presence of higher temperature due to the falling ionic interactions, while the effect is less clear as the humidity changes. These phenomena are also presented in various membranes, such as Nafion® 111 [58], Nafion® 115 [59, 60], Nafion® 117 [61], Nafion® 211 [62], Nafion® 212 [63, 64] and Gore-Select® membranes [65]. Tang et al. [65]'s experimental results using GORE® membrane material with expanded polytetrafluoroethylene (ePTFE) showed much higher Young's modulus and proportional limit stress, along with higher break stress and lower in-plane swelling than unreinforced membranes. Hence, the reinforced composite membrane has a better resistance to mechanical degradation in the fuel cell's operation. Nonlinear behavior occurs in both the elastic and plastic phases of the stress-strain curve. The linear regression of the initial linear curve (for example, 0-0.5% strain) and "proportional limit" yield or the offset yield in the ASTM D882 standard [66] could be adopted to evaluate the stress-strain curve as shown in Figure 5 (c). In addition, the varying hygrothermal conditions result in different resistance to mechanical failure for a PEM [67]. According to Dillard et al. [68, 69] who conducted trouser tear tests on commercial membranes of Nafion® NRE 211, Nafion® N111-IP, and Gore-Select® 57, the submerged specimens were an order of magnitude lower than dry membranes in terms of their tear energy. The decreasing rate of fracture energy resulting from the increasing humidity became slower at higher temperatures. This means that the formation and propagation of mechanical failure will be accelerated faster by increasing temperature than humidity if the cell is operated at high temperatures. This relates to the more sensitive response of mechanical properties to increasing temperature.

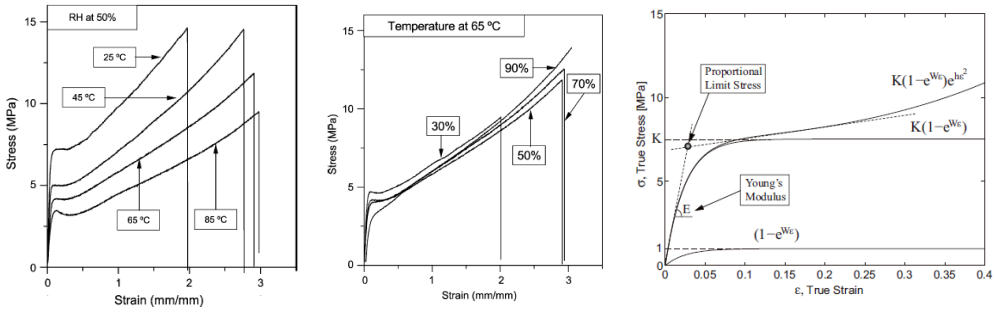

(a) (b) (c)

Figure 5. Experimental engineering stress-strain data from tensile tests of Nafion® 112 (machine direction): (a) various temperatures of 25 ℃, 45 ℃, 65 ℃ and 85 ℃ at 50% relative humidity; (b) various relative humidities of 30%, 50%, 70% and 90% at 45 ℃ [57]; and (c) Young's modulus and proportional limit stress (Permission from [56], copyright Elsevier).

In general, the water content serves as a plasticizer, reducing the membrane's stiffness, as is shown in Figure 6. The elastic modulus decreases exponentially with increasing water content. However, anomalous behavior is observed between relatively dry membranes and wet ones. With the increasing temperature, the elastic modulus of dry Nafion® membranes showed a faster decrease in a dry state than those with higher water content in Bauer et al. [70] and Li et al. [71]'s tests. Therefore, when the temperature is high enough, the membrane's elastic modulus at 0% RH is lower than that at a certain humidity. This finding corresponds to various membranes in other studies [59, 72, 73]. Taking Nafion® N1110 as an example in Figure 6 (b), the temperature is 60 ℃ at a humidity of 10 % RH and 68 ℃ at a humidity of 95 % RH [74]. Hence, Bauer et al. [70] conclude that water plasticizes membranes at lower temperatures, but that it stiffens the material at higher temperatures. They offer the explanation that higher water content shifts the bonding energy within sulfonic acid groups, thus increasing the glass transition temperature, where ionic clusters of membranes become mobile. Hence, the elastic modulus of dry membrane at higher temperature is lower than that of wet membrane because of the effect of water bonding [75, 76]. Benziger et al. [74] displayed the effect of water on the structure transition by lamellar structure as shown in Figure 7. For dry Nafion, the sulfonic acid head groups and perfluoroether tails have the same projected area, resulting in lamellar packing. However, the water absorbed induces the sulfonic acid groups to a larger effective diameter than the perfluoroether side chain. Increasing the size of the head group causes the packing to curve and form the rod type structure. Hence, water absorption increases the attractive interaction amongst sulfonic acid groups, which connect with mechanical properties.

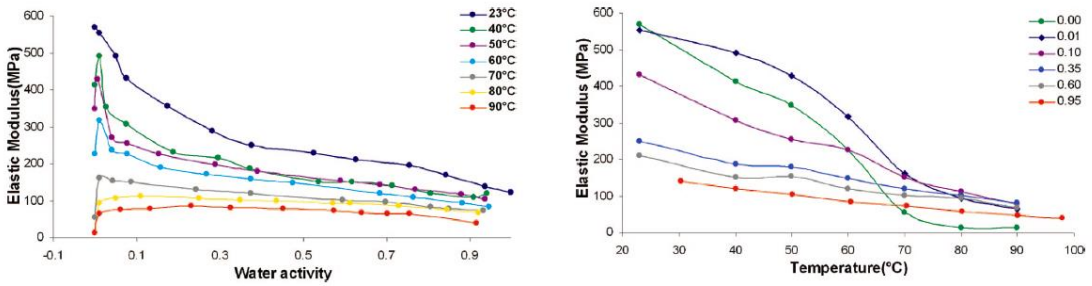

Figure 6. Instantaneous Nafion N1110's elastic response (a) on the basis of water activity at 23-90 °C; and (b) on the basis of temperature for films that is in equilibrium with constant water of 0 %-95% RH (Permission from [74], copyright ACS).

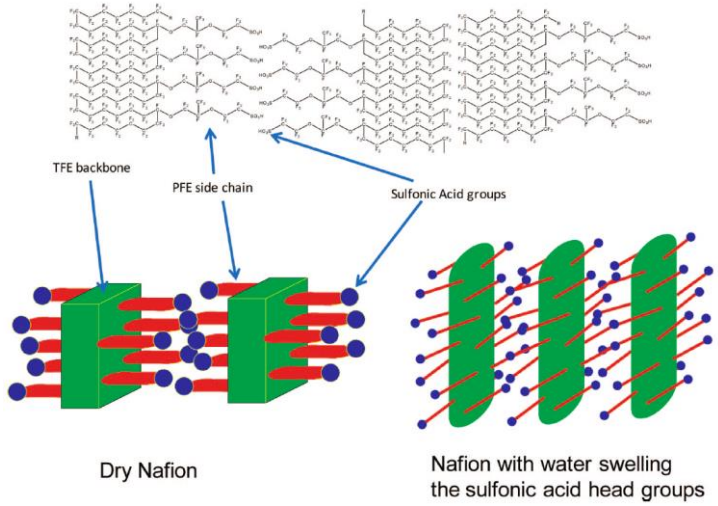

Figure 7. Schematic of the structural transitions in Nafion during water absorption (Permission from [74], copyright ACS).

The time dependence of the material can be explained by free volume theory, which asserts that polymeric chains tend to rearrange themselves into a more compact construction and lower entropy state due to the existence of free volumes [71]. As a result, the material exhibits visco-elastic and visco-plastic stress response with the strain in the testing of Nafion® membranes [77, 78]. Young's modulus and the yield stress become larger and even more obvious than the humidity response, as the stain rate increases [62]. After an aging treatment (temperature and humidity cycling), an apparent decrease can also be observed in the elastic modulus and yield stress. Moreover, the aging of the humidity has a larger influence, as the water cannot be removed through evaporation [79]. Hence, the creep and fatigue phenomenon will contribute to the development of the membrane mechanical failure as important inducing factors when subjected to constant and cycled stress in the cell [80]. Especially with the softening of higher humidity and temperature, the failure resulting from creep and fatigue can be exacerbated. More details about creep and fatigue will be reviewed in section 4.1.1.1.

3.3 Constitutive model

An accurate constitutive model of the material is the basis of the failure analysis and durability prediction of the membrane. For example, it can be incorporated into analytical tools to investigate the stress state histories of the membrane in the complex cell environments, where measurements are not feasible. In general, current models could be classified into two categories: physical model and phenomenological model [81]. The physical model interprets the macro stress-strain behavior based on the micro molecular chains mobility and interchain interaction, which are affected by various parameters such as humidity, temperature and loading rate. The phenomenological model accounts for the mechanical behavior of the polymer by the typical elastic-plastic theory in a linear/nonlinear, viscous/non-viscous way. Compared with the physical model, the phenomenological model is more widely used in the fuel cell by virtue of its convenience and intelligibility in the application.

3.2.1 Physical model

As polymeric material, the properties of the membrane are strongly controlled by the chain architecture. The physical model assumes that the chain segment tends to rearrange themselves into a more relaxed state when the polymer is subject to an external load. In the early phase, the initial physical models were devoted to the equilibrium response of polymeric materials [82-84]. These works accounted for the characteristics of the load-stretch curve in uniaxial tension of the viscous and hyperelastic material, thus failing to describe the constitutive relationship of the material in various deformation states. Arruda and Boyce [85] considered eight orientations of chains in space as shown in Figure 8, and developed eight chain model with two parameters, an initial modulus and a limiting chain extensibility, to represent the three-dimensional state of underlying macromolecular network deformation and its orientation. Eq. (1) shows a compressible version of the eight chain network model [86, 87].

$$\sigma_i = C_R\sqrt{N}\,\frac{(\lambda_i)^2-(\lambda_{chain})^2}{\lambda_{chain}}L^{-1}\left(\frac{\lambda_{chain}}{N}\right)+B\ln(I_3) \tag{1}$$

where

$$\lambda_{chain}=\frac{1}{\sqrt{3}}\left[(\lambda_1)^2+(\lambda_2)^2+(\lambda_3)^2\right]^{1/2} \tag{2}$$

$$I_3=\left(\lambda_1\lambda_2\lambda_3\right)^2 \tag{3}$$

where C_R and $\sqrt{N}$ are the initial modulus and limiting network stretch, and can be established based on a compression or tension experiment. λ_i represents the applied chain stretch. *B* is the bulk modulus, while $L^{-1}(x)$ is the inverse of the Langevin function. This physically based model has been a classic method for exploring the constitutive behavior of the membrane and other

viscoelastic materials.

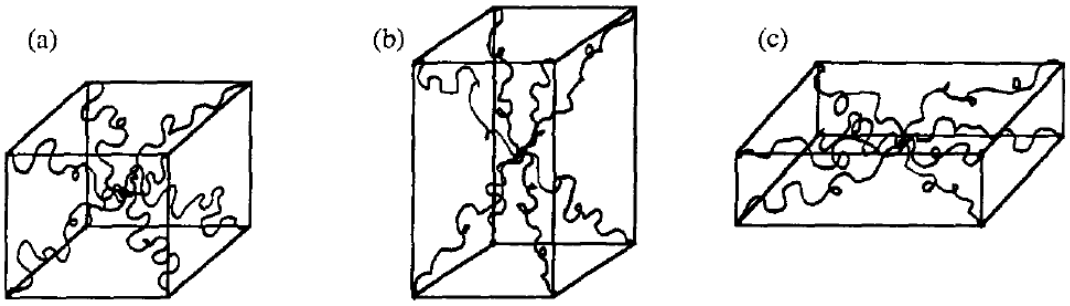

Figure 8. Eight chain elasticity model for (a) undeformed; (b) uniaxial extension; and (c) biaxial extension configurations (Permission from [85], copyright Springer).

Subsequently, Bergström and Boyce [87] expanded the 8-chain model to predict the time-dependent, large strain behavior of the elastomeric material based on the assumption that two networks acting in parallel resulted in the behavior: one network captured the equilibrium state (A) and the second network (B) yielded the time-dependent deviation from the equilibrium. The time-dependent is regarded as having been caused by the reputational motion of molecules with sufficient freedom into strain kinematics framework. In their subsequent work [88], a new constitutive framework that took into account time and temperature-dependent behavior was developed for fluoropolymers, which was referred as a Dual Network Fluoropolymer (DNF) model, as depicted in Figure 9. A visco-plastic response resulted from irreversible molecular chain-sliding and a time-dependent visco-elastic response are decomposed from the material behavior. The visco-elastic response is further decomposed into the viscoelastic response's equilibrium (A) and visco-elastic equilibrium response (B), as above [87]. Accordingly, researchers can change the decomposition results with A and B in different arrangements according to the behaviors of various materials. On the basis of the 8-chain model, the Cauchy stress conducting on network A is provided by the following [88]:

$$T^A = f_{8ch}(F^{ve}) = \frac{\mu_A^0(\theta)}{J^{ve}\overline{\lambda^{ve*}}} \frac{L^{-1}(\overline{\lambda^{ve*}}/\lambda^{lock})}{L^{-1}(1/\lambda^{lock})} dev\left[B^{ve*}\right] + \frac{\kappa^0 \ln\left[J^{ve}-1\right]}{J^{ve}} 1 \tag{4}$$

where $\mu_A^0(\theta)$ represents a temperature-dependent initial shear modulus, while F^{ve} is the visco-elastic deformation gradient. λ^{lock} represents the chain-locking stretch. For network B, its response is regarded as a scalar factor s_B times the eight-chain expression of network A with deformation gradient F^e as:

$$T^B = s_B f_{8ch}(F^e) = s_B \left(\frac{\mu_B^0(\theta)}{J^e \overline{\lambda^{v*}}} \frac{L^{-1}(\overline{\lambda^{e*}}/\lambda^{lock})}{L^{-1}(1/\lambda^{lock})} dev\left[B^{e*}\right] + \frac{\kappa^0 \ln\left[J^e-1\right]}{J^e} 1 \right) \tag{5}$$

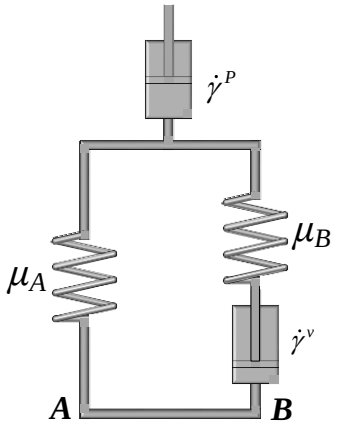

Figure 9. Rheological representation of the constitutive model

Based on previous studies of the polymer, physical models of membranes incorporating cell environments characteristics have been established recently. Boyce et al. [89] developed two models to simulate the monotonic loading behavior and cyclic behavior of Nafion® membranes, respectively, which are in capable of capturing the loading rate, with temperature and hydration dependent on the stress response. Riku and Mimura [90] used Hooke's law and the eight-chain model to express the elastic and plastic strain rates, separately, during the deformation process. Later, Yoon and Huang [78] also introduced hydration-temperature dependence into Bergström and Boyce's model by means of empirical equations to build a nonlinear, viscoelastic-viscoplastic model for the membrane.

Although physical model represents the micro molecular chains mobility and interchain interaction in the membrane, the mechanism of effects of humidity, temperature and loading rate on the molecular chains remains unclear. In these studies, humidity and temperature are assumed to remain constant during the deformation process, which is an idealized scenario. In reality, considering the dynamic hygrothermal conditions in the fuel cell, the membrane is subjected to a unequilibrium state of heat and water [78]. The volumetric expansion and transient temperature and water should be incorporated into the material model as a kinematic description for the membrane due to its time-dependent behavior. The disequilibrium state of the membrane in the fuel cell is believed to be important to the prediction of its stress state and durability. More attention should be paid to the coupled water transport and mechanical deformation models, as well as to the multi-axial stress in constrained membrane.

3.2.2 Phenomenological model

Phenomenological models are developed by fitting the experimental stress-strain response to variable functions without considering the internal micro molecules activation and motion. In the early attempts [55, 91, 92], the isotropic, linear elastic with strain hardening plasticity model was adopted to describe the membrane's behavior. Thermal and hygro expansion were taken into account by linear temperature–moisture superposition principles and hygrothermo-elasticity theory. This type of model has been further used in much recent work [93-95], in which the membrane undergoes

applied stress without time accumulation. In these models, the total strain tensor is decomposed into elastic strain ε_{ij}^{el}, plastic strain ε_{ij}^{pl}, thermal strain ε_{ij}^{th} and swelling strain ε_{ij}^{sw} as follows:

$$\varepsilon_{ij} = \varepsilon_{ij}^{el} + \varepsilon_{ij}^{pl} + \varepsilon_{ij}^{th} + \varepsilon_{ij}^{sw} \tag{6}$$

These elastic strain and plastic region are predicted by the linear Hooke's law and Mises yield criterion (J2-flow theory), respectively [96]:

$$\sigma_{ij} = \frac{E}{(1+\nu)(1-2\nu)}\left[\nu\varepsilon_V^{el} + (1-2\nu)\varepsilon_{ij}^{el}\right] \tag{7}$$

$$f(\sigma_{ij}, \bar{\varepsilon}^{pl}) = \sqrt{\frac{3}{2}S_{ij}S_{ij}} - \sigma^Y(\bar{\varepsilon}^{pl}, \phi_w, T) \tag{8}$$

The thermal strain is given by the linear response:

$$\varepsilon_{ij}^{th} = \alpha(T - T_0)\delta_{ij} \tag{9}$$

By introducing a swelling's anisotropy ratio ξ_i, which meets the condition $\xi_x + \xi_y + \xi_z = 1$, The dimensional changes due to swelling are then:

$$\varepsilon_{ij}^{sw}(i) = \delta_{ij}\xi_i \ln\frac{V}{V_0} = -\delta_{ij}\xi_i \ln\phi_p \tag{10}$$

However, since the ionomers also show strong time-dependent behavior which is also expected in the model, the linear elastic and plastic model cannot fully capture the stress-strain of the membrane in response to sustaining and cylic stress. Hence, the Boltzmann convolution integral was utilized to incorporate the time-varying nature of the material properties [97]. For example, Lai et al. [98, 99] considered the Nafion® membrane as a linear viscoelastic model with the time-temperature-moisture superposition principle on the basis of the fundamental studies of Christensen's viscoelasticity theory [100]:

$$\begin{aligned}\varepsilon_{ij}(\sigma, t, T, \lambda) = {} & \frac{\delta_{ij}}{3}\int_0^t B(t-\omega)\dot{s}(\omega)d\omega + \frac{1}{2}\int_0^t J(t-\omega)\dot{s}_{ij}(\omega)d\omega \\ & + \delta_{ij}\int_0^t \alpha(t-\omega)\dot{T}(\omega)d\omega + \delta_{ij}\int_0^t \beta(t-\omega)\dot{\lambda}(\omega)d\omega\end{aligned} \tag{11}$$

where B and J are the bulk and shear creep compliance; and α and β are the linear coefficients of thermal and hygro expansion. This is also used to describe the the Gore® membrane's mechanical response [101]. For the plastic deformation, Solasi et al. [102] established a two-layer viscoplastic model comprising an elastoplastic model in parallel to a Maxwell elastic-viscous model developed on the basis of the observations of the uniaxial mechanical test from the experiments. The two-layer viscoelastic-plastic constitutive model was further modified by incorporating a strain-rate dependence and determining the time, temperature and humidity-dependent parameters according to experimental data for Nafion® 211 membrane in Khattra et al. [77]'s work. In order to describe the stress–true strain behavior with single equation, Kusoglu et al [56] modified a version of G'Sell and Jonas' constitutive equation, which captured the viscoelasticity and viscoplasticity behaviors of

polyvinyl chloride and high density polyethylene, and showed more information on how humidity and orientation acted on the membrane behavior. Due to its convenience, the phenomenological model has been more adopted in contemporary studies [103, 104].

However, the above models are built based on the material linear behavior, which often fails when either a large deformation (>10%) or long-term behavior is needed. Time–temperature–moisture superposition and pure Boltzmann theory cannot account for nonlinear behavior. The nonlinear effect of the material may arise from the interaction changes and conformation changes of the polymer chains, such as the chain splitting and the space decrease between the chains. This complex behavior is usually approached by empirical [105] or semi-empirical methods [106] using numerous fitting parameters. In order to investigate the purely nonlinear modelling, May et al. [81] captured nonlinear a viscoelastic response of the membrane with the constitutive form suggested by Schapery's constitutive formulation [107], a nonlinear extended integral expression of the Boltzmann convolution. The nonlinear viscoelastic constitutive model is:

$$\varepsilon^{NLVE}(t) = g_0(t)D_0\sigma(t) + g_1(t)\int_0^t \Delta D(\varphi(t)-\varphi(\tau))\frac{dg_2(\tau)\sigma(\tau)}{d\tau}d\tau \tag{12}$$

where D_0 and ΔD are, respectively, creep compliance's linear elastic and time-dependent elements. g governs the nonlinear elastic response.

The viscoplastic term can be described by the Zapas–Crissman viscoplastic equation [108] or Tobolsky and Eyring equation [109] as:

$$\varepsilon^{VP.ZC}(t) = \left[C\int_0^t \sigma(\tau)^p d\tau\right]^q \tag{13}$$

$$\varepsilon^{VP.TE}(t) = \left[C\int_0^t \sigma(\tau) d\tau\right]^q \tag{14}$$

where C, p and q are fitting coefficients. Uniaxial recovery and creep experiments can be conducted to fit the coefficients of the nonlinear viscoplastic and viscoelastic models. Burlatsky et al. [110] modeled the nonlinear response of the stress to applied strain by extended Eyring model, which assumed polymer deformation as a motion of polymer chain segments that overcome potential barriers at the entanglement points.

However, the membrane in the fuel cell is highly constrained in a biaxial configuration, in which the in-plane directions are constrained and the thickness direction is free. Feasibility and accuracy of the current constitutive model based on uniaxial tension have not been validated. Moreover, the hygrothermal conditions are coupled and transient during the fuel cell operation. Incorporating varying operation parameters is still needed to improve the model. In addition, although there have been several studies of the failure process [110-112], the failure criteria of this material, such as initiation and evolution of pinholes, tears and delaminations, has not drawn enough attention, especially given the cyclic humidity and temperature. Deficiency of the failure criteria

leads to barriers to quantitative understanding of the failure mechanism and predicting the durability of the membrane.

4. Mechanical failure and mitigation strategies for the membrane

4.1 Membrane defects during the fabrication process

4.1.1 Membrane defects

It is well known that the inherent defects of the membrane significantly contribute to mechanical failure regardless of the cell lifespan process. According to Bender et al.'s [113] in-situ accelerated stress test (AST) of the fuel cell, the circumference of the defect was the most prominent location with degradation of the MEA. The tear energy of the membrane would be sharply reduced by the existence of flaw features, which underpin fracture propagation [68]. Various factors influences membrane quality during the fabrication process. These undesirable defects at the micro scale are difficult to distinguish with the naked eye and induce local weakness of mechanical resistance. To improve the membrane's durability, it is necessary to explore what the problematic features are.

In Kundu et al.'s [34] research, six morphological anomalies, namely cracks, thickness variations, delamination, catalyst orientation, electrolyte clusters and platinum clusters, were observed on the catalyst coated membrane (CCM)with Nafion® 112 as the electrolyte and carbon-supported platinum as the catalyst as shown in Figure 10. Cracking is caused by the breaking of the CL in thin region because of solvent vaporization from the inner mixing catalyst powder to the top layer during the fabrication process and the bending and stretching of the MEA in the assembly and application processes. The cracking of CL induces a concentered force on the membrane, which may accelerate the membrane cracking [114, 115]. Thickness variation is generated in the course of membrane manufacturing or the large catalyst agglomerates in the catalyst ink. The delamination causes an interval between the membrane and catalyst due to the uneven catalyst casting, local surplus solvent and a flaw in the freeze-fracturing process [34]. The uneven catalyst features of orientation, electrolyte clusters and catalyst clusters should be concerned in the catalyst particles, the mixing of catalyst ink, and slurry spreading under the force of equipment. These defects lead to a weakness in mechanical strength, contact resistance, and the inhomogeneity of reaction efficiency, the flooded area, heat generation and catalyst erosion, thus increasing the degradation speed of the membrane. The propagation of defects is also influenced by the fuel cell's operating conditions. Experimental testing shows that the fuel cell's polarization curves with a pinhole in the membrane are not significantly degraded in reactant gases of 0.1 MPa operation, but obviously decline in larger gas pressure conditions [106].

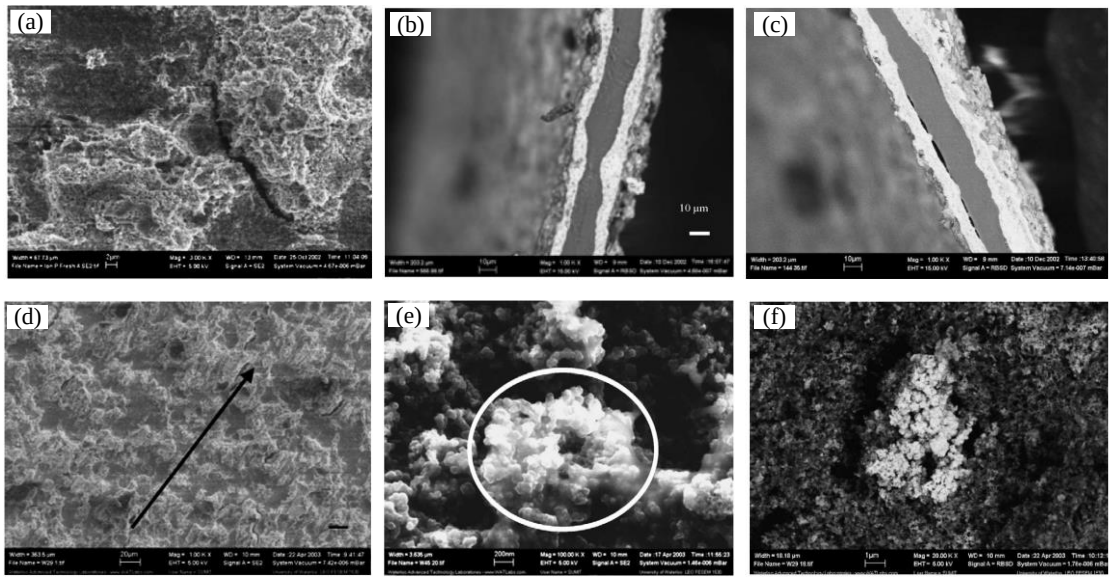

Figure 10. Typical defects of membrane: (a) cracks; (b) thickness variations; (c) delamination; (d) catalyst orientation; (e) electrolyte clusters; and (f) platinum clusters (Permission from [34], copyright Elsvier)

Although the high sensitivity of defects area to mechanical degradation is accepted by the researchers, there is little literature that addresses the impacting mechanism and developmental process of defects. This could be due to the difficulty in the observation by experiment and kinematics analysis by modeling. Patankar et al. [69] built knife-slit testing equipment to measure the fracture energies of membranes used with minimum cracks. A significant decrease in fracture energy was caused by the plastic zone before the crack tip. Due to the presence of sharp defects, the membrane's facture energy was shown to be two orders of magnitudes smaller than that of high-quality membrane [116]. This provides macroscopic evidence that defects are the weak spots in the membrane. To simulate the craze formation under hygrothermal fatigue, Kusoglu et al. [25] developed a numerical model by considering the crazing criterion and growth process as the precursor to crack propagation. Elastic-plastic properties were used to reflect the overall response of the membrane, although crazes emerge in special regions with pinholes, crack-tips and surface defects. This concept of the overall response of the membrane based on damage accrual model was also adopted in Burlatsky et al.'s [110] study. Studying mechanical failure through the overall and equivalent response of the membrane provides an easier way to conduct the analysis. In reality, weak mechanical strength is likely to exist around the defect region of the membrane. Concentrated force is drawn under the hygrothermal stress. However, the local failure resulting from micro defects has been underestimated in current studies. The relationship between defects and occurrence of membrane damage remains unclear. Novel in-situ techniques of detecting the failure process from defects are still lacking. To better evaluate mechanical failure, the effect of membrane defects on the damage evolution must be evaluated in greater detail.

4.1.2 Mitigation strategies

Improving the fabrication process is important to increase the membrane quality. Membranes reinforced by PTFE have be demonstrated to have higher resistance to mechanical degradation. Experiments have shown that the lifetime of Gore-Select® membranes with reinforced e-PTFE exhibits an order of magnitude longer lifetime than un-reinforced membranes of similar thickness [5]. Tang et al. [117] converted the Nafion ionomers into the Na+ form by fixing the PTFE frame micropores and then heat treated the material at 270 °C to improve the membrane durability. The introduction to the membrane of an inorganic material can change its chemical and mechanical properties of interest, such as working temperature, proton conductivity, mechanical strength and response to water content [60, 118]. Hence, much work have been dedicated to developing the composite membrane with SiO_2 [119], ZO_2 [120], TiO_2 [121], graphene oxide (GO) [122, 123], zirconium phosphate (ZP) [124], etc. For example, Nafion/TiO_2 composite membrane in Satterfield et al. [60]'s work shows better mechanical durability, which exhibits a lower decrease in elastic modulus when subjected to water and a 40% drop in creep at 25 ℃ and 100% RH compared with pure Nafion. Higher elastic modulus and yield stress are also obtained in H_3PO_4/Nafion–PBI membrane (20 wt.% Nafion and 80 wt.% PBI, immersing in 85% H_3PO_4 at 60 °C for 60 min) [125]. However, little concrete rules are discerned in the mechanism of these improvements. The direct connection between additive material and the mechanical properties in membranes has not been revealed in current studies.

A greater thickness can increase the durability of the membrane, but reduce the proton conductivity. The H_2 and O_2 crossover rates will decrease with an increase in membrane thickness [126]. Yuan et al. 's [14] accelerated test on a four-cell stack with Nafion® membranes (N117, N115, NR212, and NR211) of different thicknesses under idle conditions shows that the fuel cell with a thinner membrane (NR211) has a lower open circuit voltage (OCV) because of the greater hydrogen crossover, but outputs best performance before degradation. The cell with greater thickness (N117) features a much lower degradation rate throughout the test ($0.09 mV h^{-1}$), compared to that with NR211 ($0.26 mV h^{-1}$).

Good initial contact between the membrane and CL is helpful for improving cell performance and reducing mechanical degradation. In order to flatten the membrane's surface, ion beam morphology is used before being coated [127] and the interfacial structure between the membrane and catalyst layer seems to be more flat. Hot pressing process on CCM is also helpful for improving contact between the membrane and electrodes. Although there are some concerns about a possible decrease in porosity after pressing, the contributions of this procedure to performance and durability are still proven [128]. The membrane with hot-pressing showed smaller ionomer layers thinning, better cell performance and much lower degradation after AST in Wu et al.'s study [26]. The thinning of membranes with hot-pressing is not much severe compared to membranes without hot-

pressing, which was thinned to about 1 μm at the ionomer of the cathode side.

The introduction of a diffusion media (DM) between CCM and gas diffusion layer (GDL) has been proven to moderate membrane degradation. In the operating fuel cell, a static friction force generated between membrane and DM can prevent wrinkling and buckling of the membrane caused by hygrothermal conditions [129]. It provides the barrier to membrane expansion and excess water intrusion, which is also helpful in the freeze/thaw cycling conditions [31].

4.2 Mechanical failure during the assembly process

After a membrane with coated catalyst is fabricated, it is inserted between the GDLs to form a five-layer MEA, which are in turn bonded together by the surrounding MEA frame. Then, the MEAs, BPPs and sealants are clamped together by the endplate as a fuel cell stack. Although the membrane is difficult to damage through the compression, uneven contact pressure between the ribs of the flow field and GDL will induce bending and shear stress on the MEA, contributing to wrinkle of membrane and delamination between the membrane and CL [130]. Uchiyama et al. [129] reported that the membrane would be in severe wrinkle deformation after humidity cycles if the fastening force from the BPP is not enough to constraint the membrane. Furthermore, the non-uniform pressure plays a significant role in the distribution of current density and temperature in the anaphase operation of the fuel cell, and accelerates the deterioration of the membrane [131].

Although the adverse effect resulted from the lacking assembly process has been demonstrated, a quantitative relationship between the fuel cell assembly and membrane lifetime has not been directly revealed in many studies due to the invisible behavior in the stack and combined influence of the following operating conditions. This part mainly reviews studies of the membrane mechanical response during the assembly process, which is significantly affected by process parameters, manufacturing error and bonding by the MEA frame.

4.2.1 Effect of the assembly process

4.2.1.1 Geometric structure of components

Under the assembly force/displacement, the MEA is compressed by ribs of the BPP. The geometry structure of ribs plays an important role in the pressure distribution. As is shown in Figure 11 (a), the rib/channel is usually in a regular rectangle or trapezoid shape with minor round corners, which induces a pressure concentration at the interface. The contact pressure at the round corner of 0.02 mm is more than twice that under the rib [132]. According to Tang et al. [133], the shear pressure in the membrane has the highest value along the corner when the temperature and RH of the cell change. Moreover, the concentrated pressure is notably increased as the round corner decreases [134]. Salaberri et al. [132] used a FE model to compare three different values of the corner radius: 40, 80 and 160 mm by the same GDL intrusion. Reducing the round corner made the first point of contact surface move forward to the channel and also significantly increased the contact pressure peak.

The membrane close to round corner of ribs is vulnerable to intense physical and chemical damage. Hottinen et al. [135] reported that a current density peak in this region (Figure 11(b)) was caused by the lowest contact resistance and converged current flow produced below the channel. This phenomenon was also found in Su et al.'s [136] study. For the cell suffered temperature cycling, a line crack in CCM was first observed along the round corner interface as shown in Figure 11 (c) [31]. When the temperature decreased as low as −40 ℃, a worse crack occurred under the round corner and middle channel. This is caused by the abominable working conditions around the corner region during fuel cell operation, such as the concentration of pressure, current density, heat and water. Hence, the round corner region is susceptible to the cell environment, and more attention should be paid to its geometric structure during the BPP design.

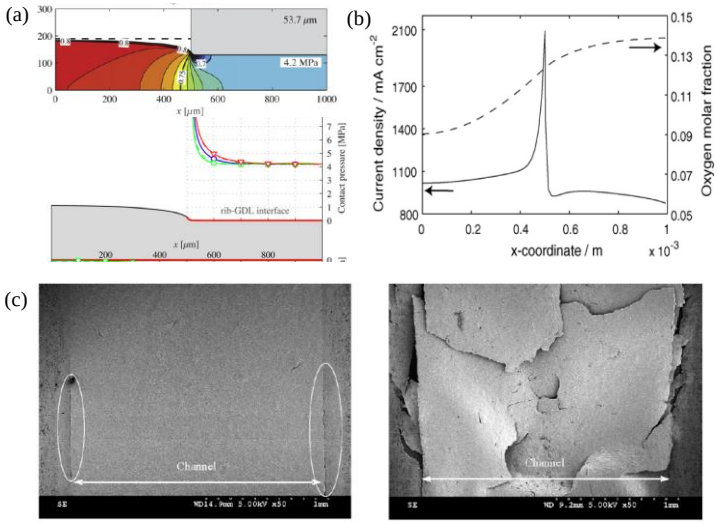

Figure 11. (a) Contact pressure distribution at the rib/MEA interface [132]; (b) oxygen molar fraction and distribution of current density between electrode and GDL at 0.4V [135]; (c) surface images of CCM under the channel locations without DM under thermal cycling of 5 ℃/70 ℃ and −40 ℃/70 ℃ (Permission from [31], copyright Elsvier).

In addition to the round corner, the ratio of the channel to the land is also an important factor in membrane damage. Due to the spaced constraint under the ribs of the flow field, clearance between the CCM and GDL is unavoidable even if the compression is large enough after the fuel cell assembly. It provides the space for the membrane deformation. Reducing the channel width could lower the clearance, thus slowing down the wrinkle of membrane and membrane/CL delamination. Uchiyama et al. [137-139] reported that a narrow channel was useful for constraining the swelling of membrane by transmitting contact pressure from the GDL to CCM. The rib with a larger width can also improve membrane resistance to mechanical degradation in freeze/thaw conditions, but too wide a rib results in a dead region in the middle of the rib and more flooding, which accelerate the crack formation as a result of ice expansion [31].

4.2.1.2 Endplate deformation

A typical fuel cell stack is composed of many single cells, which are usually clamped by endplate with bolts. The bending of the endplate under the bolts torque make an important influence to the uneven contact pressure distribution. The compression pressure in the central area of the membrane is smaller than that of the margin area, thus inducing membrane stretch. According to Kusoglu et al. [140], plastic deformation is likely to occur in the membrane under the excessive stress. It is considered as an important contributor to the mechanical failure of the membrane. In order to reduce the bending of the endplate, Liu et al. [141] developed a robust design method of bolts position and assembly pressure based on response surface methodology (RSM). Lin et al. [142] optimized the structure of the endplate to reduce the weight and increase the stiffness through topology optimization based on a FE model. Wang et al. [143], Karvonen et al. [144] and Yu et al. [145] have also proposed some novels endplate designs such as pre-curvature endplate and ribbed endplate . All of these studies improved the contact pressure distribution in the stack by optimizing the loading method of the assembly force or increasing the endplate stiffness.

4.2.1.3 Assembly force/displacement

In the assembly process, the contact pressure changes in accordance with the alteration of assembly force/displacement fastened by the endplate, causing variation in the mass, heat, and charge transfer during cell operation [146]. Proper assembly force/displacement is also critical to preventing leakage and reducing the ohmic loss. However, the excessive assembly force/displacement results in physical damage and hostile working conditions to components [147]. Zhou et al. [148] reported that too much assembly force led to a lower current density on the CL surface due to the increasing resistance of oxygen diffusion, with the current density distribution becoming slightly more non-uniform. A higher water saturation may exist on the membrane when higher compression is adopted [149].

To obtain a better assembly design, experiments [150-152] and finite element (FE) models [148, 153-155] have been widely used in most efforts. The assembly force of around 1.0 MPa is suggested as the optimal choice in the fuel cell stack. However, experiments cost too much time and money, and FE simulations are mostly carried out by 2D models because of the huge computation necessary for ideal 3D models with multi-scale structures and complicated contact behaviors to be achieved. In recent years, more effective theoretical models are developed to investigate the design of assembly force/displacement [156-158]. In Peng et al. [159, 160], a design methodology was developed for the entire fuel cell on the basis of the continuous equivalent model and optimization methods to balance the total electrical resistance and gas transfer. In general, these studies focus on the effect of assembly force/displacement on output performance at the beginning of the cell's operation. The mechanical durability change resulted from various assembly force/displacement in the long time operation has not yet proposed in literatures. For example, water saturation and local hot spots occur in the membrane if the cell is not assembled well.

4.2.2 Effect of manufacturing error

As is mentioned above, a uniform distribution of contact pressure is necessary during the fuel cell assembly. It requires a high degree of fabrication accuracy for the components. However, manufacturing error is avoidable in the forming process, especially for the fuel cell with metallic BPPs, which are considered as promising candidates of conventional graphite BPPs by virtue of good mechanical strength, electrical and thermal conductivity, and low cost in mass production [161]. As the component with maximum stiffness in the cell, the manufacturing error of metallic BPPs plays a significant role in the assembly quality of the stack. In terms of the deficiency of the fabrication, the effects of shape error, dimensional error and assembly error, as shown in Figure 12, are reviewed in this section.

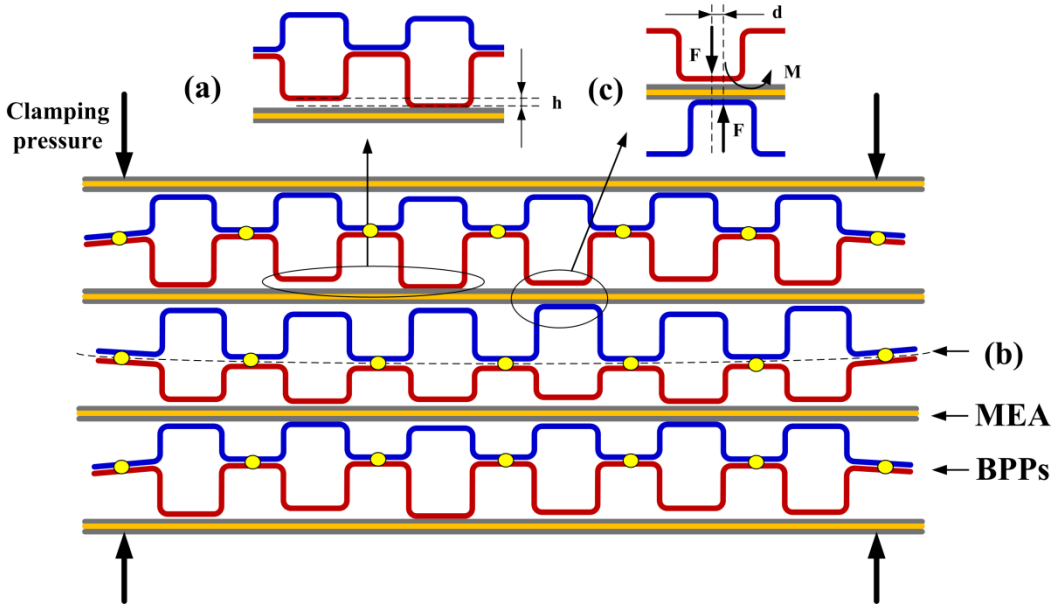

Figure 12. Schematic of PEM fuel cell stack metallic BPPs' (a) dimensional error; (b) shape error; and (c) assembly error (Permission from [162], copyright Elsvier)

4.2.2.1 Dimensional error

The dimensional error is defined as the deviation from the ideal dimensions of structures in the fuel cell. For BPPs, due to the intrinsic material springback and localized non-uniform forming force, the dimensional error of channel heights is avoidable on the formed metallic BPPs as shown in Figure 12 (a). The maximum variations of 4.1 % and 1.3% in 26-parallel channel heights were captured on stamped and hydroformed metallic BPPs, respectively [163]. In our previous study [164], a linear decrease in channel heights was also found from the border position to center position of the stamped BPP. The largest dimensional error reached up to 30 μm on the channels of designed height with 0.40 mm. In recent years, the influence of dimensional error of BPPs has drawn some attention. Turan et al.'s [165] experiments showed that stamped BPP samples generated higher interfacial contact resistance than hydroformed BPPs because of severe dimensional error and

surface condition. In order to investigate the effect of accumulated dimensional error in the multi-cell stack, several studies have been conducted by the authors [159, 164, 166]. It was found that dimensional error led to not only a non-uniform pressure distribution on MEA for the in-plane direction, but also a pressure change in the adjacent cells for the through-plane direction. A more obvious pressure variation was noted in the first several cells next to the endplate, which was termed as "edge effect". In order to improve the consistency in each cell of the stack, the maximum allowed dimensional tolerance was suggested as 0.4 ± 0.015 mm [167]. The effect of channel height non-uniformity on the performance of the fuel cell was investigated by Shimpalee et al. [168], who found that a larger dimensional error created a higher gas pressure drop and non-uniform current distribution, which led to worse working conditions on membrane.

For GDLs, the dimensional error mainly results from the thickness variation. Although little effect was found on contact pressure in the membrane because of lower compression stiffness of the GDLs [167], the dimensional error in GDL thickness provided clearance between the GDL and CCM . As a result, more severe wrinkles in the membrane and delamination between the membrane and CL are generated when subjected to hygrothermal conditions. Worst of all, the hackly GDL cannot support CL and is likely to intrude on the soft PEM, resulting in pinholes or tears in the material [169].

4.2.2.2 Shape error

The shape error of the BPP, warpage deformation of the frame, is caused by residual stress after the forming process and heat stress during the welding process [170]. During the forming process, elastic deformation gives rise to the springback of the metallic sheet to balance the residual stress status after the forming force is removed. The fabricated single plates with rough shape are then bonded together by means of a laser welding process with a high heat source, resulting in a worse BPP shape due to thermal distortion. Yi et al. [171] proposed an numerical model to predict the shape error of BPP by combining transverse and angular distortion based on inherent strain theory. Shape deformation of 3.20 mm was obtained even using improved fabrication process. In Qiu et al.'s [170] clamping experiments, the center of the MEA tended to be unloaded if BPPs with shape error were assembled in fuel cell, whereas the assembly force centralized on the peripheral part of the MEA. This serious uneven pressure distribution is unacceptable for fuel cell operation, bringing about the uneven distribution of reactant gases, contact resistance and heat generation. The membrane in the peripheral part of MEA is subjected to more intense stretch and chemical reaction. However, the parts in the central position are easier to swell because of the insufficient constraint. In order to reduce the shape error's influence, the largest acceptable shape error was suggested as 1.52 mm for the BPPs [170].

4.2.2.3 Assembly error

The high performance and long durability of the fuel cell require a highly accurate stack

assembly. Otherwise, the assembly error, deficient alignment of the cell components, will lead to assembly force being asymmetrically transmitted and in turn bring an additional moment to the MEA, which generates stress concentrations and seriously deforms the MEA [172]. The error is apt to be enlarged in ambient vibration during the fuel cell operation, especially with the transport application.

Tang et al. [92] compared in-plane, through-plane and shear stress in the membrane by two fuel cell models in which the upper and lower channels were aligned or misplaced. The simulation showed that misplaced gas channels produced much larger hygrothermal stresses than aligned channels, especially for in-plane stress and shear stress. Banan et al. [104] reported that assembly error led to an increase in the delamination propagation rate between the PEM and CL. A delamination of 0.10 mm long was reached after 1.41 $\times 10^4$ humidity cycles when the anode/cathode channel offset was 0.1 mm, which was much faster than 3.47 $\times 10^4$ humidity cycles for the aligned channels. Thus, the assembly error should be reduced to as small a size as possible to improve the operated fuel cell's stability.

However, it should be noted that the assembly error is still inevitable given the current manual assembly process. A more practical alternative is to reduce the assembly error within a certain range by fixing the fuel cell components. Liu et al. [172] developed a method on the basis of the least squares-support vector machine (LS-SVM) to investigate the assembly error effect on the MEA's pressure distribution and stress failure. The statistical results indicated that the failure probability increased quickly with increasing assembly error. The maximum allowed assembly tolerances for the three-cell configuration were obtained at 0±0.15, 0±0.12 and 0±0.111 mm based on the "Six Sigma" theory.

4.2.3 Effect of bonding by the MEA frame

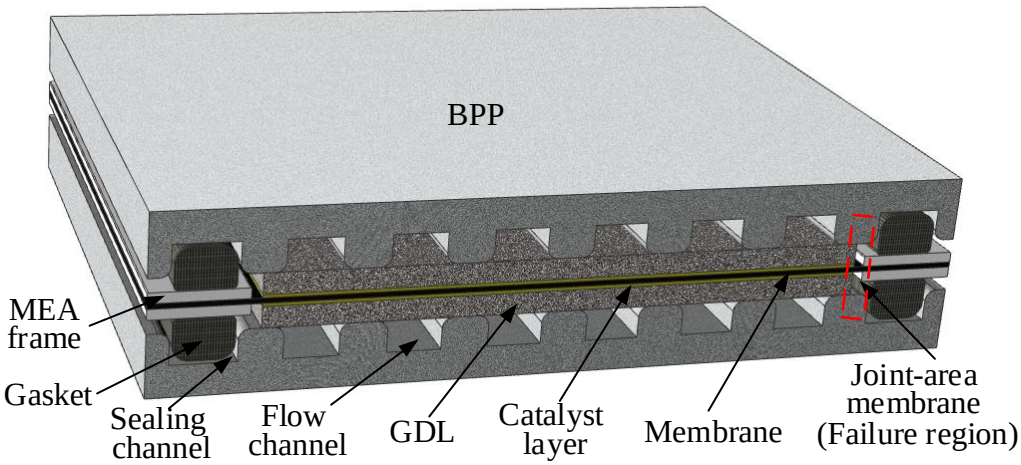

Figure. 13 Schematic drawing of the joint-area membrane in the PEM fuel cell (Permission from [173], copyright Elsvier)

As shown in Figure. 13, in practice, the frame of the MEA is needed to unite the five-layer MEA into one component. It is usually made of a polymer material, macromolecular material, composite material or rubber material that seals and insulates the adjacent cells. Various material properties of MEA components may cause stress concentration problems at the joint area between the frame and membrane. Ye et al. [130] investigated effects of the frame material and frame structure on mechanical stress in the membrane during the fuel cell assembly procedure. They found that the shear stress at the frame/membrane joint area increased with the softening of the frame. Due to the constraint the frame imposed, the tensile strain in the membrane around the joint area is much bigger than that of the central region. A peak strain of 2.675% was also found near the corner of the frame in Huang et al.'[55] study. Bograchev et al. [174] simulated the stress and plastic deformation of the MEA during cell assembly. A peak of shear and normal stress/strain was then observed under the frame/membrane joint area. This is possibly caused by the bending of the components (frame and BPP) under compression and the stiffness differences between the frame and GDL [173]. Plasticity may occur in the connection zone of the membrane if the bolt torque of stack is large enough. Hence, the zone around the frame/membrane's joint area is primarily sensitive to failure during fuel cell assembly.

4.2.4 Mitigation strategies

According to previous research, it can be seen that although the possibility of direct membrane mechanical failure is relatively small during the assembly process, improper assembly can reduce the membrane's mechanical reliability and increase the degradation rate in the following operation procedure. The stack's uniform pressure distribution in is beneficial to the durability of the membrane and performance of the fuel cell.

To prevent the bending of the endplate, many novel designs were proposed in patents that were carefully reviewed by Kim et al. [175]. Fundamentally, these designs fall into two forms: a) those which improve the flexural stiffness of endplates [176]; and (b) those that change loading methods such as applying force by bands [143, 177]. For the flow field, reducing the channel width and increasing the round corner size contribute to the constraint and pressure uniformity in the membrane, although they may increase the ohmic loss in the fuel cell [178]. In order to reduce the adverse effects from the manufacturing error, the accuracy of the components can be improved by optimizing the forming parameters and selecting a preferable forming process. For example, the hydroforming process is considered an effective method to reduce manufacturing error for metallic BPPs instead of stamping process [162]. For the MEA frame, material with mechanical characters close to the membrane is preferred in order to generate less stress concentration at the joint area [130]. All of these strategies intend to minimize/avoid the non-uniform stress distribution that can result in a higher degradation rate of the membrane.

4.3 Mechanical failure during the short-term operation phase

Once the assembled cell stack commences operation, the PEM is exposed to the varying operating conditions, such as humidity, temperature variation and the filling of reactant gases. Not only are the material properties of the membrane sensitive to the operating conditions, but also the external stress and deformation of the membrane would drastically change due to water sorption and the thermal effect. In extreme freeze-thaw conditions, the failure speed will be accelerated quickly by the thermal effect and freezing of residual water from the last operation [31, 179, 180]. On the other hand, as a constrained part, the mechanical connections with the MEA frame are a relatively weak region to suffer the ordeal under the operational conditions. Hence, mechanical failure during the short-term operation stage is a common mode during operation of the fuel cell [26, 130, 181]. A number of studies related to mechanical failure during this period are available in the literature.

4.3.1 Effect of humidity and temperature

4.3.1.1 Basic requirement by transport function

In the running fuel cell, the cyclic humidity and temperature are unavoidable for the real working environment. PEM serves as a transportation medium for protons between the anode and cathode side, while preventing gases mixing and electric conductivity. During the electrochemical reaction, water is absorbed by the hydrophilic membrane to ionize acid groups and serves to transport the of protons [182, 183]. On the molecular level, the produced proton transport in the anode is described by two principle mechanism: hopping from the hydrolyzed ionic site ($SO_3^{-1}\,H_3O^+$) to the next one or diffusing in the manner of hydrated proton (H_3O^+) by electroosmotic drag and concentration gradients across the membrane, namely “proton hopping” and “diffusion mechanism”, respectively [37]. Hence, proper RH is necessary for proton conduction. It is reported that the conductivity of dry membranes is significantly lower than that of a completely saturated membrane [60]. Moreover, hydration of the polymer electrolyte is strongly dependent on the thermal effect because of the water vapor saturation pressure increasing exponentially with temperature [184]. Hence, proper humidity and temperature are essential for proton conductivity and fuel cell’s high performance.

Nevertheless, too much water gives rise to flooding and blocking of gas transfer. A high fuel cell temperature above 80 ℃ increases the vapor pressure resulting in water loss and high proton resistivity, while too low a temperature causes water condensation and electrode flooding [185-187]. It is reported that catalytic activity becomes higher as RH increases in the range of 0-60%, while a further enhancement of RH above 60% does not contribute to the catalytic activity [188-190]. In addition, the membrane failure is intensified by the unfavorable hygrothermal conditions during cell operation. Chen and Fuller [191] showed that a decrease in humidity increased the side chain scission process, generating massive weak end groups and driving degradation. In Ballard Power

Systems's [8] comparisons of fuel cell operation under various humidity conditions, the gas crossover (>10 cm^3/min at 2 bar pressure differential) resulted from a pinhole in the membrane that occurred after the lifetime test of less than 200 h with dry reactant gases, which was much faster than any other conditions (3200 h @ 100% anode and 70% cathode, 1100 h @ 100% anode and 0% cathode, and 550 h @ 0% anode and 100% cathode).

4.3.1.2 Mechanical behavior of the constrained membrane

During fuel cell operation, humidity and temperature play a dominant role in the mechanical deformation of the PEM. In reality, water exists as a product of internal electrochemical reaction and the introduction of external humidified reactant gases. Higher RH and temperature levels lead to varying memebranes' mechanical properties, as well as in-plane compression and swelling in the membrane. The in-plane stress was found to be the dominant stress factor in the membrane in Tang et al.'s [92, 192] simulation where the membrane was assumed to be in linear elastic material, followed by shear stress and out-plane stress. The maximum measured in-plane stress lay in the part of membrane along the mid-channel. Subsequently, Kusoglu et al. [91] incorporated the plastic material behavior in the FE model, and found that plastic deformation might occur in the membrane during fuel cell operation, causing residual tensile stresses after unloading. The accumulation of residual in-plane stresses may explain the initiation and propagation of cracks or pinholes through the defect in the membrane after short-term operation. Substantial in-plane plastic strain in the membrane above 0.1 was also found in Khorasany et al. [193] and Verma et al.'s [194] simulation cells. Solasi et al. [58] made further improvements to the material behavior with a non-linear visco-plastic model in the FE analysis to describe mechanical response of ionomer membranes. Hydration is confirmed to have a more significant influence than the temperature in generating mechanical stresses within the membrane. Shear effect is also found in the in-plane of the membrane due to the non-uniformity constraint configuration of the cell. Especially when there is a defect in the membrane, the shear stress may exceed the ultimate capacity of the material.

In fact, the distribution of humidity and temperature is not uniform in the real fuel cell, and is proved to have a negative effect on the membrane's durability. Maher et al. [195, 196] reported that the temperature gradient induced non-uniform distribution of the strain, resulting in localized bending of the membrane. This bending behavior can be intensified by the moisture change and contributes to the delaminating between PEM and CL, as well as that between the CCM and GDL. This phenomenon is in accordance with Kusoglu et al.'s [140] membranes under a humidity gradient between the anode (30% RH) and cathode (95% RH). They found that the gradient loading would result in higher stress levels than those of uniform humidity on the cathode side, while the stress was very small on the anode side. However, it was found that the anisotropy of swelling property in the material was helpful for reducing the in-plane stress amplitude. For fully anisotropic swelling, the in-plane stress of membrane remained compressive. These results indicate that optimizing a

membrane with respect to the swelling anisotropy is a possible means of improving the membrane durability.

4.3.2 Mechanical degradation during the freeze–thaw process

PEM fuel cells become stable during operation at temperatures between 60 ℃ and 80 ℃. However, they are subjected to subfreezing operation or start-up from subfreezing temperature in some applications, such as in fuel cell vehicles. Therefore, fuel cell must be able to run smoothly in low-temperature environments. The potential problems, including freezing survivability, fast start-up and durability, are the primary challenges arising from the tough working requirements. As the ultimate criterion from the DOE [4], the unassisted startup of a fuel cell should be achieved at a temperature as low as -30 ℃ and takes less than 5 seconds with the consumption of < 5 MJ of energy to finish 50% of the rated power from a -20 ℃ ambient temperature. For the membrane, previous studies have regarded its mechanical damage as one of main problem because of the thermal effect and freezing of residual water from last operation [179, 197]. This mode of failure is rapid in the cycling of freeze-thaw operation. In this section, the effect of subfreezing temperatures on the membrane and start-up from freezing temperatures are presented to illustrate mechanical degradation resulting from subfreezing operation.

4.3.2.1 Subfreezing temperature conditions

The effect of a subfreezing environment on the membrane's properties is of great interest for understanding the mechanical durability during the freezing operation. However, only few studies evaluate the effect of mal-conditions on its mechanical properties. McDonald et al.[198] exposed Nafion® 112 membranes to 385 cycles between –40 ℃ and +80 ℃ in a dry state. UTS and the final strain showed an obvious decrease in both the machine direction and cross direction of the material, especially the final elongation at the break, which was reduced by over one order of the magnitude. Although no sign of increased order or disorder at molecular level was found in the tested membrane by X-ray diffraction scans, they kept the speculation that a decrease of chain entanglement and dispersion of sulfonic acid-containing hydrophilic area happened during the freeze/thaw, which induced an opening up of molecular structure, thus reducing the material strength and toughness. Furthermore, water swelling behavior and oxygen permeability were also demonstrated to be on the decrease.

In terms of the literature reviewed, research on the membrane's mechanical properties is fairly limited in this severe environment. In fact, water molecules existing in/on the membrane can be characterized in different states, including non-freezing, freezing bund and free water [199], associated with thermodynamic activity and a polymer matrix. The temperature at which water freezes is determined by the pore size which traps the water and the material properties. Non-freezing water would not crystalize since it is highly polarized in hydration shells. The free water will freeze as bulk water at sub-zero temperature [200], while the bound water trapped in the

polymer chain exhibited no apparent phase transition between −73 and 0 °C and remains in the non-frozen state, due to the strong interaction with the polymer [201]. The mechanism of proton conductivity in the freeze/thaw conditions has drawn much attention [199, 201-203]. However, the change of the membrane mechanical property in the freezing environment still need to be investigated in greater details, such as the effect of the water content and state on the material.

4.3.2.2 Start-up at subfreezing temperature

Another issue of concern is the degradation of the fuel cell's start-up from such a cold environment. Although some earlier literature indicated that little degradation was caused in this process [204, 205], significant physical damage and performance degradation were demonstrated in many recent achievements. Focusing on the mechanical damage of the membrane, cracks [31, 179, 206] and delamination from CL [31, 207, 208] are the common modes.

In the ordinary start-up above freezing point, moderate residual water from the last run is beneficial to proton conductivity and activation of the fuel cell. However, when the cell is shutdown in subfreezing temperature, the remaining water in the cell turns to solid ice with a volume expansion of 9%, resulting in the porosity change of the material, a loss of the catalyst area and structural damage to the components. It has been found that the stack with freeze/thaw cycling has little degradation when it is dried out after previous shutdowns, while severely degrading in the wet state [209]. Hence, the water content plays vital role in the degradation of fuel cell at sub-zero temperature. Cho et al. [197] examined the fuel cell in the environment chamber with 10 humidified reactant gases and thermal cycles from 80 to - 10°C. Evaluated by the nitrogen adsorption method and Brunauer-Emmett-Teller (BET) analysis, the number of pores with diameters of less than 25 nm was reduced while more pores with diameter of larger than 25 nm was found in electrode. In addition, average pore size was enlarged from 9.51 to 15.8 nm. These changes indicate that formed ice may deform the pore electrode structure, loosening the contact between the CL and membrane. The increased ohmic resistance, including the constant proton conductivity within the membrane, provides further evidence of the increased contact resistance between the PEM and CL. This higher contact resistance between CL and PEM was also found using electrochemical impedance spectra in Oszcipok et al.'s [210] single cell cold start-up measurement under isothermal conditions at - 10 °C. These detected results are likely contributed by the ice formation, resulting in delamination and structural damage to the PEM, CL and GDL at subfreezing temperature.

However, with regard to mechanical damage at the membrane, conflicting results were demonstrated in the literature. Yan et al. [179] performed a cold-start of a single cell at temperature of - 5 ℃, - 10 ℃, and - 15 ℃. The reactants were supplied at room temperature without humidification. Figure. 14 displays the morphology of MEAs and PEMs from different operating conditions. It can be seen that water freezing causes delamination between the PEM and CL at temperature of - 10 ℃ and - 15 ℃, while no delamination is found during normal startup as shown

in Figure. 14 (a). From the magnification image of the PEM as shown in Figure. 14 (b), pinhole damage and micro-cracking are also observed after operation at sub-zero temperatures. These provide evidences as to why the ohmic resistance increases and how performance degrades. The delamination is also found in Wang et al.'s [208] work. However, Alink et al. [209] reported that the membrane-electrode interface seemed not to be damaged during five start-up cycles of six cells in sub-zero conditions (-40 ℃), while a decrease of 1000 mV in voltage (at 500 mA/cm^2), an increase in porosity and a decrease in electrode surface area were detected. Given the limited details about these experiments, such as membrane type, humidity conditions and rate of heating, it is hard to distinguish the source of the difference and quantitatively evaluate the effects of various factors. Nevertheless, as far as the achievements reviewed, theses harsh working conditions present a major hidden danger for the acceleration of membrane mechanical damage.

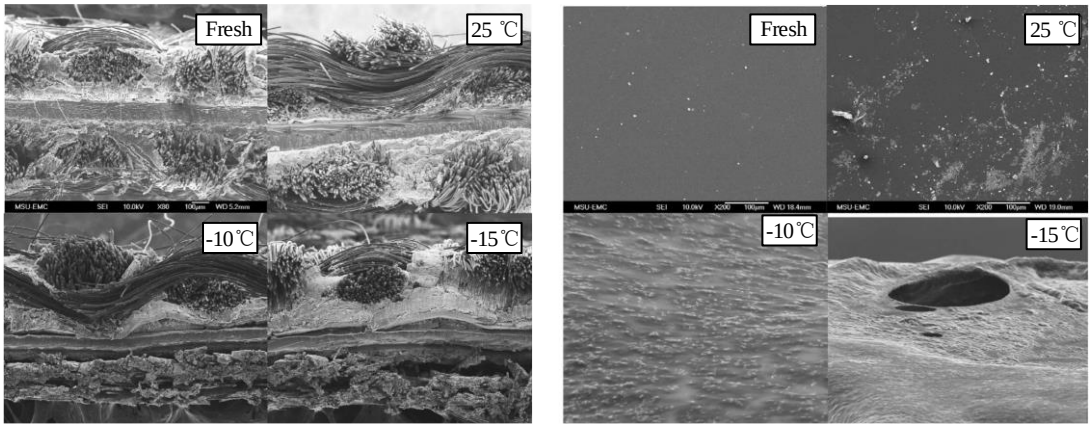

(a) (b)

Figure. 14 (a) MEA after operation at various temperatures; and (b) membrane after operation at various temperature (Permission from [179], copyright Elsvier)

To determine the key factors causing membrane's physical damage, Kim et al. [31] subjected the tested cell stack with different types of MEA to freeze/thaw cycling (- 40℃/70℃) in conditions of water immersion. Given that the MEA with 35 μm thick membrane had much more severe CL damage and delamination than that with 18 μm thick membrane, they speculated that more frost heave of water inside the 35 μm membrane was the main source of interfacial delamination. Moreover, the MEA with a virgin CL crack suffered more damage than that with the non-cracked CL. These can be explained by the shear stress that resulted from the ice expansion of the trapped water in the crack gap as shown in Figure 15 (a) and (b). According to the comparison of the bottom gap and surface gap in the CL depicted in Figure 15 (c) and (d), the inverted V-shaped crack contributed more to the damage. Samples with DM/ micro porous layer (MPL) showed much less damage on the CCM than that without DM/MPL. This may be due to the stiff boundary inhibiting expansion and eliminating interfacial gaps, as well as the hydrophobic barrier against water intrusion. However, the MPL in turn contributes to liquid water trapped after the fuel cell is stopped.

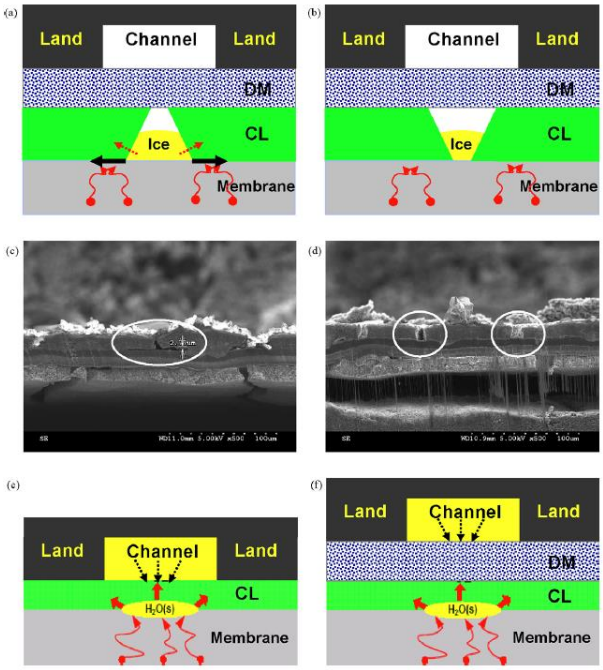

Figure 15. Schematic of potential damages by ice expansion: (a) Inverted v-shaped, damaged MEA; (b) v-shaped damaged MEA; (c) and (d) proof of inverted v-shaped cracks; (e) non-cracked MEA without DM/MPL; and (f) non-cracked MEA with DM/MPL(Permission from [31], copyright Elsvier)

These studies demonstrate that while rapid degradation of fuel cell during freeze-thaw condition results from multiple deteriorations in components, the mechanical property's change and mechanical damage of the membrane influence the degradation of the fuel cell's performance. A decrease in the mechanical strength, pinhole and delamination have been found to be the main change in the membrane. However, considering the conflict of results and deficiency in the mechanism studies, the effect of freeze-thaw operation on the membrane should be investigated in greater detail, such as water state and content in the material and particle size of the CL.

4.3.3 Mechanical failure along the MEA frame

Another common mechanical failure of the PEM is due to a tear or hole along the MEA frame as shown in Figure 16 (a). In Wu et al. [26]'s accelerated stress tests on the fuel cell, abrupt and drastic jump in hydrogen crossover was found after 300 h. The sudden failure after 72 h operation was also noted in Li et al. [181]'s study. Severe crossover suddenly occurred in a short time, and was accompanied by a sharp decrease in OCV. However, the cell voltage under light duty load dropped slowly. It is believed that a fracture at the membrane edge (along the frame) is the source of the fast change in gas crossover and performance decay. Ralph et al. [211] report that the lifetime of the commercial membrane with and without membrane edge protection was around 300h and 2500 h, respectively, on the basis of their test method. The electron probe microanalysis (EPMA) showed that the membrane was thinner at the edge, where the tear was caused.

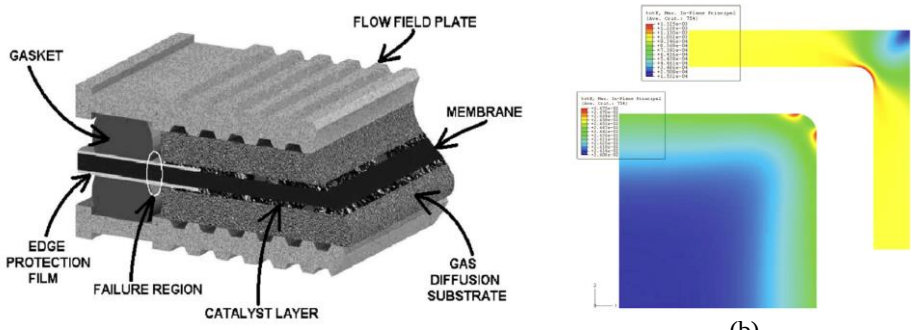

Figure 16. (a) Schematic drawing of fuel cell including the edge protection film [211]; and (b) model predicted distribution of maximum principal tensile strain in the MEA as a result of RH variation from 75 to 0% (Permission from [55], copyright Elsvier).

Some studies explained this issue with reference to the mechanical response of the membrane. Bograchev et al. [212] used a two-dimensional numerical model of an operating fuel cell to observe the development of stresses and deformation in the membrane. The peak stresses were localized within the seal joint/GDL interface, especially with a value of more than 3.5 MPa during the humidification step. Plastic deformation would be initiated at the membrane's edge, especially at the corner with peak in-plane strain. Qiu et al. [173] built a model to investigate the stress evolution in the membrane along the MEA frame throughout the assembly, operation and gas filling procedures. It was found that gas filling in the cell was the primary driving force in the fast degradation of membrane along the MEA frame. These findings regrading "edge stress" are in accordance with those of Huang et al. [55] and Solasi et al. [58]. Hence, from a mechanical perspective, the membrane along with the MEA frame is the most viable zone. Cracks of a larger size are prone to marginal distribution during the short-term opertating phase of the fuel cell [15, 26].

This far higher "edge stress" at the weaker region of the joint-area membrane is probably caused by several factors: 1) The compression from GDL pushes the membrane to the MEA's edge, which is fixed by gasket, thus creating mechanical stress due to the bending of the membrane; 2）due to the different material properties, variances in water swelling and thermal expansion lead to concentrated force during the cyclic physical loading; 3) a shock of reactant gases emerges on the edge of membrane, especially the region close to the gas inlet when the fuel cell starts. 4) the flaw is formed at the bonding area during fabrication process of MEA; and 5）the hot spot or H_2O_2 around the reaction area may intensify the degradation of the bonding region between the membrane and MEA frame [181].

4.3.4 Mitigation strategies

According to pre-existing studies, the membrane's resistance to mechanical failure would be reduced because of lower mechanical strength in hygrothermal conditions. Hence, some researchers

have advised methods for improving PEM durability by making the new materials more stable under vibrational humidity and temperature. One of the more useful method is to add reinforced structure to the membrane [211]. According to Kusoglu et al.[94], the in-plane swelling in the reinforced membrane and, consequently, the stresses and plastic deformation were reduced compared to an unreinforced PFSA membrane. The deformation of the PEM can be affected and restricted by additional MPL and GDL with high stiffness. Mustafa et al.[213] studied the effect of anisotropy of GDL on the loading of PEM. It is seen that improving the stiffness in the through-plane direction is an effective means of reducing the swelling of the membrane. In addition, the mechanical constraints resulting from the cell's clamping may mitigate the swelling in the membrane and thus reduce adverse stress.

In order to slow the degradation of a PEM during freeze/thaw operation, the fabrication method of the MEA, the operational protocol of shutdown and start-up, and measure of pre-heating should be improved on the cell. In the fabrication process of MEA, strong adhesion between the PEM and CL can reduce the delamination that resultes from ice formation. The MPL is helpful for reducing the residual water at the CCM, while it aggravates the water remaining in the GDL.

Before the fuel cell is shutdown, operating the stack with dry reactant gases could minimize the water inside the stack. A high air/nitrogen flow through the hot cathode side can be operated to sweep the vaporized liquid water from the MEA as much as possible. Coolant in the stack should be removed from the stack to minimize the thermal transfer when the fuel cell is heated. During the start-up process, in order to prevent abrupt operation of fuel cell because of insufficient mass transfer, it is not desirable to accelerate the power too rapidly. A dry membrane and high air flow rate are helpful for the charge transfer rate [210]. Operation at high cathode stoichiometry (at low current or at high flow) can provide more water vapor for the reaction of the fuel cell. However, there should be an optimized balance considering the capacity of the air supply system and convection of generated heat by air flow [214].

Preheating is the usual method for accelerating the start-up of the fuel cell at sub-freezing temperature. This can be provided by an external battery, the hydrogen's catalytic combustion, or by the preheating of the reactant gases [215]. However, Ahluwalia et al. [214] found that preheating feed gases and employing the power produced to heat the stack electrically only had a small effect on rapid self-start. Reverse voltage was also chosen to apply to the fuel cell at a subzero temperature to warm the stack and reduce its starting time. According to Wang et al. [208], the PEM is not damaged by the reverse voltage of less than 0.85 V, while cell performance is degraded if the reverse voltage is above 0.85 V.

The joint-area membrane along the frame is a weak region and must be specially protected to improve its resistance to fracture. The gasket seal or adhesive protection layer are used to eliminate the fast failure around the edge of the active area [55, 216, 217]. Li et. al [181] added a thin adhesive

protection layer covering the edge line, and no sudden crack or fracture was observed at the membrane's edge. A set of rigid sub-gaskets were bonded to minimize the edge effects in Crum et al.'s MEA [218]. A diamond-shaped active area is useful for achieving an alternated compression between the rib and channel at the edge so that the local "edge pressure" is reduced. Apart from the additional protection method, the pre-heating of the fuel cell, lower gas pressure difference between the anode and cathode sides, and decreasing of the seal joints stiffness (close to PTFE) are helpful for reducing the concentrated force at the joint-area membrane [173, 212].

4.4 Mechanical failure during long-term operation

During long-term operation, the fuel cell undergoes cyclical mechanical loadings due to dynamic temperature, hydration and reactant gas pressure. Especially in transportation applications, the cell stack is also avoidable to exposed to high-magnitude vibrations and shocks [112, 219]. Accompanying these physical loads, chemical degradation would simultaneously reduce the membrane durability and accelerate its mechanical failure. The failure is also adversely affected by the membrane's adherence to the outer-layer electrode. According to the previous studies, the influences during the long-term operation can primaly fall into three categries: physical load, chemical acceleration and the impacts of other components.

4.4.1 Mechanical degradation under physical loads

During long-term operation, the mechanical damage may arise as a result of various types of physical loads: 1) expansion and contraction induced by the cyclic temperature and RH; 2) pressure difference of reactant gases at anode and cathode sides； and 3) vibrations of the stack. Hence, the influence of physical loads on mechanical degradation are reviewed in the following three aspects.

4.4.1.1 Cyclic humidity and temperature

During the running cycles (the working status of startup/shutdown and variation of electric loading conditions), the constrained membrane undergoes cyclic swelling/shrinkage in response to the hygrothermal content results. Accompaned with alternated mechanical properties, wrinkle, creep, fatigue and final fracture are usually caused in the membrane after cyclic loading. Currently, many researchers focus on this point and have undertaken significant work in the absence of chemical degradation.

1) Mechanical property

In Section 3.2 of the mechanical property of the membrane, the strong dependence on humidity and temperature have been presented. For cyclic hygrothermal conditions, mechanical prosperity also undergoes a large change after cyclic aging [56, 57]. Xiao and Cho [79] subjected the Nafion® N117 membranes to 12 humidity cycling (30% RH-80% RH) and temperature cycling (30 ℃-80 ℃) separately. They found that initial yielding stress of 12.1 MPa and elastic modulus of 320.1 MPa at room conditions were reduced to 9.3 MPa and 265.0 MPa after humidity aging, while temperature aging induced more decrease to 8.4 MPa and 186.0 MPa, respectively. The final strain-to-failure

was also reduced after both aging treatments. These findings are in accordance with Alavijeh et al.'s [115] in-situ hygrothermal fatigue test, in which UTS, strain and fracture toughness were significantly reduced with increasing humidity cycling. 11% of ionic groups and 40% of the molecular weight are lost in a triazole-containing sulfonated polyimides (SPI-8) after 10000 wet/dry cycles [220]. The ductile membrane is transformed into a brittle material by hygrothermal aging. However, the elastic modulus is reported to be in decreasing trend in Xiao et al.'s [79] study but constant in Alavijeh et al.'s [115] study. Although they did not provide the calculation methods, the difference is probably due to the nonlinear behavior and thinning of the membrane during the aging treatment.

2) Wrinkle

Wrinkle deformation, caused by the swelling of the membrane under the flow channel, is generated as an initial degradation phase to accelerate the membrane failure after repeated humidity and temperature cycles [129]. As is shown in Figure. 17 (a), even if the fuel cell is well assembled, clearance in several hundred micrometers actually exists between GDL/CCM within the channel. Water absorption and thermal expansion force the swelled membrane into the clearance, thereby buckling the membrane. The insufficient compression between the GDL and BPP also contributes to this problem [219].

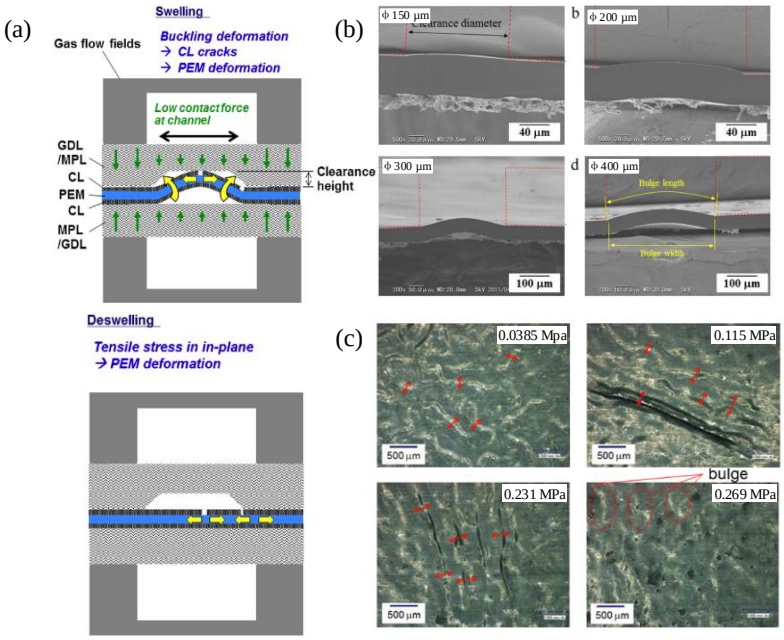

Figure. 17 (a) The proposed mechanism of wrinkle deformation under multiple humidity cycles, (b) wrinkle deformation of NR211-CL after humidity cycles under clearances in various diameters of ϕ 150μm, ϕ 200μm, ϕ 300μm, and ϕ 400 μm, and (c) deformations NR211-CL after humidity cycles at several contact pressures of 0.0385 MPa, 0.115 MPa, 0.231 MPa and 0.269 MPa. Arrows in the pictures indicate wrinkle width (Permission from [129, 137], copyright Elsvier)

Focusing on the generation of wrinkle deformation, Uchiyama and co-workers [129, 137-139]

conducted a continuous study and present another explanation on the crack on the membrane. Combining the NR211-CL bulking test and cell simulation with the clearance of 200 μm, they found that maximum tensile stress located at the topside of bulge (as much as 2.9 MPa at 100% RH) and then on the entire membrane as deswelling, while the membrane at the round corner of the clearance endured the largest shear (as much as 2.7 MPa at 100% RH). As the humidity cycles increases, the bulge deformation becomes larger. As a result, CL cracked and propagated to the membrane surface with final pinhole due to the concentrated force between the CL crack and membrane.

Wrinkle deformations become more severe as the clearance extends and the compression pressure is insufficient. As is shown in Figure. 17 (b), more obvious buckling deformation occurred under the clearance of diameter of a 400 μm in the buckling test. Severe wrinkles and slight bulge deformation are generated separately at the smaller and higher contact pressure in Figure. 17 (c), respectively, due to various friction between the CCM and GDL/MPL. Moreover, the compression on the membrane is likely to reduce the water content [221]. Hence, smaller clearance and higher contact pressure (static friction force) between CCM and MPL/GDL can reduce wrinkle deformation, especially for the thicker CCM with lower in-plane swelling.

3) Creep

The membrane exhibits viscous characteristics due to the sliding of polymeric chains into a more compact construction and lower entropy state. Creep, a time-dependent increase in strain in response to constant stress, is unavoidable even at room temperature. During the cell's operation, the membrane is likely to gradually elongate until the final rupture when the time is long enough under the constant swelling force and pressure difference of reactant gases. In Li et al. [222]'s conducted fatigue (cycling gas pressure 18 of kPa) and creep (constant gas pressure of 18 kPa) to leak test on three membranes (Nafion® NRE-211, Gore-Select® 57 and Ion Power® N111-IP) using pressure-loaded blisters at conditions of 90 ℃ and 2% RH. No obvious difference between fatigue and creep results are found in these experiments. This means that the viscous behavior of this material plays a predominant role in the lifetime of the membrane rather than cyclic loading. Solasi et al. [223] consider that creep induced the membrane to fail in two modes: excessive deformation causing wrinkle and thinning of membrane, and formation of fracture such as pinhole and crack.

Creep failure is due to the fact that the polymer chain could no longer accommodate the applied stress. During the creep process, the membrane stretches rapidly over the first several minutes, then increases at a much slower rate. When the constant stress is relieved, a certain amount of permanent creep strain would be remained inside the membrane after an instantaneous relaxation and gradual recovery. At least of 30 % of the total creep strain was permanently left in PFSA membrane under various humidity (23 ℃ and 70 ℃) and temperature conditions (50% and 90%) after 120 min of 2.5 MPa in Kjeang et al.'s [224] study. The permanent creep strain would also gradually accumulate with the multi operation steps until the finial fracture.

The creep and creep-fracture effects on the membrane should be considered for various humidity and temperature conditions in the fuel cell. Benziger and coworker et al. [60] compared the strain changes of Nafion® 115 membrane and Nafion®/3 wt% Titania (TiO2)115 membrane when subjected to the constant tensile stress. More than 20 % strain crept into the both membranes at room conditions with an applied load of 7.5 MPa after two days, whereas it reached up to 100%-120% at full humidity. The introduction of Titania particles led to a lower creep in Nafion®/TiO2 composite membranes owing to the more difficult molecular disentanglement [59]. However, an anomalous creep behavior was observed in Benziger et al.'s [74] creep test on Nafion® N110 under the conditions of temperatures, 25 ℃-110 ℃, and water activity, 0%-95%. For constant humidity, the creep strain becomes larger with increasing tempe the as reported in other studies [224, 225]. The increase of creep deformation, along with temperature, is due to the enhancement of molecular motion, especially when it is higher than the glass transition temperature [215]. However, the monotone increasing with humidity is not always obtained for each constant temperature. When the temperature is below 40 ℃, the creep strain increases with water content, while above 80 ℃, the higher humidity leads to a larger resistance to creep and smaller strain is obtained. In the region of 40 ℃-80 ℃, the creep strain decreased and then increases with rising humidity. The relatively higher dependence of creep deformation on hydration in a dry state was also found in Solasi et al.'s [223] test. They considered that the transformation of water state in the membrane, from bound water to bulk-like free water in a dry state, accelerated the creep behavior. From Benziger et al.'s perspective, this piecewise behavior is possibly caused by the glassy state transitions by the water bonding within the sulfonic acid group as is shown in Figure 7, or microphase structural variation in surfactant solutions or block copolymers [74]. However, there is no evidence of the water cluster in the membrane influencing the slippage or disentanglement of molecular chain.

4) Fatigue

High relative humidity and temperature levels lead to in-plane compression and swelling in the membrane, while diminished humidification and dry conditions create in-plane tension and shrinkage under the constraint of the adjacent seal and axial loading by the assembly. In consequence, with the temperature and moisture changes, the PEM experiences alternating expansion and contraction. Comparatively speaking, water content plays a more significant role in the mechanical failure because of the much higher swelling from water uptake than the expansion from thermal effect in the cell [94]. According to Yeh-Hung et al. [98], swelling of 15% and shrinkage of 4% were noted in the Nafion® NR111 membrane under a running condition and de-hydration status, respectively. Subjected to repeated hygrothermal stresses due to water content changes, the membrane is believed to undergo an internal fatigue process, in which bonds amongst the inner elements gradually deteriorate. Even the cyclic stress level is far below the monotonic stress-to-failure, and eventual damage can be caused over a number of cycles. Fatigue lifetime is primarily

affected by temperature, applied stress and relative humidity [30, 226]. As is shown in Figure. 18 conducted at General Motors [35], fatigue of Gore-Select® 57 membrane deteriorated with the increase of relative temperature from 70 ℃ to 90 ℃ because of softening the material. As the amplitude of the humidity was increased from 80-150 % to 0-150% at 80 ℃, the fatigue cycles of the membrane dropped significantly. Hence, fluctuation range was regarded as the most critical parameters to the fatigue lifetime [18]. Because of the time-dependent nature, the rate of fatigue also shows dependence on the frequency of cycling. Reducing the amplitude and frequency of humidity/current cycling is an effective way to increasing the membrane durability.

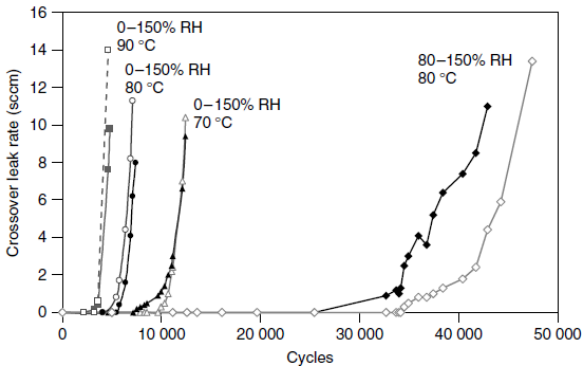

Figure. 18 Crossover leak progression of Gore-Select® series 57 membrane subjected to humidity cyclic testing under the test conditions of 70 ℃/0–150% RH, 80 ℃/0–150% RH, 90 ℃/0–150% RH, and 80 ℃/80–150% RH (Permission from [35], copyright ASME)

In order to investigate the fatigue lifetime, an ex-situ characterization of mechanical fatigue behavior has been conducted by exposing the membrane to cyclic working conditions [227] or mechanical loading [32, 80, 222, 226, 228]. Aindow and Neill [227] applied the humidity cycle (from 30 % or 10 % to 90%) on the fixed-strain membrane to build the humidity cycle-to-failure (S-N) curve as the membrane lifetime. Khorasany et al. [226] subjected the membrane to cyclic uniaxial tensions at controlled temperatures and RH. The effect of the temperature was discovered to be more powerful than humidity. Dillard et al. [80, 222, 228] simulated the equal biaxial stress to simulate the hygrothermal stress state in the constrained membrane with pressure-loaded blister tests. Using this method, they characterized the strength and durability of various membranes under different applied load, temperature and humidity conditions.

Considering the actual environment in a fuel cell, an in-situ AST test is carried out to study mechanical fatigue and observation methods have been devised in recent years. Kjeang et al. [115] designed a membrane fatigue test through applying rapid, deep wet/dry cycles (90%/0% RH) at a fairly high temperatures (80 ℃/95℃), as well as leakage location test using an IR camera. The membranes suffered more severe damage at temperature of 95℃ as a result of higher temperature and quicker humidity cycling. Vengatesan et al. [182] studied the mechanical failure underwent unsymmetrical RH cycling. The results showed that the cathode RH cycling cell owned a longer

lifespan than the anode RH cycling one.

Modelling of the ex-situ and in-situ fatigue response is also carried out in some studies [18, 25, 103, 229]. The material description with the constitutive model and failure criteria are the main challenges to understanding the fatigue mechanism and accurately predicting the lifetime. A material model with nonlinear viscoelastic and/or viscoplastic effect in temperature and humidity is necessary for calculating the fatigue process with high fidelity. In order to predict the lifetime, improvement on the fatigue model is still needed to determine the membrane failure, despite the Smith-Watson-Topper (SWT) approach having been utilized [18].

4.4.1.2 Cyclic gas flow

A significant part of the membrane's water content is brought about by the external humidified reactant gases. In the meantime, the gas pressure difference between the cathode and anode is applied on the thin membrane in tens of kPa. Bender et al. [113] applied three sets of differential anode/cathode pressures (0, 2, 4 psi) in the in-situ AST experiments. OCV degradation was found to be insensitive to the pressure difference of 4 psi in the first 18 h, while a quicker voltage drop was observed in the subsequent time. Therefore, increasing the pressure difference of the gas flow between the anode and cathode can accelerate membrane degradation, especially in a the membrane with defects.

The flow rate of hydrogen and air is important to the distributions of RH, heat and electric current in a cell. Higher flow rates quickly remove the water generated and make the membrane dry out, however, lower flow rates result in water concentration in the membrane. The non-uniformities in current density could create hotspots that cause irreparable damage to membrane [230]. In addition, a higher frequency of current change has been demonstrated to increase the fluoride release and accelerate PEM degradation [231]. Hence, the hydrogen and air flow rates, as well as the RH in the flows, must be controlled to prevent too dry or flooding membrane.

Inside a fuel cell, the degradation rate and earlier-failure position of the membrane depends on the reactants flow directions. Lai et al. [232] compared the thinning and crossover leak rate of Ion Power™ N111-IP membrane between the gas counter-flow and co-flow configuration by an in-situ shorting/crossover diagnostic method. As is shown in Figure 19, with the strong current (80 to 800 mA cm^{-2}) and hydration cycling, the locations of maximum thinning and crossover fall in the middle area of counter-flow configuration and gas outlet area of co-flow configuration, respectively. A significant leak rate exceeds 50×10^{-3} sccm cm^{-2} at several locations after the 8000 min counter-flow test, while it is below 30×10^{-3} sccm cm^{-2} at most of the area after the 11900 min co-flow test. From the perspective of achieving lower membrane degradation, the co-flow configuration in the fuel cell is preferable. The higher degradation position in the outlet area of H_2 is also found by Vengatesan et al.'s [182], although the configuration of reactant gases was not stated. Based on the infrared thermography technique, Moor et al. [15] detected the flaw size and distribution in the membrane

after 1500 h operation of the fuel cell. Compared with flaws of small size in random distribution, those of larger size were all located in the air outlet region. They noticed that the orientations of the crack formed in the membrane (air outlet) were in the same direction along the gas path. Their measurements provide evidence that the gas outlet region is the weak area of the membrane due to variation of the RH (sometime it is flooding), high gas velocity and high current.

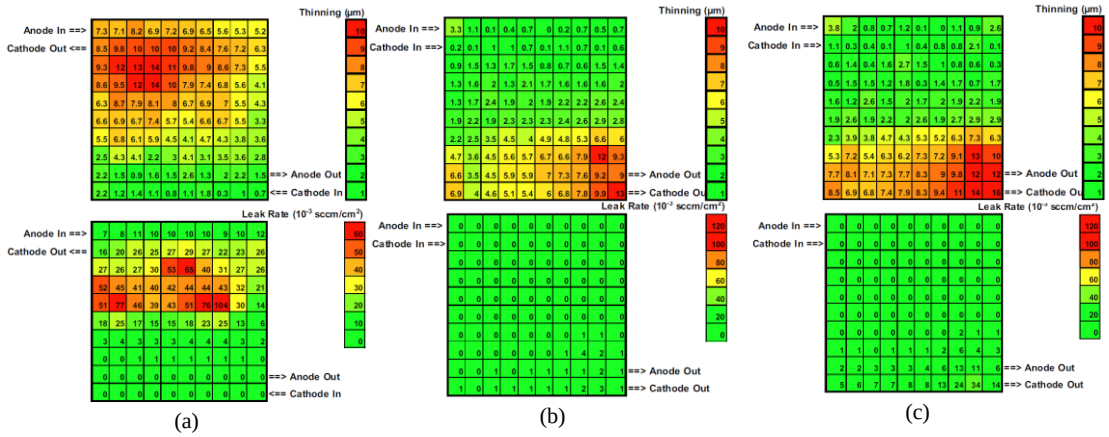

Figure 19. (a) thinning and leak rate maps from the counter-flow test at t=8000 min; (b) thinning and leak rate maps at t=11200 min from the co-flow test; (c) thinning and leak rate maps at t=11900 min from the co-flow test (Permission from [232], copyright Elsvier).

4.4.1.3 Vibrations of the fuel cell

In transportation or auxiliary power device applications, vibrations and impact loads are well-known sources of mechanical damage to fuel cell. In vehicles, a range of 8-16 Hz vibration is generated as a result of oscillations in the suspension systems in conditions where the road surface is rough [233]. With auxiliary power devices such as those which provide energy for compressors, the fuel cell generally experiences vibration in a wide range of 0.9-40 Hz due to rough road and engine vibrations [112, 234]. These dynamic loads would result in over compression and shear stress, thus precipitating the fatigue and initiation of sudden crack in the membrane.

Up until now, studies of the effect of vibrations on membrane failure are limited. Diloyan [234] found that the Pt particle size after 300 h accelerated test with vibrations grew from 2-2.5 nm to ~ 5.47 nm, which was 10 % smaller than that in the test without vibrations. Delamination becomes more severe with increasing amplitudes and frequencies of the vibrations. Banan et al.[112] compared segregation between PEM and CL under a range of stack vibrations conditions (amplitudes of 1 g, 2 g, 3 g and 4 g with frequencies of 5 Hz, 10 Hz, 20 Hz and 40 Hz,) based on the cohesive zone modeling (CZM) approach. The simulation of 40 Hz and 4 g caused the most severe damage. It was identified that non-linear relationships existed between the damage propagation and amplitudes, with the frequency playing the dominant role at larger amplitudes. In general, the effect of vibrations on mechanical damage in the fuel cell has not been revealed in detail. Only several studies addressed its effect on the stack's final power performance [235-237]. To

elucidate the fuel cell reliability, the membrane's mechanical failure, as well as the stack and other components should be studied closely under vibrational conditions, such as fatigue, crushing damage and water transport.

4.4.2 Acceleration of chemical degradation

In practice, the membrane durability is believed to be affected by the combined actions of mechanical and chemical degradation, which is a synergistic process. Each type of degradation would be increased by the presence of the other components. The chemical decomposition of the PEM, caused by radical attack originating from the formation and movement of hydrogen peroxide, metal ion contaminants, and catalyst dissolution and recrystallization, will then be accelerated by the hot condition, high reactant gas pressures and low relative humidity [238-240]. Mechanical failure, such as the crack and thinning of membrane, is inevitable to contribute to the chemical degradation. In return, the mechanical failure will also be intensified by the chemical degradation. This section mainly reviews the effect of chemical degradation on mechanical failure, which is this study's core purpose.

4.4.2.1 Influence on mechanical failure

The mechanical failure of the membrane in the fuel cell is significantly accelerated by the presence of chemical degradation. Various membranes were tested under several degradation modes at Los Alamos National Laboratory (LANL) [241]. The crossover of these membranes from RH cycling of N_2/N_2, OCV, and RH cycling of H_2/air are displayed Figure 20. OCV induced the worst crossover of membranes, followed by those in the H2/Air RH cycling and N_2/N_2 RH cycling. Although the OCV creats very severe working conditions for the membrane, it indicates that faster membrane failure occurs under combined effect of mechanical and chemical degradation.

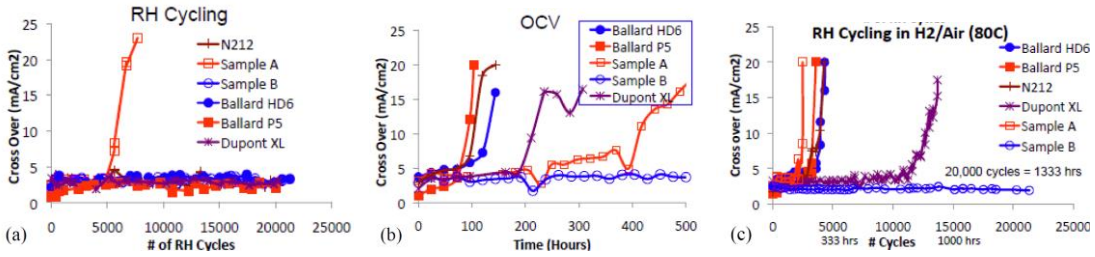

Figure 20. AST results for several different membranes from LANL a) RH cycling in N2/N2; b) OCV testing; and c) RH cycling in H2/air at 80 °C (Permission from [241], copyright ECS).

The membrane's mechanical strength is reduced by chemical attack. According to Huang et al.'s [55] ex-situ tensile test (25 °C and 50% RH) of the CCM cut from the operating MEA, the strain (average 3.55%)/stress (average 9.5 MPa)-to-failure after 48 h of chemically in-situ OCV degradation was much smaller than the original strain (average 132.5%)/stress (average 16.3 MPa) to failure and those (average failure strain 40%, failure stress 15.8 MPa) after 50 RH cycles from 80 to 120% RH. A long crack is observed on the chemically OCV degraded samples instead of

distributed microcracks on the samples after the RH cycle. According to in Kjeang et al.'s [242, 243] work, immediate fracture occurs in the OCV-degraded samples even before the yield points in the tensile test. However, the facture prior to the yield points is not found in the samples after pure mechanical degraded samples [115]. The failure of chemically degraded membranes at low strain indicates reduced ductility post-degradation. Elastic modulus slightly increases with the cycling of the OCV AST test, and as much as a 40% increase was found up until the end of the test (13 AST cycles), indicating stiffening due to chemical degradation [24]. In the AST, the membrane's thinning was about 5% after accelerated mechanical stress test, whereas it dramatically increased to 48% when the membrane was exposed to combined mechanical and chemical degradation.

4.4.2.2 Acceleration mechanism

In order to evaluate the membrane's durability, it is necessary to explore the kinetic of the membrane failure process as a function of the synergistic effect of the combined chemical aging and RH cycling. However, the technical task about identifying chemical and mechanical degradation mechanism are still challenging. Several studies have been conducted to investigate chemical acceleration mechanism in three aspects: 1) the microstructure change of the membrane; 2) the effect of Pt dispersion; and 3) the degradation rate in different stages.

1) Molecular structure

The molecular structure of the membrane would be degraded and disentangled due to the chemical degradation, thus decaying its mechanical strength. Figure 21 (a) and (b) show the stress-strain curves, open voltage and leak detection with respect to the number of OCV AST cycles [242]. It can be seen that the first fracture is observed instead of the notable elongation of membranes after only 2 ATS cycles, where leaks from pinholes or cracks are not detected as shown in Figure 21 (b). We speculate that this is due to the chain scission and molecular weight reduction resulting from the continuous chemical degradation, whereby the shortened chains would easily slip through the entanglements, making the ductile membrane transit to the brittle and stiff material. Compared with membrane surfaces after various OCV degradations and similar creep tests as shown in Figure 21 (c) [244], the surface of the membrane with 72 h OCV degradation features a larger local rupture than those with 0 h and 45 h degraded membranes. Hence, after chemical attack the membranes are prone to local rupture to release pressure instead of chain slippage within high molecular weight polymers.

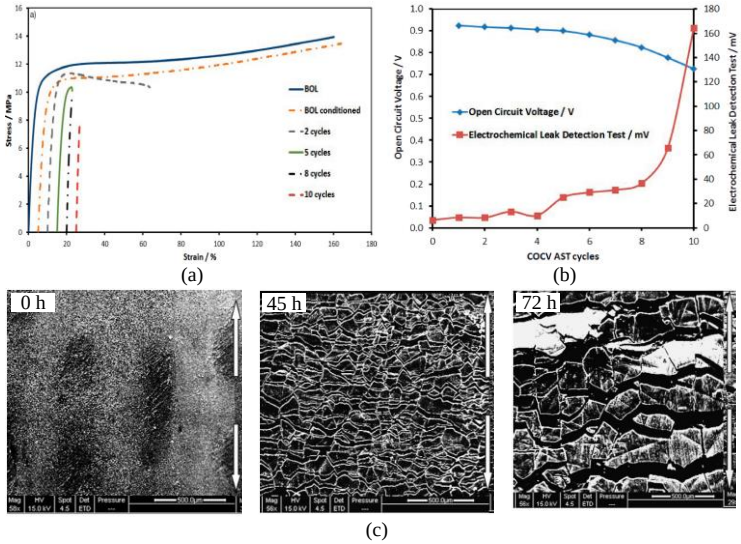

Figure 21. (a) Stress-strain curves as measured in ambient conditions; and (b) variation in OCV and leak detection test after different numbers of OCV AST cycles [242], and (c) surface SEM micrographs of 0 h, 45 h,72 h degraded membrane after the 10MPa creep test. Arrow indicates the direction of applied stress (Permission from [244], copyright ECS)

2) Pt dispersions

After long term cell operation, small Pt particles are usually found in decayed membranes generally because of dissolution and migration from cathode CL [245-248]. The size and location of the developed Pt band in the membrane are reported as various results due to flux of hydrogen permeating and differences in degradation [249], such as the diameter of 10-30 nm and 1.3-7.6 μm away from the cathode observed by Fenton et al. [247], and 3.8 μm away from the cathode in Bi et al. [250]. In general, the Pt band is closer to cathode/membrane interface [251, 252].

Using membranes with synthetic or in-situ degraded Pt bands, the effects of Pt dispersions on the membrane durability are demonstrated with conflicting results based on in current studies. As a more easily controlled approach, synthetic methods of incorporating intended amount of Pt powders in the membrane have been used to explore the adverse effect on the material. For example, the membrane of mixing Nafion® 117 solution with Pt dispersion shows growing elastic modulus as the Pt dispersion amount increases, while an earlier fracture happens at lower stress, namely UTS [253]. This is due to the fact that fracture resistance is reduced due to the initiation of crack around the Pt cluster and propagation through the regions with Pt dispersion. Higher sensitivity to humidification and more ionomer decomposition are found during the OCV degradation tests with deposited Pt in the membrane [254]. However, for the in-situ formed Pt band after chemical degradation in a cell, on the one hand the further degradation of the membrane with the developed Pt band would be accelerated because of more radical formation [255, 256], while on the other hand an extended lifetime with smaller material thinning and better mechanical strength is observed in the degradation test of the membrane with the Pt band [249, 257]. Furthermore, the presence of contaminant ions in

hydrated membrane increased material stiffness noted by Kundu et al. [61] due to the possible generation of the physical crosslinking of ionic clusters, therefore, reduces the chain mobility and increases the strength and stiffness. In general, the effect of Pt dispersion on the membrane is still unclear. The growth process of the further dynamic of the Pt band in the membrane, as well as its influence mechanism on durability, still needs more investigation.

3) Degradation rate

Through the overall evolutions of mechanical failure, the predominant role in the membrane degradation is successively played by chemical and mechanical stressor with respect to the failure stages. In Kjeang et al.'s [257] experiments, degradation of the membrane under AST with constant RH showed a similar level of membrane degradation under AST with cyclic RH at the beginning. In later stages, the membrane with RH cycling showed a higher rate and early failure, which had more severe micro pinholes of 50-300 μm in diameter and density of 2.9 cm^{-2} than those with constant RH (diameter of 40 μm and density of 1.2 cm^{-2}). In addition, the hygrothermal expansion of the membrane after long in-situ test was observed at about 2%, which is in the same range of its strain-to-failure in the tensile test [242]. These indicate that the first phase of the membrane degradation in the fuel cell is dominated by chemical degradation due to fast radical attack, followed by a propagation of failure accelerated primarily by the action of mechanical degradation. Up until now, although feasible, evidence supporting this conclusion is limited. More details about degradation in different stages should be considered in addressing this problem, such as real operation conditions and various membrane compositions.

4.4.3 Effect of catalyst layer

Most current studies focus on pure membrane failure. In practice, the anode and cathode CLs adhere to the membrane to form a catalyst-coated membrane (CCM)[258]. Together, the membrane and two CLs act in response to mechanical degradation as a composite material, which has different mechanical properties to the pure membrane [259]. The interaction between the membrane and CL is avoidable for producing a more complex impact than those with a single membrane. When the adhesive stress disappears, delamination between the membrane and CL occurs, serving to intensify the membrane failure. Hence, the effect of CL on the mechanical failure process is important to understand.

4.4.3.1 Combination of material property

The bonded CLs contribute to the mechanical properties of the fuel cell's composite CCM. Several studies have been conducted comparing the mechanical properties of pure polymer and CCM, as well as behavioral changes under cell operation conditions. Testing transition temperature of CCM, related to polymer molecules and the disintegration of the crystallized domains into an amorphous network, has shown the same value with a pure membrane indicating coated process of CL makes no observed impact on the polymer chain network [260]. On the basis of the ex-situ

tensile test under various hygrothermal conditions, it is found that the CLs induced a lower level of elastic modulus, yield stress and yield strain because of their lower stiffness.

More of a decrease in mechanical strength and stiffness is obtained in CCM than pure membrane from room conditions to operation conditions (70 ℃, 90% RH) [260]. Due to the reinforcement of CL and composite nature of CCM, the swelling length of CCM with respect to hydration is shown to be half that of the pure membrane (16.8 % and 8.8% increase in length for pure membrane and CCM, respectively, at 70 ℃, 90% RH), thereby reducing the stress/strain during the cyclic humidity. In contrast, the CCM tends to have more thermal expansion than the pure membrane because of the relatively high expansion ratio of the catalyst [242]. As a result, in Khorasany et al.'s [226, 259] fatigue test on the pure membrane and CCM, the humidity cycles lead to more severe fatigue for the pure membrane, whereas the CCM suffers relatively more fatigue under the thermal cycles.

4.4.3.2 Crack acceleration

Unlike the above studies that regard it as a composite material [242, 260] or single component [193, 259], the other work holds that the interaction between the membrane and CL accelerates crack in the membrane. Uchiyama et al. [138] state that the cracks initiate at the topside of the bulge in the CL with an increasing humidity cycle. As a result, the PEM under CL cracks are kept in tensile state in the dehydration state. Crazes are then propagated into the PEM from CL cracks by creep and fatigue. The same results were also obtained by Pestrak et al. using in-situ humidity cycling fatigue test of Gore-Primea® series 57 [32]. They reported that tested MEA samples were prone to leakage a lot earlier than tested membrane samples without CL, and small cracks initiated in the membrane under the mud-cracks of the CL. It means that catalyst cracks contribute to the premature failure in the membrane by concentrated stress. According to the ex-situ low-cycle tensile test of the CCM, cracks immediately generate on the surface of the CL after the membrane yield due to the following drastic elongation mismatch between the PEM and CL [261]. Therefore, from the above studies, different material properties and the micromorphology of the catalyst accelerate the mechanical failure of the membrane. Reducing the deformation mismatch in the three-layer CCM is therefore effective in suppressing crack formation.

4.4.3.3 CL and PEM Delamination

Delamination between the PEM and CL is another common failure mode during the fuel cell operation, which blocks proton transportation and the hydration reaction and causes particles aggregation in CL during middle-term life tests [262]. In order to understand the delamination mechanism and competition with crack in the membrane, a cohesive zone model and fractional contact model are utilized to figure the response of the interfacial behavior between the PEM and CL by FE models in several studies. It is accepted that there is an initiation competition between the accumulation of plasticity energy, inducing crack of the membrane and accumulation of

delamination energy at the interface under the hygrothermal cycles. Rong et al. [263] reported that fast frequent RH and temperature cycles at the startup and shutdown of fuel cell induced an earlier delamination and later crack initiation. However, a contrasting results were obtained by Banan et al.[104] using a half-channel model, which states that the crack in the membrane grew faster than delamination.

The difference amongst these studies may result from the developed CL models, which are C/Pt agglomerate model and single layer model in the representing of CLs, respectively. The agglomerate model contributes to more interaction and higher delamination energy accumulation between CL and PEM. As a result, delamination occurs earlier than the crack if the agglomerate model is used. In contrast, the crack in the membrane is initiated more rapidly if a single layer model is selected. It can be seen that the delamination prediction between PEM and CL is significantly influenced by the simulation of CL model. In reality, CL is demonstrated to own varying mechanical properties with respect to depth at the nano-scale [264]. The stress concentration at the interface is caused by the graded behavior of the CL throughout the discrete model. Hence, considering naturally random and heterogeneous microstructure of CL, constructing models according to the micromorphology of practical CLs is necessary in order to understand delamination more accurately during fuel cell operation.

4.4.4 Mitigation strategies

Although the membrane's mechanical degradation is unavoidable during hygrothermal cycling in the fuel cell's long-term operation, some strategies are still intended to minimize its influences through two categories: 1) reinforcing the PEM material with better anti-swelling efficiency; and 2) adopting adequate water management to reduce the rate and swing of hydration/dehydration in the membrane.

In order to improve the dimensional stability when swelling, designing the PEM composition is crucial for controlling the expansion properties of a membrane in the fabrication process such as reinforcement. By modifying the PEM composition, lower in-plane swelling and higher durability are expected to be achieved during the hydrated expansion/contraction. A flat MPL, a rigid GDL with higher transverse stiffness and a narrow channel of flow fields are useful designs for obtaining a lower clearance height between the CCM and PEM, thus reducing wrinkle deformation and delamination [137, 265].

During the fuel cell's operation, reducing the speeds of startup and shutdown are efficient operating strategies for limiting the frequency of the wet-up and dry-out cycles that the membranes experience. Considering the high dependence of the accumulated creep damage on permanent deformation, it is suggested to decrease the temperature and assure the membrane sufficiently hydrated so as to alleviate the adverse creep effects [224]. Hydrogen and air flow rates and humidified RH significantly influence current density, membrane dry-out and electrode

flooding. Based on the current experimental results [232], the co-flow configuration for anode/cathode gases is more advantages to shift the membrane lifetime than counter-flow. Cathode RH in the range of 50-60% is also recommended to ensure reaction efficiency and prevent flooding [188, 189]. Dry H_2 conditions can sustain fuel cell operation when the cathode RH is kept in this range [266].

5. Evaluation methods and protocols of mechanical failure

During the review process, we find that it is difficult to systematically assess and compare the date of mechanical failure in the large amount of literature, because different testing and evaluation methods are used with various material, test protocols and hardware. In order to effectively explore the membrane's mechanical failure, it is crucial to develop a recognized method for evaluating durability, as well as to determining the improvement strategies. In this section, in-situ and ex-situ methods of evaluation and characterization of the membrane mechanical durability are presented to provide a guideline.

5.1 In-situ method

5.1.1 Lifetime tests

During the fuel cell's operation, the membrane is simultaneously subjected to chemical and mechanical degradation. In the lifetime test, the fuel cells are usually running at a stable loading by controlling the current density or voltage for several hundred or even thousands of hours until the cell's outperformance is no longer acceptable. This kind of method provides a more realistic process of membrane degradation. However, a large amount of time and expense is consumed by this testing, which mixes two inseparable degradation mechanism.

Table 1 has listed the lifetime tests reported in the fuel cell literature. It is apparent that if membrane failure occurs, the durability life of the fuel cell is generally less than 3000 h, depending on the membrane materials and test loading. For example, the cell with Gore-Select® membrane with the PTFE operated for 1600 h, which was much longer than that with Nafion® 101 without PTFE [5]. The Nafion® 112 membrane exhibited a shorter lifetime of 1000h at a loading of 1060 mA/cm^2 than 2088h at a loading of 300 mA/cm^2 [9, 11]. The gas crossover rate, membrane thinning and fluoride release rate are usually adopted to evaluate the degradation of membranes.

5.1.2 Accelerated stress testing

Due to the high time requirements and cost, the full lifetime test of the fuel cell is not feasible in the large-scale application of evaluating membrane durability. Accelerated stress testing (AST), which reduces testing time by more than an order of magnitude, is preferred for estimating the fuel cell system's durability and membrane. It is a powerful tool for benchmarking the durability of fuel cells and evaluating different accelerated stressors at a reasonable time and cost [176, 267, 268]. As is noted above, membrane degradation strongly depends on cell conditions like temperature, freeze-thaw cycling, RH, start-up/shut-down and transient operation. Hence, single or combined

parameters of importance are usually enhanced during the testing to observe their influences.

To date, several test protocols have been adopted in the ASTs, including (1) open circuit voltage (OCV), (2) RH cycling, (3) freeze/thaw, and (4) load cycling tests (voltage, and start/stop) [232]. In particular, the OCV AST mode is widely adopted in AST to enhance chemical stressors, while RH cycling is apt to accelerating mechanical degradation. It has been observed that OCV testing accelerates 5 to 40 times the voltage decay, around 5 times the electrochemically active surface area (ECA) losses, and 3 to 12 times the gas crossover of those in lifetime testing [247]. Table 2 lists the studies that focused on the AST of mechanical degradation or combined mechanical degradation and chemical degradation.

Table 2 Summary of achieved fuel cell ASTs with mechanical degradation or the combined mechanical and chemical degradation

Stack description	AST mode	Testing time	Operation conditions				Degradation rate	Ref.
			OCV Testing conditions	RH	Temperature	Fuel/oxidant		
Five cells, 45 cm^2, Nafion NR-211 non-reinforced	RH cycling	20,000 cycles	-	①0% RH dry (2 min) + 90% RH wet (2 min); ②0% RH dry (3 min) + 100% RH wet (1 min)	① 80 ℃ ② 90 ℃	① N_2 9.0 SLPM for both sides ② N_2 3.5 SLPM for both sides	1) Gas crossover: ① 14 sccm/per cell, ② 7 sccm/per cell 2) Catalyst layer crack	[115]
Five cells, 25 cm^2, SPI-8 membrane with different degree of polymerization	RH cycling	10,000 cycles	-	0% RH dry (2 min) + 100% RH wet (2 min)	80 ℃	H2/Argon :100 SCCM for both sides	Ionic groups loss: 11%, Molecular weight loss: 40%	[220]
Single cell 42.25 cm^2 Gore - Select® 57	RH cycling	440 h	Constant running at an idle current 10mA/cm^2	0% RH dry (10 min) + 100 % RH wet (40 min)	70 ℃	H2: 0.113 sccm, Air: 0.358 sccm	1) Cumulative fluoride release: Cathode: 24 μmol cm^{-2}, Anode: 7.5 μmol cm^{-2} 2) Delamination in the membrane layer and crack in the catalyst layer	[182]
Single cell	RH	① 400	-	0% RH dry (2 min)+	80 ℃	Air: 2	Gas crossover:	[269]

50 cm^2 ① Hydrocarbon Membrane ② Nafion® NR-111 ③ Gore-Select® 57 ④ Nafion® N111-IP	cycling	cycles ② 4500 cycles ③ 6000 cycles ④ more than 20000 cycles		150% RH supersaturated (2min)		SLPM for both sides	10 sccm/per cell	
Single cell, 50 cm^2 Gore-Select®57 membranes	RH cycling	①12000 cycles ② 6000 cycles ③ 4500 cycles ④ 42000-45000 cycles	-	① 0% RH dry (2 min)+ 150% RH supersaturated (2min); ② 0% RH dry (2 min)+ 150% RH supersaturated (2min); ③ 0% RH dry (2 min)+ 150% RH supersaturated (2min); ④ 80% RH wet (2 min) + 150% RH supersaturated (2min);	①70 ℃ ②80 ℃ ③90 ℃ ④80 ℃	Air: 2 SLPM for both sides	1）Gas crossover: 10 sccm/per cell 2) Catalyst layer crack	[35]
Five cells, 45 cm^2 PFSA membranes, Cabon-based Pt	OCV and RH	13 cycles/200h	Low load	OCV: low RH; RH cycling: N_2 dry+ oversaturated	High temperature	OCV：H_2/Air; RH cycling：N_2 for both sides	1) Fluorine release for both sides: 83 mmol cm^{-2} 2) Catalyst layer crack	[24, 242]
10 cells, PFSA membranes, Cabon-based Pt	OCV and RH	298 h	Low load of 1 A	OCV: low RH; RH cycling: cathode: 60% RH+ oversaturated;	85 ℃	N2 for both sides; Backpressure: 0.1	1) Gas crossover: 10 sccm/per cell, 2) Delamination in the membrane layer	[257]

				anode: 100 % RH		bar	and crack in the catalyst layer, Pt band in the membrane	
Single cell, 25 cm^2, Nafion® 112, 0.2 mg cm^{-2} and 0.4 mg cm^{-2} on the anode and cathode sides	OCV and RH	20 cycles/960 h	OCV: Idle 7min, Heavy of 1.8 A cm^{-2} 3 min;	OCV(24h): D.P.a/c=65/65 ℃; RH cycling (24 h): 0% RH dry (30 min) +100 % RH wet (30 min)	80 ℃	OCV: H_2:O_2 =2:3 stoich; RH cycling: H_2/N_2= 250/250 sccm	1) Gas crossover: 14.3 mA cm^{-2}; 2) Fluoride emission rate at cathode side: 1.59 μg h^{-1} cm^{-2} 3) Delamination in the membrane layer and Pt agglomeration	[26]
Single cell, 25 cm^2, ①Nafion® 111 after treatment in Fenton's reagent for 72 h ② Novel composite membrane after treatment in Fenton's reagent for 72 h, 0.2 mg cm^{-2} cabon-based Pt on both the anode and cathode sides	OCV and RH	①60000 s ② 120000s	-	OCV : H2/air= 0% dry (8min)+100 % RH wet (2 min) RH cycling: 0% RH dry (8 min) + 25 % RH wet (2 min)	90 ℃	OCV: H_2/Air; RH cycling: Air for both sides	Gas crossover: ① 21.8 ± 0.1 mA/cm^2; ②7.3 ± 0.1 mA/cm^2	[117]
Single cell, 50 cm^2, Nafion® NRE212	OCV	56 h	-	OCV: D.P.a/c=90/90 ℃ (2 min)+ D.P.a/c=20/20 ℃ (2 min);	80 ℃	H_2/Air: 2000/2000 sccm, Backpressure:150/150 kPa	Voltage Decay: 82 mV	[113]
single cell 25 cm^2 NRE211 membranes,	OCV	100 h	-	OCV: 30% RH	90 ℃	H_2/Air: 0.2 SLPM;	1) Fluoride emission rate: 0.069h + 2.65 μmol/h;	[247]

0.4 mg/cm2 Pt on both the anode and cathode sides						atmospheric pressure	2) Voltage Decay: 1.3 mV/h; 3) Delamination in the membrane layer	

As is shown in Table 2, by the single mechanical degradation, Gittleman et al. [35] compared four membrane: partially fluorinated hydrocarbon, Nafion® NR-111, Gore-Select® 57, and Nafion® N111-IP membranes until the crossover was over 10 sccm/cell. Nafion® N111-IP showed the best mechanical durability, followed by Gore-Select® 57, Nafion® NR-111 and fluorinated hydrocarbon. Kjeang et al. [115] used two developed RH cyclings with different rates to test the fuel cell. Likewise, Vengatesan et al. [182] investigated the degradation of the membrane by applying unsymmetrical RH cycling on cell's the cathode and anode sides, which was run at a minimal "idle" current. It was found that the MEA suffered more severe degradation from anode RH cycling than from cathode RH cycling. In general, the tested durability of membranes under RH cycling will be reduced by the increasing frequency and amplitude of RH, temperature and gas pressure. In order to give evaluation criteria, the mechanical protocol of the membrane through the use of RH cycling from the DOE report (Updated May 2017) is presented in Table 3 [4]. The test can be stopped until a crossover >15 mA/cm^2 or 20,000 cycles.

Table 3. Membrane mechanical cycle protocol and metrics published by the DOE [4, 19]

Test conditions and metric	Target
Cycle gases	Air/air cycles at two SLPM on anode and cathode sides, respectively, in a single cell with active area 25–50 cm^2
Relative humidity	0% RH for 2 min and 90°C dew point for 2 min in a cycle
Test pressure	Ambient or no back pressure
Temperature	80 °C
Test time	Stopped after crossover is larger than 15 mA/cm^2 or 20,000 cycles
Crossover test (each 24 h)	<15 mA/cm^2 at 0 kPa pressure differential and at anode overpressure of 50 kPa or 0.1 sccm/cm^2 for air and N2 test at a 20 kPa pressure differential
Shorting resistance test (each 24 h)	>1,000 ohm cm^2 at 0.5 V, 100% RH N_2/N_2, 80°C

The DOE recommends protocols for mechanical and chemical stability that are usually adopted as the basis for the combined degradations of the MEA. The latest chemical/mechanical testing method is shown in Table 4. Drawing on the DOE protocols, Bender et al. [113] exposed the MEA to alternated H_2/air from a dew point of 90 ℃ and 20 ℃ every 2 min in OCV conditions. The MEA with defects showed a significant rate of degradation. Wu et al. [26] investigated the importance of the hot-pressing process and edge protection of MEA fabrication with an OCV and RH cycling AST,

which used a current density of 1.8 A cm^{-2}. Ballard Power System's cyclic OCV and RH cycling of the AST protocol were also used to test the fuel cell in Kjeang et al. [24, 242]. In this test, a low steady-state RH /high temperature OCV phase is applied to increase the chemical degradation, followed by a series of dry/wet humidity cycles in N_2 to induce mechanical degradation. In order to provide a closer to realistic application for heavy duty fuel cells in bus-related conditions, a milder AST method was used by increasing the RH at the dry cycle to increase the membrane failure time from 131 h to 300 h in their study [257]. In order to establish the relationship between true cell life and AST, Rodgers et al. [247] compared the degraded membranes from the performance evaluation test (PET) protocol close to automotive drive cycles of 184 h and OCV AST of 100 h with some decay modes, such as fluoride emission, membrane thinning and voltage decay. The relationship was found to be a function of the electrode catalyst and electrode ionomer.

Table 4. Membrane chemical/mechanical cycle protocol and metrics published by the DOE [4, 19].

Test conditions and metric	Target
Cycle gases	H_2/air cycles at 40 sccm/cm^2 on anode and cathode sides, respectively, in a single cell with active area 25–50 cm^2
Relative humidity	0% RH for 30 s and 90°C dew point for 45 s in a cycle
Test pressure	Ambient or no back pressure
Temperature	90 °C
Test time	Stopped after crossover is larger than 15 mA/cm^2 or 20,000 cycles
F-release or equivalent for nonfluorine membranes (each 24 h)	No target or unmarked
Hydrogen crossover (each 24 h)	<15 mA/cm^2 at 0 kPa pressure differential and at anode overpressure of 50 kPa
Continuous OCV	≥ 0.95 V at original wet conditions, <20% OCV loss during test
High-frequency resistance at 0.2 A/cm^2 (each 24 h)	No target or unmarked
Shorting resistance (each 24 h)	>1,000 ohm cm^2 at 0.5 V, 100% RH N_2/N_2, 80°C

5.2 Ex-situ method

The in-situ methods provide the pathway for investigating the process of the membrane's degradation under cell conditions. However, considering the observational convenience, some ex-situ methods are also necessary to characterize the membrane's mechanical properties and durability in more direct ways. This section presents some ex-situ methods from the point views of mechanical properties and failure modes.

5.2.1 Tensile tests

In fact, the membrane's mechanical properties vary along with the temperature and humidity conditions. A uniaxial tensile test [59, 60, 65, 270] is usually carried out using test machine equipped with chamber that can be operated in controlled environmental conditions. The membranes in dog-bone shape are stretched to break by the tensile force to get the stress-strain curves at different temperatures and relative humidities. Given the planar constraint in the fuel cell, the biaxial behavior of membrane is also investigated in some studies [80, 271, 272].

The yield stress, elastic modulus, UTS and final strain are usually used to evaluate the membrane's mechanical properties. The elastic modulus and yield stress can be used as indications of the membrane stiffness and strength, respectively. The final strain and UTS are defined as the total strain and maximum tensile stress, respectively [242, 257]. It should be noted that the polymer material is in terms of nonlinear behavior, in both the plastic and elastic parts of the stress-strain curve. Tang et al. [57] took the elastic modulus as the linear regression of the first linear component of the stress-strain curve. The greatest slope of a fifth order polynomial fit the first section from 0 to 0.5% strain and is usually also calculated as the elastic modulus [242, 257, 260]. The yielding behavior can be defined as the offset yield in the ASTM D882 standard [66] or the proportional limit yield used in the polymer material [57, 89, 260].

5.2.2 Fatigue and creep tests

In order to evaluate the membrane failure subjected to cyclic swelling and sustained stress, fatigue and creep to leak tests have been performed in the current studies. According to the conventional fatigue test, the membrane with the dog-bone geometry is exposed to cyclic uniaxial mechanical loading relevant to the fuel cell operation [226, 227, 259]. In terms of the number of stress cycles, the membrane's fatigue lifetime is obtained until the final rupture in various environmental conditions. It is worth mentioning that the measured membrane's lifetime is determined by the amplitude and frequency of applied stress due to its viscous characteristics. Creep damage in the membrane subjected to controlled temperature and RH is also tested using a constant load [102, 224, 273]. The creep strain under the stress and permanent left strain after load release are usually observed as a function of time.

To simulate the biaxial stress state of the constrained membrane in the operating fuel cell, a pressure-loaded blister is adopted by Dillard et al. [32, 80, 222, 228]. A pressure control apparatus is designed to produce various pressure histories as shown in Figure 22. Using the electrically operated valve, the gases could be imposed at any mode, including static pressure for creep and cyclic pressure for fatigue. The membrane is well constructed for observing the fracture through gas pressure loss. Furthermore, the fatigue and creep behaviors of the membrane are also investigated by FEM simulation combined with a Smith-Watson-Topper (SWT) fatigue formulation or crazing criteria in recent years [18, 226, 229].

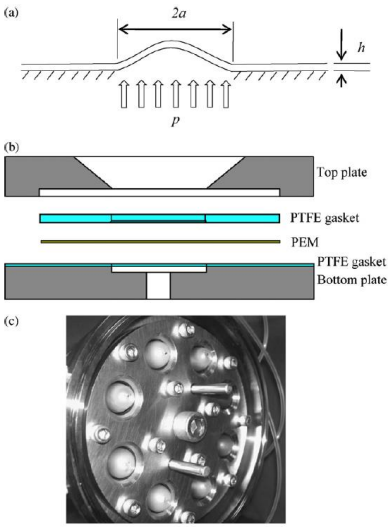

Figure 22. (a) The schematic drawing of pressure-loaded blister; (b) an single cell schematic of the device photographed in (c), which captures a test in progress(Permission from [222], copyright Elsvier)

5.2.3 Other tests

In order to investigate the wrinkle deformation, a bulking test is adopted to simulate the in-plane stress from membrane swelling. As is shown in Figure 23 designed by Uchiyama et al. [137-139], the membrane samples with the PI film are inserted between the GDLs in the fuel cell at the designated temperature. The hole in the PI film can be regarded as the clearance between the CCM and GDL. Gases with cyclic humidity are injected into the flow field. After the test, bulge deformation could be observed by microscope after the test.

Intrinsic fracture energy, consumed energy of the material that crack at an extremely low rate, is helpful for understanding the durability of the membrane under fatigue/creep loading conditions. In order to mitigate the effect of plastic deformation and the viscous dissipation close the crack tip, while a knife slit test is more feasible for obtaining intrinsic fracture energy than the double-edge notched tension test and trouser tear test [69, 116]. To approach the real intrinsic fracture energy, the tearing weight and cutting angel should be optimized with consideration to the humidity and temperature, and a small cutting rate is recommended. Using a knife slit test, Nafion® N111-IP and Gore-Select® 57 showe much higher fracture energy than Nafion NRE 211 [69]. This result is in accordance with their performance in AST tests [115, 269]. Hence, the knife slit test can be considered a tool for evaluating the various membranes.

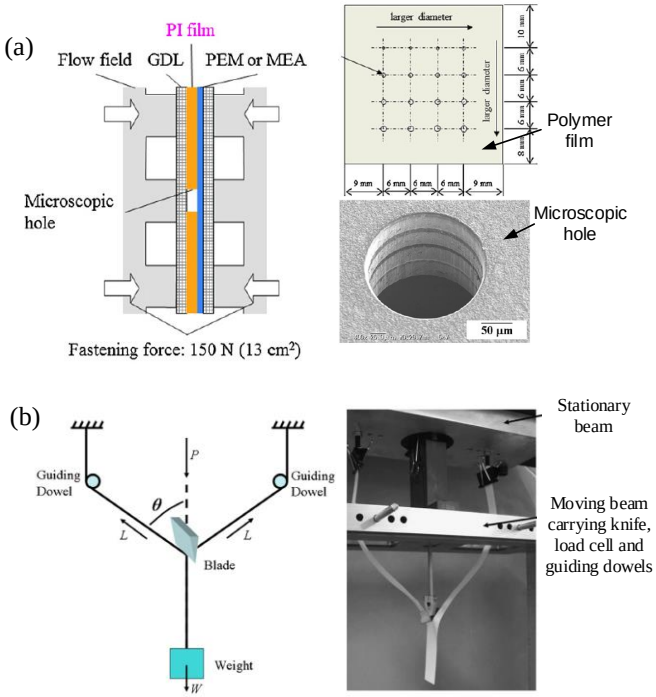

Figure 23. Schematic diagram and fixture used of (a) bulking test [139], and (b) knife slit test [116]. (Copyright Elsvier and Springer)

To observe the crack in the membrane, 2 dimentional (2D) techniques have been widely performed in current studies such as scanning electron microscopy (SEM) and atomic force microscope (AFM). However, only surface images can be genertated by these 2D methods, and the cracks have been destroyed in nature during the sample preparation process. In order to achieve the features with scope and depth in the membrane, 3D X-ray computed tomography (XCT), a non-destructive method, has been applied to obtain the insights reagrading the membrane failure in recent years. XCT is a technique that combines 2D images from different angles into 3D structure. It has proven to be a very advantageous approach to investigate mechanism of crack intiation and growth in the membrane by Kjeang et al. [274, 275].

6. Conclusion

At present, durability is still a critical issue standing in the way of the commercialization of PEM fuel cells. It has been found that in current studies, the lifetimes of fuel cell stacks achieve less than 3000 h operation once mechanical failure occurs in the membrane, and this is influenced by the material, fabrication technology and operational conditions. In particular, recent stacks have been directed to applying super thin membranes to increase proton conductivity and minimize ohmic losses in the cell. Therefore, a membrane's mechanical durability and integrity have become critical challenges and require continuing effort to rectify. This review has sought to address issues surrounding the key achievements in mechanical degradation and mitigation strategies for membrane failure to present major directions for further improvement.

In the last few years, considerable progress has been made in understanding and improving the

membrane durability. However, in accordance with our understanding of the mechanical durability of the membrane, there are still some key issues that should be addressed. A summary of the key conclusions and research interests is given as follows:

1) PFSA membranes continue to maintain their positon as the proton conducting polymer of choice due to their stability and durability in the cell condition. The durability of the membrane is highly influenced by its mechanical features, which are sensitive to humidity, temperature and time. The stress-strain curves of membranes monotonically drop with the increasing humidity and temperature because of a declining intermolecular force and amorphous domain. Water plasticizes membranes at lower temperatures, but stiffens the material at higher temperatures because of the increasing bonding energy within sulfonic acid groups caused by water. In order to analyze the membrane mechanical failure, two kinds of materially constitutive models are proposed to illustrate its mechanical behavior, including a physical model based on molecular chain mobility and a phenomenological model based on typical elastic-plastic theory in a linear/nonlinear, viscous/non-viscous way.

In order to understand its mechanical behavior and degradation in the cell environment, many studies have been conducted in recent years to address the membrane's mechanical properties. However, most of these efforts focus on the pure membrane. There is a lack of information about CCM, in which catalysts adhere to membranes as a composite material to work together. The combined action and interaction between them is important for mechanical durability when subjected to humidity, temperature and time. Moreover, constitutive models and the failure criteria of this polymeric material are still not powerful enough to precisely support the prediction of mechanical failure in the fuel cell.

2) With respect to membrane defects such as pinhole and thickness variation, these contribute to mechanical failure by weaking mechanical strength, contact resistance, and the inhomogeneity of the reaction efficiency, the flooded area, heat generation and catalyst erosion. To reduce the membrane defects and improve the fabrication process, reinforced membranes with PTFE and some inorganic materials are developed, and ion beam morphology and hot pressing are proposed to obtain good initial contact between the membrane and CL.

Although adverse effects of membrane defects are well known, various types of damage evolution through defects must be evaluated in greater depth to better understand the weaker regions. Great achievements have been made in strengthening the membrane by modifying its material composition, such as the additive PTFE. However, the requirement of ultrathin membranes in commercial fuel cells creates a higher risk of mechanical failure. Improving the material composition and fabrication process are the preferred choices for increas membrane durability.

3) Since a typical fuel cell stack is complex and consists of numerous components, degradation of the membrane depends not only on the individual component, but also the interaction with all

parts, as well as the assembly process. Uneven contact pressure between the ribs of the flow field and GDL, resulting from the channel feature, endplate deformation, assembly force and manufacturing error of components, will induce bending and shear stress on the MEA, contributing to wrinkle of the membrane and delamination between it and the CL. A common mode of mechanical failure lies at the edge of membranes due to the stress concentration on joint area between the MEA frame and membrane. The material of the MEA frame with mechanical characters close to the membrane is preferred.

Manufacturing error in the fuel cell is inevitable due to the characteristics of the fabrication process, especially the cell with promising metallic BPPs. A tradeoff is expected to balance the low error level and cost of improving accuracy. The assembly process should then be further optimized so as to provide a more comfortable mechanical environment for the membrane and avoid potential deterioration in the subsequent cell operation.

4) The membrane's mechanical failure is the main cause of a running stop during a fuel cell's short-term operation phase. During fuel cell operation, in-plane stress along the mid-channel is found to be the dominant stress factor in the membrane due to swelling. The nonuniform distribution of humidity and temperature prove to have a negative effect on the membrane's deformation. In particular, freeze/thaw cycling can seriously compromise durability. Although conflicting results are demonstrated in the literature, it is accepted by some researchers that pinhole and delamination may occur in the membrane during the freeze/thaw operation. A fracture at the membrane edge (along the frame) is the source of the fast change in gas crossover and performance decay. This is caused by the peak stresses within the seal joint/GDL interface, which can be explained by the pushment from GDL, membrane swelling, a shock of reactant gases, fabricated flaw and the hot spot.

Research on the membrane's mechanical properties in the subfreezing environment is fairly limited. Considering the various states of the water molecules at sub-zero temperatures, understanding the membrane mechanical properties at subzero temperatures needs more effort. The effect of freeze-thaw operation on the membrane should be investigated in greater detail. More effective strategies should be adopted to reduce solid ice formation, which may result in crack and delamination of the membrane, porosity changes in the material, and a loss in the catalyst area. The gasket seal or adhesive protection layer is also helpful for eliminating fast failure around the membrane edge.

5) As for long-term operation, the membrane is subjected to cyclic hydration, thermal and reactant gas pressure. Wrinkle, creep, fatigue and final fracture are usually caused in the membrane after cyclic swelling/shrinkage. CL crack and clearance between the CL and membrane contribute to the wrinkle deformation. Reducing the amplitude and frequency of humidity/current cycling is an effective way to decreasing the membrane fatigue. The pressure difference of the gas flow between the anode and cathode can accelerate membrane degradation, especially in the air outlet

region. In addition to these physical loads, chemical degradation would simultaneously accelerate its mechanical failure through the degraded and disentangled microstructure of membranes. For the combined CCM, a decrease in mechanical strength and stiffness is obtained. Catalyst cracks will also contribute to the premature failure of the membrane due to concentrated stress.

However, in order to predict the lifetime, improvement on the fatigue model is still needed to determine the membrane's failure. The effect of vibrations on mechanical damage in the fuel cell has not been revealed in detail. The question remains as to what type of failure (wrinkle, creep, fatigue, delamination, pinhole, etc.) arises, how cracks propagate and where failures first occur in the large scale ductile membrane in the cell. The synergetic mechanism of the mechanical and chemical degradation is still not clear across the whole lifetime of the fuel cell. During the cell operation, the growth process of the further dynamic of the Pt band in the membrane, as well as its influence mechanism on durability, requires more investigation.

6) It should be noted that even though there have been a large number of studies dedicated to membrane durability, it is very difficult to compare and complement these. In-situ and ex-situ methods for the evaluation and characterization of mechanical durability are summarized to pursue the measurement methods and protocols of membranes. DOE protocols for mechanical and chemical stability are usually adopted as the basis for the degradations of the membrane. The establishment of in-situ and ex-situ protocols will create a standard set of test conditions and operational procedures for membrane durability. The completion and unanimity of protocols as a whole, as well as the relationship between the test results and actual lifetime, are important research goals for the near future.

7. Acknowledgements

This work was carried out within the projects supported by the National Natural Science Foundation of China (No. 51705308), and the China Postdoctoral Science Foundation (No. 2016M601592, 2018T110393). The authors also thank Christopher Wood for the language improvement.

8. Conflicts of interest

There are no conflicts of interest to declare.

9. References

[1] Guerrero Moreno N, Cisneros Molina M, Gervasio D, Pérez Robles JF. Approaches to polymer electrolyte membrane fuel cells (PEMFCs) and their cost. Renewable and Sustainable Energy Reviews. 2015;52:897-906.

[2] Iwan A, Malinowski M, Pasciak G. Polymer fuel cell components modified by graphene: Electrodes, electrolytes and bipolar plates. Renewable and Sustainable Energy Reviews. 2015;49:954-67.
[3] Schmittinger W, Vahidi A. A review of the main parameters influencing long-term performance and durability of PEM fuel cells. J Power Sources. 2008;180:1-14.
[4] DOE U. Multiyear Research Development and Demonstration Plan: Planned program activities for 2011-2020. In: Office DFCT, editor.: US Department of Energy; 2017. p. 3.4.
[5] Liu W, Ruth K, Rusch G. The membrane durability in PEM fuel cells. J New Mater Electrochem Syst. 2001;4:227-32.
[6] St-Pierre J, Jia N. Successful demonstration of ballard PEMFCS for space shuttle applications. Journal of New Materials for Electrochemical Systems. 2002;5:263-72.
[7] Curtin DE, Lousenberg RD, Henry TJ, Tangeman PC, Tisack ME. Advanced materials for improved PEMFC performance and life. Journal of power Sources. 2004;131:41-8.
[8] Knights SD, Colbow KM, St-Pierre J, Wilkinson DP. Aging mechanisms and lifetime of PEFC and DMFC. Journal of Power Sources. 2004;127:127-34.
[9] Yu J, Matsuura T, Yoshikawa Y, Islam MN, Hori M. In situ analysis of performance degradation of a PEMFC under nonsaturated humidification. Electrochemical and solid-state letters. 2005;8:A156-A8.
[10] Yoshioka S, Yoshimura A, Fukumoto H, Hiroi O, Yoshiyasu H. Development of a PEFC under low humidified conditions. Journal of power sources. 2005;144:146-51.
[11] Liu D, Case S. Durability study of proton exchange membrane fuel cells under dynamic testing conditions with cyclic current profile. Journal of Power Sources. 2006;162:521-31.
[12] Chiem BH, Beattie P, Colbow K. The development and demonstration of technology on the path to commercially viable PEM fuel cell stacks. ECS Transactions. 2008;16:1927-35.
[13] Wu J, Yuan X-Z, Martin JJ, Wang H, Yang D, Qiao J, et al. Proton exchange membrane fuel cell degradation under close to open-circuit conditions. J Power Sources. 2010;195:1171-6.
[14] Yuan X-Z, Zhang S, Wang H, Wu J, Sun JC, Hiesgen R, et al. Degradation of a polymer exchange membrane fuel cell stack with Nafion® membranes of different thicknesses: Part I. In situ diagnosis. J Power Sources. 2010;195:7594-9.
[15] De Moor G, Bas C, Charvin N, Moukheiber E, Niepceron F, Breilly N, et al. Understanding Membrane Failure in PEMFC: Comparison of Diagnostic Tools at Different Observation Scales. Fuel Cells. 2012;12:356-64.
[16] Ruiu T, Dreizler AM, Mitzel J, Gülzow E. Evaluation of a 2.5 kWel automotive low temperature PEM fuel cell stack with extended operating temperature range up to 120 °C. Journal of Power Sources. 2016;303:257-66.
[17] Han I-S, Kho B-K, Cho S. Development of a polymer electrolyte membrane fuel cell stack for an underwater vehicle. Journal of Power Sources. 2016;304:244-54.
[18] Khorasany RM, Kjeang E, Wang G, Rajapakse R. Simulation of ionomer membrane fatigue under

mechanical and hygrothermal loading conditions. Journal of Power Sources. 2015;279:55-63.

[19] Inaba M, Kinumoto T, Kiriake M, Umebayashi R, Tasaka A, Ogumi Z. Gas crossover and membrane degradation in polymer electrolyte fuel cells. Electrochim Acta. 2006;51:5746-53.

[20] Teranishi K, Kawata K, Tsushima S, Hirai S. Degradation mechanism of PEMFC under open circuit operation. Electrochemical and Solid-State Letters. 2006;9:A475-A7.

[21] Wong CY, Wong WY, Loh KS, Mohamad AB. Study of the plasticising effect on polymer and its development in fuel cell application. Renewable and Sustainable Energy Reviews. 2017;79:794-805.

[22] Ghassemzadeh L, Peckham TJ, Weissbach T, Luo X, Holdcroft S. Selective formation of hydrogen and hydroxyl radicals by electron beam irradiation and their reactivity with perfluorosulfonated acid ionomer. Journal of the American Chemical Society. 2013;135:15923-32.

[23] Ghassemzadeh L, Holdcroft S. Quantifying the structural changes of perfluorosulfonated acid ionomer upon reaction with hydroxyl radicals. Journal of the American Chemical Society. 2013;135:8181-4.

[24] Lim C, Ghassemzadeh L, Van Hove F, Lauritzen M, Kolodziej J, Wang G, et al. Membrane degradation during combined chemical and mechanical accelerated stress testing of polymer electrolyte fuel cells. Journal of Power Sources. 2014;257:102-10.

[25] Kusoglu A, Santare MH, Karlsson AM. Aspects of fatigue failure mechanisms in polymer fuel cell membranes. Journal of Polymer Science Part B: Polymer Physics. 2011;49:1506-17.

[26] Wu B, Zhao M, Shi W, Liu W, Liu J, Xing D, et al. The degradation study of Nafion/PTFE composite membrane in PEM fuel cell under accelerated stress tests. Int J Hydrogen Energ. 2014;39:14381-90.

[27] Grigoriev SA, Dzhus KA, Bessarabov DG, Millet P. Failure of PEM water electrolysis cells: Case study involving anode dissolution and membrane thinning. International Journal of Hydrogen Energy. 2014;39:20440-6.

[28] Ye D, Tu Z, Yu Y, Cai Y, Zhang H, Zhan Z, et al. Hydrogen permeation across super-thin membrane and the burning limitation in low-temperature proton exchange membrane fuel cell. Int J Energ Res. 2014;38:1181-91.

[29] Wu J, Yuan XZ, Martin JJ, Wang H, Zhang J, Shen J, et al. A review of PEM fuel cell durability: Degradation mechanisms and mitigation strategies. J Power Sources. 2008;184:104-19.

[30] Tang H, Peikang S, Jiang SP, Wang F, Pan M. A degradation study of Nafion proton exchange membrane of PEM fuel cells. J Power Sources. 2007;170:85-92.

[31] Kim S, Mench MM. Physical degradation of membrane electrode assemblies undergoing freeze/thaw cycling: Micro-structure effects. J Power Sources. 2007;174:206-20.

[32] Pestrak M, Li Y, Case SW, Dillard DA, Ellis MW, Lai Y-H, et al. The effect of mechanical fatigue on the lifetimes of membrane electrode assemblies. Journal of Fuel Cell Science and Technology. 2010;7:041009.

[33] de Bruijn F. The current status of fuel cell technology for mobile and stationary applications. Green

Chem. 2005;7:132-50.
[34] Kundu S, Fowler MW, Simon LC, Grot S. Morphological features (defects) in fuel cell membrane electrode assemblies. J Power Sources. 2006;157:650-6.
[35] Lai YH, Dillard DA. Mechanical durability characterization and modeling of ionomeric membranes. Handbook of Fuel Cells: John Wiley & Sons, Ltd; 2010.
[36] Andújar JM, Segura F. Fuel cells: History and updating. A walk along two centuries. Renewable and sustainable energy reviews. 2009;13:2309-22.
[37] Peighambardoust SJ, Rowshanzamir S, Amjadi M. Review of the proton exchange membranes for fuel cell applications. International Journal of Hydrogen Energy. 2010;35:9349-84.
[38] Brandell D, Karo J, Liivat A, Thomas JO. Molecular dynamics studies of the Nafion®, Dow® and Aciplex® fuel-cell polymer membrane systems. Journal of molecular modeling. 2007;13:1039-46.
[39] Rikukawa M, Sanui K. Proton-conducting polymer electrolyte membranes based on hydrocarbon polymers. Progress in Polymer Science. 2000;25:1463-502.
[40] Jiang R, Fuller T, Brawn S, Gittleman C. Perfluorocyclobutane and poly (vinylidene fluoride) blend membranes for fuel cells. Electrochimica Acta. 2013;110:306-15.
[41] Zakil FA, Kamarudin SK, Basri S. Modified Nafion membranes for direct alcohol fuel cells: An overview. Renewable and Sustainable Energy Reviews. 2016;65:841-52.
[42] Dihrab SS, Sopian K, Alghoul MA, Sulaiman MY. Review of the membrane and bipolar plates materials for conventional and unitized regenerative fuel cells. Renewable and Sustainable Energy Reviews. 2009;13:1663-8.
[43] Peron J, Shi Z, Holdcroft S. Hydrocarbon proton conducting polymers for fuel cell catalyst layers. Energy & Environmental Science. 2011;4:1575-91.
[44] Wu QX, Pan ZF, An L. Recent advances in alkali-doped polybenzimidazole membranes for fuel cell applications. Renewable and Sustainable Energy Reviews. 2018;89:168-83.
[45] Mao SS, Lewinski KA, Ylitalo DA. Sulfonated perfluorocyclobutane ion-conducting membranes. Google Patents; 2003.
[46] Serpico J, Ehrenberg S, Fontanella J, Jiao X, Perahia D, McGrady K, et al. Transport and structural studies of sulfonated styrene− ethylene copolymer membranes. Macromolecules. 2002;35:5916-21.
[47] Xing P, Robertson GP, Guiver MD, Mikhailenko SD, Wang K, Kaliaguine S. Synthesis and characterization of sulfonated poly (ether ether ketone) for proton exchange membranes. Journal of Membrane Science. 2004;229:95-106.
[48] Genies C, Mercier R, Sillion B, Cornet N, Gebel G, Pineri M. Soluble sulfonated naphthalenic polyimides as materials for proton exchange membranes. Polymer. 2001;42:359-73.
[49] Guo X, Fang J, Watari T, Tanaka K, Kita H, Okamoto K-i. Novel sulfonated polyimides as polyelectrolytes for fuel cell application. 2. Synthesis and proton conductivity of polyimides from 9, 9-bis (4-aminophenyl) fluorene-2, 7-disulfonic acid. Macromolecules. 2002;35:6707-13.

[50] Steenberg T, Hjuler HA, Terkelsen C, Sanchez MTR, Cleemann LN, Krebs FC. Roll-to-roll coated PBI membranes for high temperature PEM fuel cells. Energy & Environmental Science. 2012;5:6076-80.

[51] Li N, Lee SY, Liu Y-L, Lee YM, Guiver MD. A new class of highly-conducting polymer electrolyte membranes: Aromatic ABA triblock copolymers. Energy & Environmental Science. 2012;5:5346-55.

[52] Zhang H, Shen PK. Recent development of polymer electrolyte membranes for fuel cells. Chemical reviews. 2012;112:2780-832.

[53] Reyna-Valencia A, Kaliaguine S, Bousmina M. Tensile mechanical properties of sulfonated poly(ether ether ketone) (SPEEK) and BPO4/SPEEK membranes. Journal of Applied Polymer Science. 2005;98:2380-93.

[54] Meyer G, Perrot C, Gebel G, Gonon L, Morlat S, Gardette J-L. Ex situ hydrolytic degradation of sulfonated polyimide membranes for fuel cells. Polymer. 2006;47:5003-11.

[55] Huang X, Solasi R, Zou Y, Feshler M, Reifsnider K, Condit D, et al. Mechanical endurance of polymer electrolyte membrane and PEM fuel cell durability. Journal of Polymer Science Part B: Polymer Physics. 2006;44:2346-57.

[56] Kusoglu A, Tang Y, Santare MH, Karlsson AM, Cleghorn S, Johnson WB. Stress-strain behavior of perfluorosulfonic acid membranes at various temperatures and humidities: experiments and phenomenological modeling. ASME J Fuel Cell Sci Technol. 2009;6:011012.

[57] Tang Y, Karlsson AM, Santare MH, Gilbert M, Cleghorn S, Johnson WB. An experimental investigation of humidity and temperature effects on the mechanical properties of perfluorosulfonic acid membrane. Materials Science and Engineering: A. 2006;425:297-304.

[58] Solasi R, Zou Y, Huang X, Reifsnider K, Condit D. On mechanical behavior and in-plane modeling of constrained PEM fuel cell membranes subjected to hydration and temperature cycles. J Power Sources. 2007;167:366-77.

[59] Satterfield MB, Benziger JB. Viscoelastic properties of Nafion at elevated temperature and humidity. Journal of Polymer Science Part B: Polymer Physics. 2009;47:11-24.

[60] Satterfield MB, Majsztrik PW, Ota H, Benziger JB, Bocarsly AB. Mechanical properties of Nafion and titania/Nafion composite membranes for polymer electrolyte membrane fuel cells. Journal of Polymer Science Part B: Polymer Physics. 2006;44:2327-45.

[61] Kundu S, Simon LC, Fowler M, Grot S. Mechanical properties of Nafion™ electrolyte membranes under hydrated conditions. Polymer. 2005;46:11707-15.

[62] Lu Z, Lugo M, Santare MH, Karlsson AM, Busby FC, Walsh P. An experimental investigation of strain rate, temperature and humidity effects on the mechanical behavior of a perfluorosulfonic acid membrane. J Power Sources. 2012;214:130-6.

[63] Shi S, Liu D, Liu D, Tae P, Gao CY, Yan L, et al. Mechanical properties and microstructure changes of proton exchange membrane under immersed conditions. Polymer Engineering & Science.

2014;54:2215-21.

[64] Silberstein MN. Mechanics of proton exchange membranes: time, temperature, and hydration dependence of the stress-strain behavior of persulfonated polytetrafluorethylene: Massachusetts Institute of Technology; 2008.

[65] Tang Y, Kusoglu A, Karlsson AM, Santare MH, Cleghorn S, Johnson WB. Mechanical properties of a reinforced composite polymer electrolyte membrane and its simulated performance in PEM fuel cells. J Power Sources. 2008;175:817-25.

[66] Testing ASf, Materials. Standard Test Method for Tensile Properties of Thin Plastic Sheeting: ASTM International; 2010.

[67] Zhou Y, Lin G, Shih AJ, Hu SJ. Assembly pressure and membrane swelling in PEM fuel cells. J Power Sources. 2009;192:544-51.

[68] Dillard DA, Lai Y-H, Budinski M, Gittleman C. Tear resistance of proton exchange membranes. ASME 2005 3rd International Conference on Fuel Cell Science, Engineering and Technology: American Society of Mechanical Engineers; 2005. p. 153-9.

[69] Patankar K, Dillard DA, Case SW, Ellis MW, Li Y, Lai Y-H, et al. Characterizing fracture energy of proton exchange membranes using a knife slit test. Journal of Polymer Science Part B: Polymer Physics. 2010;48:333-43.

[70] Bauer F, Denneler S, Willert-Porada M. Influence of temperature and humidity on the mechanical properties of Nafion® 117 polymer electrolyte membrane. Journal of Polymer Science Part B: Polymer Physics. 2005;43:786-95.

[71] Uan-Zo-li JT. The effects of structure, humidity and aging on the mechanical properties of polymeric ionomers for fuel cell applications. 2001.

[72] Shao Z-G, Xu H, Li M, Hsing I-M. Hybrid Nafion–inorganic oxides membrane doped with heteropolyacids for high temperature operation of proton exchange membrane fuel cell. Solid State Ionics. 2006;177:779-85.

[73] Kim YM, Choi SH, Lee HC, Hong MZ, Kim K, Lee H-I. Organic–inorganic composite membranes as addition of SiO 2 for high temperature-operation in polymer electrolyte membrane fuel cells (PEMFCs). Electrochimica Acta. 2004;49:4787-96.

[74] Majsztrik PW, Bocarsly AB, Benziger JB. Viscoelastic Response of Nafion. Effects of Temperature and Hydration on Tensile Creep. Macromolecules. 2008;41:9849-62.

[75] Satterfield MB. Mechanical and water sorption properties of Nafion and composite Nafion/titanium dioxide membranes for polymer electrolyte membrane fuel cells: Princeton University; 2007.

[76] Majsztrik P, Bocarsly A, Benziger J. An instrument for environmental control of vapor pressure and temperature for tensile creep and other mechanical property measurements. Review of Scientific Instruments. 2007;78:103904.

[77] Khattra NS, Karlsson AM, Santare MH, Walsh P, Busby FC. Effect of time-dependent material

properties on the mechanical behavior of PFSA membranes subjected to humidity cycling. J Power Sources. 2012;214:365-76.
[78] Yoon W, Huang X. A nonlinear viscoelastic–viscoplastic constitutive model for ionomer membranes in polymer electrolyte membrane fuel cells. Journal of Power Sources. 2011;196:3933-41.
[79] Xiao Y, Cho C. Experimental Investigation and Discussion on the Mechanical Endurance Limit of Nafion Membrane Used in Proton Exchange Membrane Fuel Cell. Energies. 2014;7:6401-11.
[80] Dillard DA, Li Y, Grohs JR, Case SW, Ellis MW, Lai Y-H, et al. On the use of pressure-loaded blister tests to characterize the strength and durability of proton exchange membranes. Journal of Fuel Cell Science and Technology. 2009;6:031014.
[81] May JA, Ellis MW, Dillard DA, Case SW, Moore RB, Li Y, et al. Development and Validation of a Uniaxial Nonlinear Viscoelastic Viscoplastic Stress Model for a Fuel Cell Membrane. ASME J Fuel Cell Sci Technol. 2016;12:061011.
[82] Flory P. Theory of elasticity of polymer networks. The effect of local constraints on junctions. The Journal of Chemical Physics. 1977;66:5720-9.
[83] Treloar LRG. The physics of rubber elasticity: Oxford University Press, USA; 1975.
[84] James HM, Guth E. Theory of the elastic properties of rubber. The Journal of Chemical Physics. 1943;11:455-81.
[85] Arruda EM, Boyce MC. A three-dimensional constitutive model for the large stretch behavior of rubber elastic materials. Journal of the Mechanics and Physics of Solids. 1993;41:389-412.
[86] Anand L. A constitutive model for compressible elastomeric solids. Computational Mechanics. 1996;18:339-55.
[87] Bergström JS, Boyce MC. Constitutive modeling of the large strain time-dependent behavior of elastomers. Journal of the Mechanics and Physics of Solids. 1998;46:931-54.
[88] Bergström J, Hilbert L. A constitutive model for predicting the large deformation thermomechanical behavior of fluoropolymers. Mech Mater. 2005;37:899-913.
[89] Silberstein MN, Boyce MC. Constitutive modeling of the rate, temperature, and hydration dependent deformation response of Nafion to monotonic and cyclic loading. Journal of Power Sources. 2010;195:5692-706.
[90] Riku I, Mimura K. Computational characterization on mechanical behavior of polymer electrolyte membrane based on nonaffine molecular chain network model. International Journal of Mechanical Sciences. 2010;52:287-94.
[91] Kusoglu A, Karlsson AM, Santare MH, Cleghorn S, Johnson WB. Mechanical response of fuel cell membranes subjected to a hygro-thermal cycle. Journal of Power Sources. 2006;161:987-96.
[92] Tang Y, Santare MH, Karlsson AM, Cleghorn S, Johnson WB. Stresses in Proton Exchange Membranes Due to Hygro-Thermal Loading. Journal of Fuel Cell Science and Technology. 2005;3:119-24.

[93] Kusoglu A, Karlsson A, Santare M, Cleghorn S, Johnson WB. Investigation of stress and water distribution in Membrane Electrode Assembly (MEA) during fuel cell operation. ECS Transactions. 2008;16:551-61.

[94] Kusoglu A, Santare MH, Karlsson AM, Cleghorn S, Johnson WB. Numerical investigation of mechanical durability in polymer electrolyte membrane fuel cells. J Electrochem Soc. 2010;157:B705-B13.

[95] Lu Z, Kim C, Karlsson AM, Cross Iii JC, Santare MH. Effect of gas diffusion layer modulus and land–groove geometry on membrane stresses in proton exchange membrane fuel cells. Journal of Power Sources. 2011;196:4646-54.

[96] Hill R. The mathematical theory of plasticity: Oxford university press; 1998.

[97] Ferry JD. Viscoelastic properties of polymers: John Wiley & Sons; 1980.

[98] Lai Y-H, Mittelsteadt CK, Gittleman CS, Dillard DA. Viscoelastic stress model and mechanical characterization of perfluorosulfonic acid (PFSA) polymer electrolyte membranes. ASME 2005 3rd International Conference on Fuel Cell Science, Engineering and Technology: American Society of Mechanical Engineers; 2005. p. 161-7.

[99] Lai Y-H, Mittelsteadt CK, Gittleman CS, Dillard DA. Viscoelastic Stress Analysis of Constrained Proton Exchange Membranes Under Humidity Cycling. ASME J Fuel Cell Sci Technol. 2009;6:021002-.

[100] Christensen R. Theory of viscoelasticity: an introduction: Elsevier; 2012.

[101] Patankar KA, Dillard DA, Case SW, Ellis MW, Lai Y-H, Budinski MK, et al. Hygrothermal characterization of the viscoelastic properties of Gore-Select® 57 proton exchange membrane. Mechanics of Time-Dependent Materials. 2008;12:221-36.

[102] Solasi R, Zou Y, Huang X, Reifsnider K. A time and hydration dependent viscoplastic model for polyelectrolyte membranes in fuel cells. Mechanics of Time-Dependent Materials. 2007;12:15-30.

[103] Silberstein MN, Boyce MC. Hygro-thermal mechanical behavior of Nafion during constrained swelling. J Power Sources. 2011;196:3452-60.

[104] Banan R, Zu J, Bazylak A. Humidity and Temperature Cycling Effects on Cracks and Delaminations in PEMFCs. Fuel Cells. 2015;15:327-36.

[105] Hadid M, Rechak S, Zouani A. Empirical nonlinear viscoelastic model for injection molded thermoplastic composite. Polymer Composites. 2002;23:771-8.

[106] Oliver WC, Pharr GM. An improved technique for determining hardness and elastic modulus using load and displacement sensing indentation experiments. Journal of materials research. 1992;7:1564-83.

[107] Schapery RA. On the characterization of nonlinear viscoelastic materials. Polymer Engineering & Science. 1969;9:295-310.

[108] Zapas L, Crissman J. Creep and recovery behaviour of ultra-high molecular weight polyethylene in the region of small uniaxial deformations. Polymer. 1984;25:57-62.

[109] Tobolsky A, Eyring H. Mechanical properties of polymeric materials. The Journal of Chemical

Physics. 1943;11:125-34.
[110] Burlatsky SF, Gummalla M, O'Neill J, Atrazhev VV, Varyukhin AN, Dmitriev DV, et al. A mathematical model for predicting the life of polymer electrolyte fuel cell membranes subjected to hydration cycling. J Power Sources. 2012;215:135-44.
[111] Kusoglu A, Weber AZ. A mechanistic model for pinhole growth in fuel-cell membranes during cyclic loads. J Electrochem Soc. 2014;161:E3311-E22.
[112] Banan R, Bazylak A, Zu J. Effect of mechanical vibrations on damage propagation in polymer electrolyte membrane fuel cells. Int J Hydrogen Energ. 2013;38:14764-72.
[113] Bender G, Felt W, Ulsh M. Detecting and localizing failure points in proton exchange membrane fuel cells using IR thermography. J Power Sources. 2014;253:224-9.
[114] Lu Z, Santare MH, Karlsson AM, Busby FC, Walsh P. Time-dependent mechanical behavior of proton exchange membrane fuel cell electrodes. J Power Sources. 2014;245:543-52.
[115] Alavijeh AS, Khorasany RM, Nunn Z, Habisch A, Lauritzen M, Rogers E, et al. Microstructural and Mechanical Characterization of Catalyst Coated Membranes Subjected to In Situ Hygrothermal Fatigue. Journal of The Electrochemical Society. 2015;162:F1461-F9.
[116] Li Y, Quincy JK, Case SW, Ellis MW, Dillard DA, Lai Y-H, et al. Characterizing the fracture resistance of proton exchange membranes. J Power Sources. 2008;185:374-80.
[117] Tang H, Pan M, Wang F, Shen PK, Jiang SP. Highly Durable Proton Exchange Membranes for Low Temperature Fuel Cells. The Journal of Physical Chemistry B. 2007;111:8684-90.
[118] Tripathi BP, Shahi VK. Organic–inorganic nanocomposite polymer electrolyte membranes for fuel cell applications. Progress in Polymer Science. 2011;36:945-79.
[119] Adjemian K, Lee S, Srinivasan S, Benziger J, Bocarsly A. Silicon oxide nafion composite membranes for proton-exchange membrane fuel cell operation at 80-140 C. Journal of the Electrochemical Society. 2002;149:A256-A61.
[120] Lee C, Park JH, Jeon Y, Park J-I, Einaga H, Truong YB, et al. Phosphate modified TiO2/ZrO2 nanofibrous web composite membrane for enhanced performance and durability of high temperature PEM fuel cells. Energy & Fuels. 2017.
[121] Chalkova E, Fedkin MV, Wesolowski DJ, Lvov SN. Effect of TiO2 surface properties on performance of Nafion-based composite membranes in high temperature and low relative humidity PEM fuel cells. Journal of the electrochemical society. 2005;152:A1742-A7.
[122] Lee DC, Yang HN, Park SH, Kim WJ. Nafion/graphene oxide composite membranes for low humidifying polymer electrolyte membrane fuel cell. Journal of Membrane Science. 2014;452:20-8.
[123] Farooqui UR, Ahmad AL, Hamid NA. Graphene oxide: A promising membrane material for fuel cells. Renewable and Sustainable Energy Reviews. 2018;82:714-33.
[124] Yang C, Srinivasan S, Bocarsly A, Tulyani S, Benziger J. A comparison of physical properties and fuel cell performance of Nafion and zirconium phosphate/Nafion composite membranes. Journal of

Membrane Science. 2004;237:145-61.
[125] Zhai Y, Zhang H, Zhang Y, Xing D. A novel H3PO4/Nafion–PBI composite membrane for enhanced durability of high temperature PEM fuel cells. Journal of Power Sources. 2007;169:259-64.
[126] Fenton JM, Rodgers MP, Slattery DK, Huang X, Mittal VO, Bonville LJ, et al. Membrane degradation mechanisms and accelerated durability testing of proton exchange membrane fuel cells. ECS Transactions. 2009;25:233-47.
[127] Cho SA, Cho EA, Oh IH, Kim HJ, Ha HY, Hong SA, et al. Surface modified Nafion® membrane by ion beam bombardment for fuel cell applications. Journal of Power Sources. 2006;155:286-90.
[128] Zhang J, Yin G-P, Wang Z-B, Lai Q-Z, Cai K-D. Effects of hot pressing conditions on the performances of MEAs for direct methanol fuel cells. Journal of Power Sources. 2007;165:73-81.
[129] Uchiyama T, Kumei H, Yoshida T, Ishihara K. Static friction force between catalyst layer and micro porous layer and its effect on deformations of membrane electrode assemblies under swelling. J Power Sources. 2014;272:522-30.
[130] Ye D, Zhan Z, Lee Y, Tu Z, Zhang Y, Pan M. Effects of Frame Materials and Structures on Stress Concentration of Membrane Electrode Assembly of PEMFCs. Fuel Cells. 2013;13:1205-12.
[131] Nitta I, Karvonen S, Himanen O, Mikkola M. Modelling the Effect of Inhomogeneous Compression of GDL on Local Transport Phenomena in a PEM Fuel Cell. Fuel Cells. 2008;8:410-21.
[132] García-Salaberri PA, Vera M, Zaera R. Nonlinear orthotropic model of the inhomogeneous assembly compression of PEM fuel cell gas diffusion layers. Int J Hydrogen Energ. 2011;36:11856-70.
[133] Tang Y, Cleghorn S, Johnson WB, Santare MH, Karlsson AM. Stresses in Proton Exchange Membranes Due to Hygro-Thermal Loading. ASME J Fuel Cell Sci Technol. 2005;3:119-24.
[134] Ciavarella M, Hills DA, Monno G. The influence of rounded edges on indentation by a flat punch. Proceedings of the Institution of Mechanical Engineers, Part C: Journal of Mechanical Engineering Science. 1998;212:319-27.
[135] Hottinen T, Himanen O, Karvonen S, Nitta I. Inhomogeneous compression of PEMFC gas diffusion layer: Part II. Modeling the effect. J Power Sources. 2007;171:113-21.
[136] Su ZY, Liu CT, Chang HP, Li CH, Huang KJ, Sui PC. A numerical investigation of the effects of compression force on PEM fuel cell performance. J Power Sources. 2008;183:182-92.
[137] Uchiyama T, Kumei H, Yoshida T. Catalyst layer cracks by buckling deformation of membrane electrode assemblies under humidity cycles and mitigation methods. Journal of Power Sources. 2013;238:403-12.
[138] Uchiyama T, Kato M, Ikogi Y, Yoshida T. Mechanical Degradation Mechanism of Membrane Electrode Assemblies in Buckling Test Under Humidity Cycles. ASME J Fuel Cell Sci Technol. 2012;9:061005-.
[139] Uchiyama T, Kato M, Yoshida T. Buckling deformation of polymer electrolyte membrane and membrane electrode assembly under humidity cycles. Journal of Power Sources. 2012;206:37-46.

[140] Kusoglu A, Karlsson AM, Santare MH, Cleghorn S, Johnson WB. Mechanical behavior of fuel cell membranes under humidity cycles and effect of swelling anisotropy on the fatigue stresses. Journal of Power Sources. 2007;170:345-58.

[141] Liu D, Lai X, Ni J, Peng L, Lan S, Lin Z. Robust design of assembly parameters on membrane electrode assembly pressure distribution. J Power Sources. 2007;172:760-7.

[142] Lin P, Zhou P, Wu CW. Multi-objective topology optimization of end plates of proton exchange membrane fuel cell stacks. J Power Sources. 2011;196:1222-8.

[143] Wang X, Song Y, Zhang B. Experimental study on clamping pressure distribution in PEM fuel cells. J Power Sources. 2008;179:305-9.

[144] Karvonen S, Hottinen T, Ihonen J, Uusalo H. Modeling of Polymer Electrolyte Membrane Fuel Cell Stack End Plates. ASME J Fuel Cell Sci Technol. 2008;5:41009-1.

[145] Yu HN, Kim SS, Suh JD, Lee DG. Composite endplates with pre-curvature for PEMFC (polymer electrolyte membrane fuel cell). Compos Struct. 2010;92:1498-503.

[146] Tu ZK, Liu ZC, Liu C, Gai DX, Wan ZM, Liu W. Heat and mass transfer in a flat disc-shaped evaporator of a miniature loop heat pipe. Proceedings of the Institution of Mechanical Engineers, Part G: Journal of Aerospace Engineering. 2009;223:609-18.

[147] Yi P, Peng L, NI J. A numerical model for predicting gas diffusion layer failure in proton exchange membrane fuel cells. ASME J Fuel Cell Sci Technol. 2011;8:011011.1-10.

[148] Zhou Y, Lin G, Shih A, Hu S. Multi-Physics Modeling of Assembly Pressure Effects on PEM Fuel Cell Performance. ASME Journal of Fuel Cell Science and Technology. 2008;6:041005.1-7.

[149] Zhou P, Wu CW. Numerical study on the compression effect of gas diffusion layer on PEMFC performance. J Power Sources. 2007;170:93-100.

[150] Chang WR, Hwang JJ, Weng FB, Chan SH. Effect of clamping pressure on the performance of a PEM fuel cell. J Power Sources. 2007;166:149-54.

[151] Lee W, Ho CH, Van Zee J, Murthy M. The effects of compression and gas diffusion layers on the performance of a PEM fuel cell. J Power Sources. 1999;84:45-51.

[152] Wen C-Y, Lin Y-S, Lu C-H. Experimental study of clamping effects on the performances of a single proton exchange membrane fuel cell and a 10-cell stack. J Power Sources. 2009;192:475-85.

[153] Taymaz I, Benli M. Numerical study of assembly pressure effect on the performance of proton exchange membrane fuel cell. Energy. 2010;35:2134-40.

[154] Zhou P, Lin P, Wu C, Li Z. Effect of nonuniformity of the contact pressure distribution on the electrical contact resistance in proton exchange membrane fuel cells. Int J Hydrogen Energ. 2011;36:6039-44.

[155] Lee S-J, Hsu C-D, Huang C-H. Analyses of the fuel cell stack assembly pressure. J Power Sources. 2005;145:353-61.

[156] Wang W, Hou B, Lin Z, Xia ZC. An engineering approach to improve the stamping robustness of

high strength steels. Journal of manufacturing science and engineering. 2009;131.
[157] Zhou Y, Lin G, Shih AJ, Hu SJ. A micro-scale model for predicting contact resistance between bipolar plate and gas diffusion layer in PEM fuel cells. J Power Sources. 2007;163:777-83.
[158] Wu Z, Zhou Y, Lin G, Wang S, Hu SJ. An improved model for predicting electrical contact resistance between bipolar plate and gas diffusion layer in proton exchange membrane fuel cells. J Power Sources. 2008;182:265-9.
[159] Qiu D, Yi P, Peng L, Lai X. Assembly design of proton exchange membrane fuel cell stack with stamped metallic bipolar plates. Int J Hydrogen Energ. 2015;40:11559-68.
[160] Peng LF, Qiu DK, Yi PY, Lai XM. Investigation of Thermal Influence on the Assembly of Polymer Electrolyte Membrane Fuel Cell Stacks. In: Ren N, Che LK, Jin B, Dong R, Su H, editors. Renewable and Sustainable Energy Ii, Pts 1-42012. p. 1509-14.
[161] de las Heras N, Roberts EPL, Langton R, R. Hodgson D. A review of metal separator plate materials suitable for automotive PEM fuel cells. Energy & Environmental Science. 2009;2:206-14.
[162] Peng L, Yi P, Lai X. Design and manufacturing of stainless steel bipolar plates for proton exchange membrane fuel cells. Int J Hydrogen Energ. 2014;39:21127-53.
[163] Mahabunphachai S, Cora ÖN, Koc M. Effect of manufacturing processes on formability and surface topography of proton exchange membrane fuel cell metallic bipolar plates. J Power Sources. 2010;195:5269-77.
[164] Qiu D, Yi P, Peng L, Lai X. Channel Dimensional Error Effect of Stamped Bipolar Plates on the Characteristics of Gas Diffusion Layer Contact Pressure for Proton Exchange Membrane Fuel Cell Stacks. ASME J Fuel Cell Sci Technol. 2015;12:041002.
[165] Turan C, Cora ÖN, Koc M. Effect of manufacturing processes on contact resistance characteristics of metallic bipolar plates in PEM fuel cells. Int J Hydrogen Energ. 2011;36:12370-80.
[166] Liu D, Peng L, Lai X. Effect of dimensional error of metallic bipolar plate on the GDL pressure distribution in the PEM fuel cell. Int J Hydrogen Energ. 2009;34:990-7.
[167] Peng L, Qiu D, Yi P, Lai X. An Analytical Model for Contact Pressure Prediction Considering Dimensional Error of Stamped Bipolar Plate and Gas Diffusion Layer in Proton Exchange Membrane Fuel Cell Stack Assembly. Journal of Electrochemical Energy Conversion and Storage. 2016;13:021007.
[168] Shimpalee S, Lilavivat V, Van Zee JW, McCrabb H, Lozano-Morales A. Understanding the effect of channel tolerances on performance of PEMFCs. Int J Hydrogen Energ. 2011;36:12512-23.
[169] Majlan EH, Rohendi D, Daud WRW, Husaini T, Haque MA. Electrode for proton exchange membrane fuel cells: A review. Renewable and Sustainable Energy Reviews. 2018;89:117-34.
[170] Qiu D, Yi P, Peng L, Lai X. Study on shape error effect of metallic bipolar plate on the GDL contact pressure distribution in proton exchange membrane fuel cell. Int J Hydrogen Energ. 2013;38:6762-72.
[171] Yi PY, Du XY, Kan YY, Peng LF, Lai XM. Modeling and experimental study of laser welding distortion of thin metallic bipolar plates for PEM fuel cells. Int J Hydrogen Energ. 2015;40:4850-60.

[172] Liu D, Peng L, Lai X. Effect of assembly error of bipolar plate on the contact pressure distribution and stress failure of membrane electrode assembly in proton exchange membrane fuel cell. J Power Sources. 2010;195:4213-21.
[173] Qiu D, Peng L, Liang P, Yi P, Lai X. Mechanical degradation of proton exchange membrane along the MEA frame in proton exchange membrane fuel cells. Energy. 2018;165:210-22.
[174] Bograchev D, Gueguen M, Grandidier J-C, Martemianov S. Stress and plastic deformation of MEA in fuel cells: Stresses generated during cell assembly. Journal of Power Sources. 2008;180:393-401.
[175] Kim J-S, Park J-B, Kim Y-M, Ahn S-H, Sun H-Y, Kim K-H, et al. Fuel Cell End Plates. International Journal of Precision Engineering and Manufacturing. 2008;9:39-46.
[176] !!! INVALID CITATION !!!
[177] Wozniczka B, Fletcher NJ, Gibb PR. Electrochemical fuel cell stack with compression bands. Google Patents; 1998.
[178] Qiu D, Peng L, Yi P, Lai X, Janßen H, Lehnert W. Contact behavior modelling and its size effect on proton exchange membrane fuel cell. J Power Sources. 2017;365:190-200.
[179] Yan Q, Toghiani H, Lee Y-W, Liang K, Causey H. Effect of sub-freezing temperatures on a PEM fuel cell performance, startup and fuel cell components. Journal of Power Sources. 2006;160:1242-50.
[180] Wan Z, Chang H, Shu S, Wang Y, Tang H. A Review on Cold Start of Proton Exchange Membrane Fuel Cells. Energies. 2014;7:3179.
[181] Li B, Kim YS, Mukundan R, Wilson MS, Welch C, Fenton J, et al. Mixed Hydrocarbon/Fluoropolymer Membrane/Ionomer MEAs for Durablity Studies. ECS Transactions. 2010;33:913-24.
[182] Vengatesan S, Panha K, Fowler MW, Yuan X-Z, Wang H. Membrane electrode assembly degradation under idle conditions via unsymmetrical reactant relative humidity cycling. J Power Sources. 2012;207:101-10.
[183] Thursfield A, Murugan A, Franca R, Metcalfe IS. Chemical looping and oxygen permeable ceramic membranes for hydrogen production - a review. Energy & Environmental Science. 2012;5:7421-59.
[184] Ju H, Wang C-Y, Cleghorn S, Beuscher U. Nonisothermal modeling of polymer electrolyte fuel cells I. Experimental validation. J Electrochem Soc. 2005;152:A1645-A53.
[185] Kandlikar SG, Lu Z. Thermal management issues in a PEMFC stack – A brief review of current status. Applied Thermal Engineering. 2009;29:1276-80.
[186] Sun H, Zhang G, Guo L-J, Dehua S, Liu H. Effects of humidification temperatures on local current characteristics in a PEM fuel cell. J Power Sources. 2007;168:400-7.
[187] Ozen DN, Timurkutluk B, Altinisik K. Effects of operation temperature and reactant gas humidity levels on performance of PEM fuel cells. Renewable and Sustainable Energy Reviews. 2016;59:1298-306.
[188] Xu H, Song Y, Kunz HR, Fenton JM. Effect of Elevated Temperature and Reduced Relative

Humidity on ORR Kinetics for PEM Fuel Cells. J Electrochem Soc. 2005;152:A1828-A36.

[189] Neyerlin K, Gasteiger HA, Mittelsteadt CK, Jorne J, Gu W. Effect of relative humidity on oxygen reduction kinetics in a PEMFC. J Electrochem Soc. 2005;152:A1073-A80.

[190] Mortazavi M, Tajiri K. Two-phase flow pressure drop in flow channels of proton exchange membrane fuel cells: Review of experimental approaches. Renewable and Sustainable Energy Reviews. 2015;45:296-317.

[191] Chen C, Fuller TF. The effect of humidity on the degradation of Nafion® membrane. Polym Degrad Stabil. 2009;94:1436-47.

[192] Tang Y, Santare MH, Karlsson AM, Cleghorn S, Johnson WB. Stresses in proton exchange membranes due to hydration and dehydration cycles. Proceedings of the Third International Conference on Fuel Cell Science, Engineering and Technology2005. p. 23-5.

[193] Khorasany RM, Goulet M-A, Alavijeh AS, Kjeang E, Wang GG, Rajapakse R. On the constitutive relations for catalyst coated membrane applied to in-situ fuel cell modeling. Journal of Power Sources. 2014;252:176-88.

[194] Verma A, Pitchumani R. Investigation of Mechanical Behavior of Membrane in Polymer Electrolyte Fuel Cells Subject to Dynamic Load Changes. ASME J Fuel Cell Sci Technol. 2014;11:031010.

[195] Al-Baghdadi MARS, Al-Janabi HAKS. Influence of the Design Parameters in a Proton Exchange Membrane (PEM) Fuel Cell on the Mechanical Behavior of the Polymer Membrane. Energy & Fuels. 2007;21:2258-67.

[196] Sadiq Al-Baghdadi MAR. A CFD study of hygro–thermal stresses distribution in PEM fuel cell during regular cell operation. Renew Energ. 2009;34:674-82.

[197] Cho E, Ko J-J, Ha HY, Hong S-A, Lee K-Y, Lim T-W, et al. Characteristics of the PEMFC repetitively brought to temperatures below 0 C. Journal of the Electrochemical Society. 2003;150:A1667-A70.

[198] McDonald R, Mittelsteadt C, Thompson E. Effects of deep temperature cycling on Nafion® 112 membranes and membrane electrode assemblies. Fuel cells. 2004;4:208-13.

[199] Yoshida H, Miura Y. Behavior of water in perfluorinated ionomer membranes containing various monovalent cations. Journal of membrane science. 1992;68:1-10.

[200] Rhim J-W, Park HB, Lee C-S, Jun J-H, Kim DS, Lee YM. Crosslinked poly (vinyl alcohol) membranes containing sulfonic acid group: proton and methanol transport through membranes. Journal of Membrane Science. 2004;238:143-51.

[201] Karlsson LE, Wesslén B, Jannasch P. Water absorption and proton conductivity of sulfonated acrylamide copolymers. Electrochimica acta. 2002;47:3269-75.

[202] Kim DS, Park HB, Rhim JW, Lee YM. Proton conductivity and methanol transport behavior of cross-linked PVA/PAA/silica hybrid membranes. Solid State Ionics. 2005;176:117-26.

[203] Cappadonia M, Erning JW, Stimming U. Proton conduction of Nafion® 117 membrane between 140 K and room temperature. Journal of Electroanalytical Chemistry. 1994;376:189-93.
[204] Wilson MS, Valerio JA, Gottesfeld S. Low platinum loading electrodes for polymer electrolyte fuel cells fabricated using thermoplastic ionomers. Electrochimica Acta. 1995;40:355-63.
[205] Mukundan R, Kim YS, Garzon F, Pivovar B. Freeze/thaw effects in PEM fuel cells. ECS Transactions. 2006;1:403-13.
[206] Gaylord R. Stationary application and freeze/thaw. Proceedings of the Workshop on Fuel Cell Operations at Sub-Freezing Temperatures, Phoenix, AZ, USA2005. p. 1-2.
[207] Luo M, Huang C, Liu W, Luo Z, Pan M. Degradation behaviors of polymer electrolyte membrane fuel cell under freeze/thaw cycles. International Journal of Hydrogen Energy. 2010;35:2986-93.
[208] Wang H, Hou J, Yu H, Sun S. Effects of reverse voltage and subzero startup on the membrane electrode assembly of a PEMFC. Journal of Power Sources. 2007;165:287-92.
[209] Alink R, Gerteisen D, Oszcipok M. Degradation effects in polymer electrolyte membrane fuel cell stacks by sub-zero operation—An in situ and ex situ analysis. Journal of Power Sources. 2008;182:175-87.
[210] Oszcipok M, Riemann D, Kronenwett U, Kreideweis M, Zedda M. Statistic analysis of operational influences on the cold start behaviour of PEM fuel cells. Journal of power sources. 2005;145:407-15.
[211] Ralph TR, Barnwell DE, Bouwman PJ, Hodgkinson AJ, Petch MI, Pollington M. Reinforced Membrane Durability in Proton Exchange Membrane Fuel Cell Stacks for Automotive Applications. Journal of The Electrochemical Society. 2008;155:B411-B22.
[212] Bograchev D, Gueguen M, Grandidier J-C, Martemianov S. Stress and plastic deformation of MEA in running fuel cell. International Journal of Hydrogen Energy. 2008;33:5703-17.
[213] Serincan MF, Pasaogullari U. Effect of gas diffusion layer anisotropy on mechanical stresses in a polymer electrolyte membrane. J Power Sources. 2011;196:1314-20.
[214] Ahluwalia R, Wang X. Rapid self-start of polymer electrolyte fuel cell stacks from subfreezing temperatures. Journal of Power Sources. 2006;162:502-12.
[215] Borup R, Meyers J, Pivovar B, Kim YS, Mukundan R, Garland N, et al. Scientific aspects of polymer electrolyte fuel cell durability and degradation. Chem Rev. 2007;107:3904-51.
[216] Krasij M, Rajport Jr MJ. Interfacial and edge seals for unitized electrode assemblies of fuel cell stack assembly. Google Patents; 2004.
[217] Bhaskar S, Gasteiger H, Litteer BA. Catalyst layer edge protection for enhanced MEA durability in PEM fuel cells. Google Patents; 2005.
[218] Crum M, Liu W. Effective testing matrix for studying membrane durability in PEM fuel cells: Part 2. Mechanical durability and combined mechanical and chemical durability. ECS Transactions. 2006;3:541-50.
[219] Lai Y-H, Miller DP, Ji C, Trabold TA. Stack compression of PEM fuel cells. ASME 2004 2nd

International Conference on Fuel Cell Science, Engineering and Technology: American Society of Mechanical Engineers; 2004. p. 567-71.
[220] Miyatake K, Furuya H, Tanaka M, Watanabe M. Durability of sulfonated polyimide membrane in humidity cycling for fuel cell applications. Journal of Power Sources. 2012;204:74-8.
[221] Kusoglu A, Kienitz BL, Weber AZ. Understanding the Effects of Compression and Constraints on Water Uptake of Fuel-Cell Membranes. J Electrochem Soc. 2011;158:B1504-B14.
[222] Li Y, Dillard DA, Case SW, Ellis MW, Lai Y-H, Gittleman CS, et al. Fatigue and creep to leak tests of proton exchange membranes using pressure-loaded blisters. J Power Sources. 2009;194:873-9.
[223] Solasi R, Huang X, Reifsnider K. Creep and stress-rupture of Nafion® membranes under controlled environment. Mech Mater. 2010;42:678-85.
[224] Alavijeh AS, Khorasany RM, Habisch A, Wang GG, Kjeang E. Creep properties of catalyst coated membranes for polymer electrolyte fuel cells. Journal of Power Sources. 2015;285:16-28.
[225] Kyriakides SA. Mechanical Behavior of Nafion® and BPSH Membranes. Journal of Undergraduate Materials Research. 2017;1.
[226] Khorasany RM, Alavijeh AS, Kjeang E, Wang G, Rajapakse R. Mechanical degradation of fuel cell membranes under fatigue fracture tests. Journal of Power Sources. 2015;274:1208-16.
[227] Aindow TT, O'Neill J. Use of mechanical tests to predict durability of polymer fuel cell membranes under humidity cycling. J Power Sources. 2011;196:3851-4.
[228] Grohs JR, Li Y, Dillard DA, Case SW, Ellis MW, Lai Y-H, et al. Evaluating the time and temperature dependent biaxial strength of Gore-Select® series 57 proton exchange membrane using a pressure loaded blister test. J Power Sources. 2010;195:527-31.
[229] Banan R, Bazylak A, Zu J. Combined effects of environmental vibrations and hygrothermal fatigue on mechanical damage in PEM fuel cells. International Journal of Hydrogen Energy. 2015;40:1911-22.
[230] Guvelioglu GH, Stenger HG. Flow rate and humidification effects on a PEM fuel cell performance and operation. J Power Sources. 2007;163:882-91.
[231] Jung M, Williams KA. Effect of dynamic operation on chemical degradation of a polymer electrolyte membrane fuel cell. J Power Sources. 2011;196:2717-24.
[232] Lai Y-H, Fly GW. In-situ diagnostics and degradation mapping of a mixed-mode accelerated stress test for proton exchange membranes. Journal of Power Sources. 2015;274:1162-72.
[233] Watts G, Krylov V. Ground-borne vibration generated by vehicles crossing road humps and speed control cushions. Applied Acoustics. 2000;59:221-36.
[234] Diloyan G, Sobel M, Das K, Hutapea P. Effect of mechanical vibration on platinum particle agglomeration and growth in Polymer Electrolyte Membrane Fuel Cell catalyst layers. Journal of Power Sources. 2012;214:59-67.
[235] Betournay MC, Bonnell G, Edwardson E, Paktunc D, Kaufman A, Lomma AT. The effects of mine conditions on the performance of a PEM fuel cell. Journal of Power Sources. 2004;134:80-7.

[236] Rouss V, Lesage P, Bégot S, Candusso D, Charon W, Harel F, et al. Mechanical behaviour of a fuel cell stack under vibrating conditions linked to aircraft applications part I: Experimental. International Journal of Hydrogen Energy. 2008;33:6755-65.
[237] Rajalakshmi N, Pandian S, Dhathathreyan K. Vibration tests on a PEM fuel cell stack usable in transportation application. International journal of hydrogen energy. 2009;34:3833-7.
[238] Kundu S, Simon LC, Fowler MW. Comparison of two accelerated Nafion™ degradation experiments. Polym Degrad Stabil. 2008;93:214-24.
[239] Qiao J, Saito M, Hayamizu K, Okada T. Degradation of Perfluorinated Ionomer Membranes for PEM Fuel Cells during Processing with H2O2. J Electrochem Soc. 2006;153:A967-A74.
[240] Kusoglu A, Calabrese M, Weber AZ. Effect of Mechanical Compression on Chemical Degradation of Nafion Membranes. ECS Electrochemistry Letters. 2014;3:F33-F6.
[241] Rodgers MP, Bonville LJ, Mukundan R, Borup RL, Ahluwalia R, Beattie P, et al. Perfluorinated Sulfonic Acid Membrane and Membrane Electrode Assembly Degradation Correlating Accelerated Stress Testing and Lifetime Testing. ECS Transactions. 2013;58:129-48.
[242] Sadeghi Alavijeh A, Goulet MA, Khorasany RMH, Ghataurah J, Lim C, Lauritzen M, et al. Decay in Mechanical Properties of Catalyst Coated Membranes Subjected to Combined Chemical and Mechanical Membrane Degradation. Fuel Cells. 2015;15:204-13.
[243] Lim C, Alavijeh AS, Lauritzen M, Kolodziej J, Knights S, Kjeang E. Fuel cell durability enhancement with cerium oxide under combined chemical and mechanical membrane degradation. ECS Electrochemistry Letters. 2015;4:F29-F31.
[244] Patil YP, Jarrett WL, Mauritz KA. Deterioration of mechanical properties: A cause for fuel cell membrane failure. Journal of Membrane Science. 2010;356:7-13.
[245] Madden T, Weiss D, Cipollini N, Condit D, Gummalla M, Burlatsky S, et al. Degradation of Polymer-Electrolyte Membranes in Fuel Cells: I. Experimental. Journal of The Electrochemical Society. 2009;156:B657-B62.
[246] Luo Z, Li D, Tang H, Pan M, Ruan R. Degradation behavior of membrane–electrode-assembly materials in 10-cell PEMFC stack. International Journal of Hydrogen Energy. 2006;31:1831-7.
[247] Rodgers MP, Brooker RP, Mohajeri N, Bonville LJ, Kunz HR, Slattery DK, et al. Comparison of proton exchange membranes degradation rates between accelerated and performance tests. Journal of The Electrochemical Society. 2012;159:F338-F52.
[248] Kim L, Chung CG, Sung YW, Chung JS. Dissolution and migration of platinum after long-term operation of a polymer electrolyte fuel cell under various conditions. Journal of Power Sources. 2008;183:524-32.
[249] Macauley N, Ghassemzadeh L, Lim C, Watson M, Kolodziej J, Lauritzen M, et al. Pt band formation enhances the stability of fuel cell membranes. ECS Electrochemistry Letters. 2013;2:F33-F5.
[250] Bi W, Gray GE, Fuller TF. PEM Fuel Cell Pt/C Dissolution and Deposition in Nafion Electrolyte.

Electrochemical and Solid-State Letters. 2007;10:B101-B4.
[251] Yasuda K, Taniguchi A, Akita T, Ioroi T, Siroma Z. Platinum dissolution and deposition in the polymer electrolyte membrane of a PEM fuel cell as studied by potential cycling. Physical Chemistry Chemical Physics. 2006;8:746-52.
[252] Zhang J, Litteer BA, Gu W, Liu H, Gasteiger HA. Effect of hydrogen and oxygen partial pressure on Pt precipitation within the membrane of PEMFCs. Journal of The Electrochemical Society. 2007;154:B1006-B11.
[253] Jia R, Han B, Levi K, Hasegawa T, Ye J, Dauskardt RH. Mechanical durability of proton exchange membranes with catalyst platinum dispersion. Journal of Power Sources. 2011;196:8234-40.
[254] Helmly S, Ohnmacht B, Gazdzicki P, Hiesgen R, Gülzow E, Friedrich KA. Influence of the Distribution of Platinum Deposits on the Properties and Degradation of Platinum-Impregnated Nafion Membranes. Journal of The Electrochemical Society. 2014;161:F1416-F26.
[255] Stucki S, Scherer GG, Schlagowski S, Fischer E. PEM water electrolysers: evidence for membrane failure in 100kW demonstration plants. Journal of Applied Electrochemistry. 1998;28:1041-9.
[256] Kundu S, Cimenti M, Lee S, Bessarabov D. Fingerprint of automotive fuel cell cathode catalyst degradation: Pt band in PEMs. Membrane Technology. 2009;2009:7-10.
[257] Macauley N, Alavijeh AS, Watson M, Kolodziej J, Lauritzen M, Knights S, et al. Accelerated membrane durability testing of heavy duty fuel cells. Journal of The Electrochemical Society. 2015;162:F98-F107.
[258] Han B, Carlton CE, Kongkanand A, Kukreja RS, Theobald BR, Gan L, et al. Record activity and stability of dealloyed bimetallic catalysts for proton exchange membrane fuel cells. Energy & Environmental Science. 2015;8:258-66.
[259] Khorasany RMH, Singh Y, Sadeghi Alavijeh A, Kjeang E, Wang GG, Rajapakse RKND. Fatigue properties of catalyst coated membranes for fuel cells: Ex-situ measurements supported by numerical simulations. International Journal of Hydrogen Energy. 2016;41:8992-9003.
[260] Goulet M-A, Khorasany RMH, De Torres C, Lauritzen M, Kjeang E, Wang GG, et al. Mechanical properties of catalyst coated membranes for fuel cells. Journal of Power Sources. 2013;234:38-47.
[261] Kai Y, Kitayama Y, Omiya M, Uchiyama T, Kato M. Crack Formation in Membrane Electrode Assembly Under Static and Cyclic Loadings. Journal of Fuel Cell Science and Technology. 2013;10:021007-.
[262] Xie J, Wood DL, Wayne DM, Zawodzinski TA, Atanassov P, Borup RL. Durability of PEFCs at high humidity conditions. J Electrochem Soc. 2005;152:A104-A13.
[263] Rong F, Huang C, Liu Z-S, Song D, Wang Q. Microstructure changes in the catalyst layers of PEM fuel cells induced by load cycling: Part I. Mechanical model. J Power Sources. 2008;175:699-711.
[264] Poornesh KK, Cho CD, Lee GB, Tak YS. Gradation of mechanical properties in gas diffusion electrode. Part 1: Influence of nano-scale heterogeneity in catalyst layer on interfacial strength between

catalyst layer and membrane. J Power Sources. 2010;195:2709-17.
[265] Zhan Z, Xiao J, Li D, Pan M, Yuan R. Effects of porosity distribution variation on the liquid water flux through gas diffusion layers of PEM fuel cells. Journal of Power Sources. 2006;160:1041-8.
[266] Saleh MM, Okajima T, Hayase M, Kitamura F, Ohsaka T. Exploring the effects of symmetrical and asymmetrical relative humidity on the performance of H2/air PEM fuel cell at different temperatures. J Power Sources. 2007;164:503-9.
[267] Zhang S, Yuan X, Wang H, Mérida W, Zhu H, Shen J, et al. A review of accelerated stress tests of MEA durability in PEM fuel cells. Int J Hydrogen Energ. 2009;34:388-404.
[268] Miller M, Bazylak A. A review of polymer electrolyte membrane fuel cell stack testing. Journal of Power Sources. 2011;196:601-13.
[269] Gittleman CS, Lai Y-H, Miller D. Durability of perfluorosulfonic acid membranes for PEM fuel cells. Extended Abstract in the AIChE 2005 Annual Meeting, Cincinnati, OH, Oct2005.
[270] Shi S, Chen G, Wang Z, Chen X. Mechanical properties of Nafion 212 proton exchange membrane subjected to hygrothermal aging. J Power Sources. 2013;238:318-23.
[271] Silberstein MN, Pillai PV, Boyce MC. Biaxial elastic–viscoplastic behavior of Nafion membranes. Polymer. 2011;52:529-39.
[272] Jia R, Han B, Levi K, Hasegawa T, Ye J, Dauskardt RH. Effect of cation contamination and hydrated pressure loading on the mechanical properties of proton exchange membranes. Journal of Power Sources. 2011;196:3803-9.
[273] Cheng S, Johnson L, Wang S-Q. Crazing and strain localization of polycarbonate glass in creep. Polymer. 2013;54:3363-9.
[274] Singh Y, Orfino FP, Dutta M, Kjeang E. 3D visualization of membrane failures in fuel cells. J Power Sources. 2017;345:1-11.
[275] Singh Y, Orfino FP, Dutta M, Kjeang E. 3D Failure Analysis of Pure Mechanical and Pure Chemical Degradation in Fuel Cell Membranes. J Electrochem Soc. 2017;164:F1331-F41.